Regulation of *Caenorhabditis elegans* MCAK by Aurora Kinase Phosphorylation

by

Xue Han

A thesis submitted in partial fulfillment of the requirements for the degree of

Doctor of Philosophy

in

Molecular Biology and Genetics

Department of Biological Sciences
University of Alberta

Abstract

Regulation of microtubule dynamics is essential for many cellular processes, including proper assembly and function of the mitotic spindle. One mechanism for temporal and spatial regulation of microtubule dynamics is provided by the kinesin-13 microtubule depolymerizing enzymes, among which MCAK is the most extensively studied. Vertebrates MCAK locates to chromatin, kinetochores, spindle poles, microtubule tips, and the cytoplasm, implying that the regulation of MCAK activity and subcellular targeting is complex. It has been established that MCAK activity and subcellular localization is regulated by Aurora kinase phosphorylation. However, the *in vivo* regulatory mechanism is highly complex and is still not fully understood. In this thesis I describe the function and regulation of KLP-7, the *C. elegans* kinesin-13 homologue. KLP-7 locates to chromosomes and spindle poles during meiosis and mitosis, and to the chromosomal passenger complex region in meiosis. Loss of KLP-7 results in meiotic and mitotic defects that are consistent with an increase in the amount of microtubules in the cytoplasmic and spindle regions of meiotic embryos, and an increase in the number of microtubules emanating from centrosomes. I found that KLP-7 protein is phosphorylated *in vivo* and *in vitro*. Finally, by performing a structure-function analysis I identified S546 as a putative Aurora kinase site essential for KLP-7 activity *in vivo*.

Preface

The FRAP experiments (Figure 3-32) were designed and conducted by Martin Srayko, and the data analysed by Ellen Sykes. Some of the microscopy data used to characterize the meiotic defects of *klp-7(tm2143)* embryos (Table 3-2) was collected by Kelly Adames. The experiment to image *C. elegans* motor neurons (Figure A-4) was designed by me, but image acquisition was done by Kelly Adames. The rest of the thesis is my original work and has not been published.

Acknowledgements

First of all, I would like to express my sincere gratitude to my supervisor, Dr. Martin Srayko, for giving me the opportunity to work on this project. His patient guidance and support throughout my Ph.D. studies are extremely valuable in my training. I would like to thank my committee members, Dr. Gordon Chan and Dr. Shelagh Campbell for their great suggestions and advice on my project. Thanks also to Dr. Andrew Waskiewicz and Dr. David Sharp for serving as my examiners.

Many thanks to past and present members of the Srayko laboratory. Thanks to Ellen, Kelly and Nobu for their effort and assistance on my project. Thanks also to Donna, Eva, Karen L, Maryam, Megha, Ina, Jay, Tegha, Karen C, Jen, Ashkan, Caitlin, David, Jeffery, Justin, Phil and Ritika for making the lab a cheerful and fun place to work.

I'd like to give special thanks to my friends, Danielle, Juan, Sophie and Ran for listening to me and encouraging me to do my best. Finally, I want to express my deepest love and thanks to my family, mom, dad and my husband Xiao Li, for their understanding and support.

Table of Contents

List of tables

List of figures

List of abbreviations and symbols

2D gel electrophoresis two dimensional gel electrophoresis

+TIP plus end tracking protein

°C degrees Celsius

γ-TuRC gamma-tubulin ring complex

γ-TuSC gamma-tubulin small complex

λ PPase Lambda Phosphatase

µCi microcurie

µg microgram

µL microliter

µm micrometer

µM micromolar

A alanine

A-P anterior-posterior

AA (or a.a.) amino acid

AIR Aurora/Ipl1 related

ALM anterior lateral microtubule

APC adenomatous polyposis coli

ATP adenosine-5'-triphosphate

bp base pair

BSA bovine serum albumin

cDNA complementary DNA

Cdc cell division cycle

Cdk cyclin-dependent kinase

CENP centromere protein

CGC Caenorhabditis Genetics Center

CHAPS 3-[(3-cholamidopropyl)dimethylammonio]-1-propanesulfonate hydrate

cM centimorgan

CPC chromosomal passenger complex

DAF abnormal dauer formation

DAPI 4',6-diamidino-2-phenylindole

DIC differential interference contrast

DLK dual-leucine zipper kinase

DMSO dimethyl sulfoxide

DNA deoxyribonucleic acid

DTT dithiothreitol

dNTPs deoxyribonucleotide triphosphate

dsRNA double-stranded RNA

E glutamic acid

EB end binding

EDTA ethylene diamine tetraacetic acid

EGTA ethylene glycol tetraacetic acid

EBP end binding protein

FRAP fluorescence recovery after photobleaching

GDP guanine diphosphate

GFP green fluorescent protein

GPR G protein regulator

GPS group-based phosphorylation scoring method

GST glutathione s-transferase

GTP guanine triphosphate

h hour

HEPES 4-(2-hydroxyethyl)-1-piperazineethanesulfonic acid

HRG human retinal gene

HRP horseradish peroxidise

icp inner centromere protein

IEF isoelectric focusing

IgG immunoglobulin G

IP immunoprecipitation

IPG immobilized pH gradient

IPTG isopropyl β-D-1-thiogalactopyranoside

KD kinase-dead

kDa kilodalton

KIF kinesin superfamily protein

Kin-I kinesin internal

KLH keyhole limpet hemocyanin

KLP kinesin like protein

L liter

L4 larval instar stage 4

LB Luria Bertani broth

LC-MS/MS liquid chromatography-tandem mass spectrometry

lf loss of function

M molar

MALDI-TOF matrix assisted laser desorption /Ionization- time of flight

MAPs microtubule associated proteins

MAPK mitogen-activated protein kinase

MAS Martin A. Srayko (lab designation for *C. elegans* strains)

MCAK mitotic centromere-associated kinesin

min minute

mL milliliter

mm millimetre

mM millimolar

MTOC microtubule organizing centres

MTs microtubules

MW molecular weight

mW milliwatt

NA numerical aperture

NAD+ nicotinamide adenine dinucleotide

NEB nuclear envelope breakdown

NGM nematode growth medium

nm nanometre

OD optical density

PAGE polyacrylamide gel electrophoresis

PAK p21-activated kinase

PBS phosphate buffered saline

PCM pericentriolar material

PCR polymerase chain reaction

pie pharynx and intestine in excess

PLM posterior lateral microtubule

Plk polo-like kinase

PP2A protein phosphatase 2

ptr patched related family

Rac ras-related C3 botulinum toxin substrate

RNA ribonucleic acid

RNAi RNA interference

RRG rat retinal gene

RSA regulator of spindle assembly

S serine

SDS-PAGE sodium dodecyl sulfate polyacrylamide gel electrophoresis

sec second

T threonine

TBST Tris buffered saline Tween 20

TPX2 targeting protein for *Xenopus* Klp2

tpxl targeting protein for *Xenopus* Klp2 like

ts temperature-sensitive

unc uncoordinated

V Voltage

WT wild type

ZYG zygote defective, embryonic lethal

1 Introduction

1.1 Introduction to microtubule structure and regulation of microtubule dynamics

1.1.1 Structure of microtubules

Microtubules (MTs) are a cytoskeleton component responsible for multiple essential cellular processes in all eukaryotic cells. They function in maintaining cell structure and polarity. They are also integral components of meiotic and mitotic spindles, which are used by eukaryotic cells to separate DNA during cell divisions. MTs also provide routes for intracellular transport of secretory vesicles and organelles. Since MTs are so critical to cellular functions, it is important to understand the structure of MTs and how they are assembled and disassembled in a regulated manner throughout the cell cycle.

MTs are polymers of α/β-tubulin heterodimers, which are conserved in amino acid sequence and protein structure. The monomers α- and β-tubulin contain a core of two β-sheets surrounded by α-helices and can be divided into three functional domains. The N-terminal domain is formed by β-strands and α-helices and is responsible for nucleotide-binding. An intermediate domain is formed by β-strands and α-helices. In β-tubulin this domain contains a binding site for paclitaxel (taxol), a well-known anticancer drug. The C-terminal domain contains two α-helices that may serve as the binding surface for motor proteins (Nogales et al., 1998).

The α/β-tubulin heterodimers assemble end-to-end to form protofilaments, which associate side-by-side to form the MT lattice (Amos and Klug, 1974). In most eukaryotes, thirteen protofilaments associate laterally to form a single MT (Evans et al., 1985; Ledbetter and Porter, 1964; Tilney et al., 1973), although this can vary between different organisms and between different cell types within a single organism. MTs are polarized with a fast growing “plus” end and a slow growing “minus” end (Allen and Borisy, 1974). The MT polymers can rapidly switch between growth and shrinkage phases, allowing quick assembly or disassembly of MT structures to meet the cell’s needs. This intrinsic “dynamic instability” property of MTs is linked to GTP hydrolysis in β-tubulin. GTP-bound tubulin is incorporated into the polymer at the plus end, and this “GTP-cap” structure confers stability to the growing plus end. Sometime after subunit addition, the β-tubulin-bound GTP hydrolyzes to GDP. Unlike GTP-bound tubulin, the GDP-bound tubulin has a curved conformation which is prone to depolymerisation when exposed at the MT ends (Weisenberg et al., 1976). In the middle of the MT lattice, a GDP-bound tubulin is constrained to adopt a straight conformation, thus the energy released from GTP hydrolysis is stored in the MT lattice as conformation strain. When the GTP-cap is lost, MTs undergo rapid depolymerization (Mitchison and Kirschner, 1984).

MT growth spontaneously occurs in the presence of GTP, Mg^{2+} and high concentrations of α/β-tubulin *in vitro* (Voter and Erickson, 1984).

However, inside cells, the concentration of α/β-tubulin is below the concentration required for efficient de novo MT formation (free MT nucleation) (Hyman and Karsenti, 1998). In cells, MTs are nucleated by microtubule organizing centers (MTOCs), such as the centrosomes. One protein, γ-tubulin has been found to provide a kinetically favorable site for MT nucleation *in vivo* [for review, see (Wiese and Zheng, 2006)]. γ-tubulin protein complexes isolated from *Drosophila* embryo or *Xenopus* egg extracts can nucleate MTs *in vitro* (Oegema et al., 1999; Zheng et al., 1995). However, knocking down γ-tubulin by RNAi does not eliminate centrosomal MTs in *C. elegans*, indicating that it is not absolutely required for MT nucleation at the centrosomes (Bobinnec et al., 2000; Hannak et al., 2002; O'Toole et al., 2012; Srayko et al., 2005; Strome et al., 2001). Further electron tomography followed by 3-D reconstruction analysis revealed that γ-tubulin plays an important role in organizing MT minus ends at the centrosomes (O'Toole et al., 2012). γ-tubulin subunits associate with other proteins to form a large γ-tubulin ring complex (γ-TuRC) and the γ-tubulin small complex (γ-TuSC). Structural data support the idea that γ-TuRC serves as a template in which γ-tubulin catalyzes MT-nucleation. A separate capping activity has also been revealed for γ-TuRC at the MT minus end, indicating a role of γ-tubulin in modulating end-dynamics (Moritz and Agard, 2001).

Other than GTP-dependent polymerization/depolymerization at both ends, MT dynamics are also regulated extrinsically by interactions

between the polymer and microtubule-associated proteins (MAPs). The MAP family includes a variety of proteins that carry out a wide range of functions, such as stabilizing/destabilizing MTs, transporting vesicles or organelles along MTs and cross-linking MTs.

1.1.2 Microtubule-associated proteins (MAPs)

MAPs were first identified by their high affinity for MTs *in vitro*. Over the past 50 years, the majority of work has been done on MAPs purified from brain tissues using cycles of temperature-dependent assembly and disassembly [for review, see (Olmsted, 1986)]. Other studies have also identified MAPs from cultured mammalian cells, sea urchin eggs and *Xenopus* oocytes (Jessus et al., 1985; Olmsted, 1986). One important class of MAPs binds to MTs to regulate polymer behavior. For example, the microtubule-associated protein XMAP215 promotes MT polymerization (Brouhard et al., 2008; Gard and Kirschner, 1987), whereas MCAK (mitotic centromere-associated kinesin) induces MT depolymerization (Walczak et al., 1996).

Microtubule plus-end tracking proteins (+TIPs) represent a specific class of MAPs that are characterized by their accumulation at the growing MT plus ends (termed tip-tracking). It is unclear whether +TIPs associate with the growing MT plus ends by co-polymerizing with tubulin at the MT tip followed by dissociation from the older MT lattice, or by binding to the open lattice of the growing MT end, or via transportation to the end by plus-end directed motor proteins. +TIPs not only interact with MT ends but

also form complex interaction networks with each other to regulate MT dynamics. In the center of the networks are highly conserved end-binding family proteins (EBs), which associate with MT plus ends independently of other +TIPs. End-binding protein 1 (EB1) was first identified in a yeast two-hybrid screen for proteins that interact with the C-terminus of adenomatous polyposis coli (APC) tumor suppressor protein (Su et al., 1995). Homologs of EB1 have been identified in every organism and various cell types (Tirnauer and Bierer, 2000). EBs target other MT-associated proteins to the plus end to regulate MT stability and MT interaction with various cellular organelles. Most +TIPs stabilize MTs and are implicated in linking MTs to diverse cellular components, such as the kinetochores and cortex [reviewed in (Akhmanova and Steinmetz, 2008)].

A specialized class of MAPs are the MT motors, which utilize the chemical energy of ATP hydrolysis to move along MTs. Representatives of the MT motors are dyneins and kinesins. Dyneins participate in a variety of cellular processes including cell division, intracellular transport and cilia beating. They can be divided into two general groups: axonemal dyneins and cytoplasmic dyneins. One key function of cytoplasmic dyneins is to transport various cargos along the MT surface towards the minus ends, which are usually anchored in the centrosomes of the cell [reviewed in (Roberts et al., 2013)]. In contrast to dyneins, most kinesins use MTs to drive plus-end directed transport (the plus-end directed motors).

1.2 General introduction to kinesin family proteins

The kinesin superfamily comprises 14 classes of proteins (termed kinesin 1 to kinesin 14) with diverse structures and functions [reviewed in (Hirokawa et al., 2009)]. Members of kinesin family proteins are characterized by a highly conserved motor domain, which contains the MT-binding and ATPase-active sites. X-ray structural analysis revealed that the motor domain is composed of multiple β-sheets and α-helices (Kull et al., 1996; Sack et al., 1997). Although the motor domains of kinesins are relatively well-conserved, other domains, such as a stalk and tail domain, are divergent and class-specific (Figure 1-1). Depending on the position of the motor domain within the primary sequence, kinesins can be broadly classified into three major groups: N-type kinesins (kinesin 1-12) with the motor domain located at the N-terminal region, C-type kinesins (kinesin 14A and 14B) with the motor domain close to the C-terminus and M-type kinesins (kinesin-13) with the motor domain in the middle (Figure 1-1, Table 1-1). MT plus-end-directed and minus-end-directed transport is driven by N-type kinesins and C-type kinesins, respectively. A general mechanism of kinesin-mediated cellular transport includes: the motor domain hydrolyses ATP to generate force, and the stalk and tail domains function in dimerization and/or cargo-binding [reviewed in (Hirokawa et al., 2009)]. Here I focus on the unique M-type kinesins (kinesin 13), a kinesin family that use the energy of ATP to

depolymerise MTs rather than to move along MTs (Desai et al., 1999; Hunter et al., 2003; Maney et al., 2001; Wordeman and Mitchison, 1995).

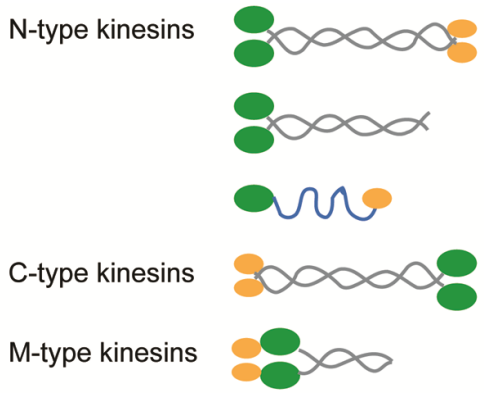

Figure 1-1 Domain structure of some representative N-, C-, and M-type kinesins

Many kinesins comprise a motor domain (green) and a coiled-coil domain for oligomerization (grey). Other domains are class-specific (orange and blue). Figure is drawn according to (Hirokawa and Takemura, 2004; Verhey and Hammond, 2009).

Table 1-1 Classification of kinesin superfamily proteins

Standardized name	Other names	direction of movement
Kinesin-1	N-1	to the plus-end of MTs
Kinesin-2	N-IV	
Kinesin-3	N-III	
Kinesin-4	N-V	
Kinesin-5	N-II	
Kinesin-6	N-VI	
Kinesin-7	N-VII	
Kinesin-8	N-IIX	
Kinesin-9		
Kinesin-10		
Kinesin-11		
Kinesin-12		
Kinesin-13	M	
Kinesin-14	C	to the minus-end of MTs
Orphan kinesins		

Standardized names of kinesins are listed (the left column). Kinesins were also classified by other criteria, such as the location of the motor domain within the primary sequence of the protein (the right column) (Vale and Fletterick, 1997). Table adapted from (Lawrence et al., 2004).

1.3 Kinesin-13 family proteins

1.3.1 General introduction to kinesin-13 family proteins

As previously mentioned, the M-type kinesins (also called Kin-I kinesins, for kinesin internal) refer to the kinesin-13 family of proteins that catalyze MT-depolymerisation from both MT ends *in vitro* (Desai et al., 1999). Most organisms have multiple Kinesin-13 variants (Table 1-2)

[reviewed in (Ems-McClung and Walczak, 2010)]. This is, perhaps, expected, considering the many diverse functions associated with MT depolymerisation, such as its requirement for proper axonal growth and regeneration, mitotic spindle assembly, and accurate chromosome segregation. Next, I focus on evidence that implicates kinesin-13s in mitotic functions and on pathways that regulate kinesin-13s to control the MT cytoskeleton.

Table 1-2 Kinesin-13 proteins from representative model organisms

species	Protein
Caenorhabditis elegans	KLP-7 (MCAK)
Cricetulus griseus	Kif2A, Kif2B, Kif2C (MCAK)
Drosophila melanogaster	Klp10A (Kif2A), Klp59C (MCAK), Klp59D (Kif2B)
Homo sapiens	Kif2 (Kif2A), Klp17q22 (Kif2B), Kif2C (MCAK)
Mus musculus	Kif2A, Kif2B, Kif2C
Xenopus laevis	XKCM1 (MCAK), XKIF2 (Kif2A)

Name in the brackets is what a particular protein is orthologous to. Putative orthologues are identified by pairwise comparisons of full-length and motor domain sequences (The Kinesin Home Page: http://labs.cellbio.duke.edu). Abbreviations: KLP for kinesin like protein, MCAK for mitotic centromere-associated kinesin, KIF for kinesin superfamily proteins, XKCM1 for *Xenopus* kinesin central motor 1.

1.3.2 Structure and MT-depolymerisation mechanism of kinesin-13 proteins

Structural analysis revealed that, similar to motor domains of conventional kinesins, the centrally-located catalytic core domain of kinesin-13s contain the conserved MT- and ATP- binding sites (Figure 1-2). Targeting kinesin-13s to MT ends induces a conformational change of protofilaments, which disrupts the MT end structure (Desai et al., 1999; Moores et al., 2006; Moores et al., 2002). ATP hydrolysis recycles kinesin-13s by releasing them from tubulin dimers generated by MT-depolymerisation (Desai et al., 1999). A study on the crystal structure of mouse Kif2C (the mouse homologue of MCAK) demonstrated that the MT-binding surface of the motor domain adopts a convex surface that facilitates interaction with the concave surface of a curved protofilament (Ogawa et al., 2004). This suggests that Kif2C preferentially binds to the curved MT ends rather than actively bending MTs. Ogawa et al. proposed that Kif2C binds to and stabilizes the curved conformation of MT ends. This can result in the initial cycles of MT depolymerisation (Ogawa et al., 2004).

MT-depolymerising activity was shown to be intrinsic to the motor domain of the MCAK family of kinesin-13s (Moores et al., 2002). However, motor-only MCAKs depolymerise MTs less efficiently than full length MCAKs *in vitro*, and they barely work at all *in vivo*, indicating contributions of other domains to MT-depolymerisation (Andrews et al., 2004; Hertzer et

al., 2006; Maney et al., 2001; Ogawa et al., 2004). N-terminal to the motor domain is a positively charged “neck” region, which is required for MT depolymerization activity *in vivo* (Maney et al., 2001; Ogawa et al., 2004; Ovechkina et al., 2002). One role proposed for the neck region is that it interacts with the negatively charged MT surface via electrostatic interactions, which facilitate one-dimensional diffusion along the MT lattices (Helenius et al., 2006; Hunter et al., 2003; Ogawa et al., 2004; Ovechkina et al., 2002). Further, the motor-proximal neck region was found to form a rigid α-helix structure that points towards the MT surface and inhibits MCAK binding to a straight protofilament in the interior MT lattice (Ogawa et al., 2004). Structures formed by the motor domain and neck region seem to facilitate interactions of MCAK with the curved protofilament, similar to the mechanism hypothesized for Kif2C. This provides one explanation for the end-recognition mechanism by which kinesin-13s are targeted to MT ends to depolymerise MTs [reviewed in (Moores and Milligan, 2006)].

Except for the highly conserved motor domain and neck region, kinesin-13s also contain more divergent N- and C-terminal domains (*i.e.*, 75% identity between the catalytic domain of *Xenopus* MCAK and KIF2A, 20% identify between the N- or C- terminal domains) (Figure 1-2). The N-terminal domain of the MCAK family of kinesin-13s is required for proper subcellular localisation, while the C-terminal domain is required for dimerization (Ems-McClung et al., 2007; Hertzer et al., 2006; Kline-Smith

et al., 2004; Maney et al., 1998; Moore and Wordeman, 2004; Walczak et al., 2002; Wordeman et al., 1999). Monomeric truncated neck+motor domain MCAK targets to MT ends with lower efficiency compared to dimeric full-length MCAK, indicating potential roles of C-terminal regions in promoting end-recognition (Hertzer et al., 2006).

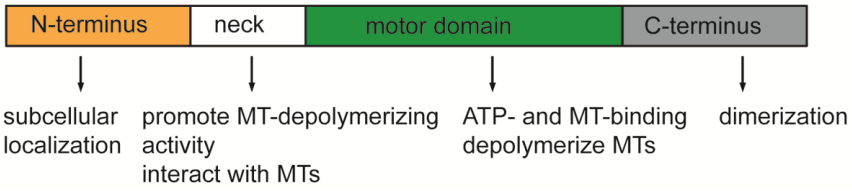

Figure 1-2 A general schematic structure of kinesin-13 proteins

The structure of MCAK (mitotic centromere-associated kinesin), the best-characterized family of kinesin-13s, is shown. The function of each domain is indicated. This figure is adapted from Ems-McClung and Walczak 2010.

1.3.3 Functions of kinesin-13s during mitosis

After mammalian kinesin-13 proteins (Kif2A and MCAK) were first identified (Noda et al., 1995; Wordeman and Mitchison, 1995), extensive studies revealed the diverse functions of kinesin-13 MT-depolymerases, such as spindle assembly during cell division, correction of improper MT-kinetochore attachments, participation in axonal growth and regeneration, and regulation of ciliary and centriole length [reviewed in (Walczak et al., 2013)]. MCAK and vertebrate homologues represent the best characterized kinesin-13 proteins. Studies on these proteins have clearly established that MT-depolymerization is critical for proper spindle

assembly and function, but many questions remain regarding how depolymerization activity is regulated spatially and temporally.

1.3.3.1 Spindle assembly during cell division

Assembly of a MT-based bipolar spindle is essential for accurate chromosome segregation during cell divisions. Previous studies demonstrated that the morphology of mitotic spindles is sensitive to MCAK levels, indicating a role of MCAK in spindle assembly. When MCAK is removed from *Xenopus* egg extracts, large asters (a “star”-shaped structure formed by MTs emanating in all directions from the centrosomes) with long MTs form instead of bipolar spindles (Walczak et al., 1996). Similarly, inhibition of MCAK in cultured mammalian cells results in bipolar spindles with longer than normal spindles and astral MTs, or monoastral spindles, which have two centrosomes in the centre of the cell, surrounded by a halo of chromosomes (Holmfeldt et al., 2004; Kline-Smith and Walczak, 2002; Stout et al., 2006). On the contrary, over-expression of MCAK results in an increase in monopolar spindles, which have two centrosomes at one side of the cell, with all chromosomes attached to microtubules on the other side. In addition excess MCAK causes monoastral spindles and also small prometaphase-like spindles (Kline-Smith and Walczak, 2002). Monoasters with short MTs are also observed when excessive MCAK is added to *Xenopus* extracts during meiotic spindle assembly (Ohi et al., 2007). Overall, these findings suggest that abnormal MCAK levels result in a failure in assembling spindles with

proper morphology and functions. Furthermore, when bipolar spindles are observed, there seems to be a correlation between relative MCAK activity and spindle size.

The spindle assembly defects associated with disruption of MCAK may result from altered MT dynamics. It has been established that one important role of MCAK is to induce MT catastrophe (the switch from growth to shrinkage) and make MTs more dynamic (Gardner et al., 2011; Kline-Smith and Walczak, 2002; Newton et al., 2004; Tournebize et al., 2000; Walczak et al., 1996). Work by Ganem and Compton demonstrated that inhibition of another kinesin-13 protein, KIF2A, also results in formation of monopolar spindles in cultured human cells (Ganem and Compton, 2004). Addition of nocodazole (a drug that induces MT depolymerisation) or depletion of MCAK restored spindle bipolarity in cells lacking KIF2A. This finding suggests that spindle bipolarity requires balanced activities of MCAK at kinetochores and KIF2A at spindle poles in human cells (Ganem and Compton, 2004).

1.3.3.2 Kinetochore-MT attachments and chromosome segregation

Chromosome segregation errors can cause diseases and cell death. To ensure faithful chromosome segregation during mitosis, sister chromatids are kept together by a protein complex (cohesin) until they are properly attached to MTs emanating from the opposite poles of the spindle. In normal cases sister kinetochores are anchored to MTs from opposite spindle poles (amphitelic). However, abnormal attachments

spontaneously arise, resulting in either two kinetochores being attached to one spindle pole (syntelic), or one kinetochore being attached to both poles (merotelic) or one kinetochore is attached to one spindle pole while the other kinetochore is unattached (monotelic) [reviewed in (Gorbsky, 2004; Musacchio and Salmon, 2007; Nicklas, 1997)]. A “correction mechanism” must be employed by cells to resolve kinetochore-MT attachment errors (Figure 1-3).

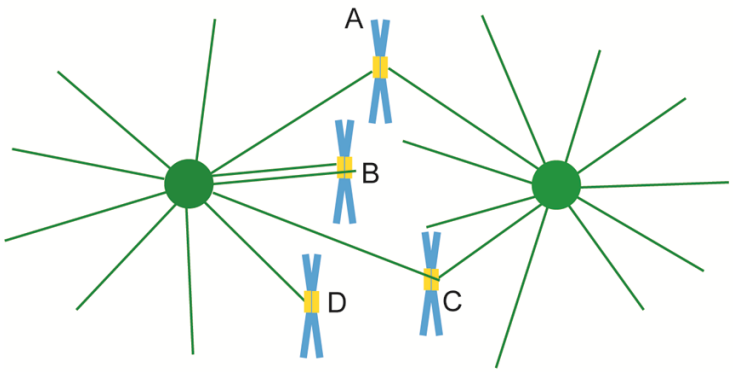

Figure 1-3 MT-kinetochore attachments during chromosome alignment

Proper MT-kinetochore attachment allows sister chromatids to be attached by MTs from different spindle poles (amphitelic attachment, A). Improper MT-kinetochore attachments (syntelic, merotelic and monotelic attachments, B, C and D, respectively) occur during chromosome congression. To correct syntelic and merotelic attachments, MTs are released from the kinetochore to allow new attachments to form. Monotelic attachment is very common in early mitosis before bi-orientation. Correction of monotelic attachment does not require MT depolymerisation. This figure is adapted from Gorbsky 2004. MTs and centrosomes are in green. Chromosomes are in blue. Kinetochores are in yellow.

The MT-depolymerase MCAK accumulates at the kinetochores and centromeres during mitosis, indicating a role for MCAK in correcting

improper kinetochore-MT attachments. Indeed, inhibiting MCAK activity at the centromeres results in chromosome misalignment and segregation errors in *Xenopus* and cultured mammalian cells (Maney et al., 1998; Walczak et al., 2002). Further studies by Kline-Smith et al. demonstrated that disruption of centromeric MCAK function leads to multiple kinetochore-MT attachment errors, which are likely responsible for chromosome segregation defects observed in anaphase. Interestingly, chromosome movement rates were not affected. These findings suggest that the primary role of MCAK at the centromere is to prevent and/or correct improper kinetochore-MT attachments, rather than to move chromosomes (Kline-Smith et al., 2004). In *Xenopus* tissue culture cells defects in chromosome congression were also observed with inhibition of Aurora B kinase, which localizes to the inner centromere during prometaphase and metaphase (Kallio et al., 2002). Furthermore, MCAK localization and activity at the centromere/kinetochore is negatively regulated by Aurora B kinase (Andrews et al., 2004; Lan et al., 2004; Ohi et al., 2004). This established a pathway for MT regulation at the kinetochore: the inner centromere region is enriched with Aurora B kinase while the outer kinetochore is phosphatase-rich. When merotelic attachment occurs, MCAK is stretched out of the Aurora B kinase-rich region. Syntelic attachments results in a loss of tension in the centromeric region. This makes the outer, phosphatase-rich kinetochore move inward.

In both cases MCAK inhibition by Aurora B kinase is relieved to release erroneous MT-kinetochore attachments (Gorbsky, 2004).

The above studies from vertebrate systems suggest that MCAK does not play a role in chromosome movement during anaphase. However, this may not be the case in *Drosophila melanogaster*. All identified *Drosophila* kinesin-13 proteins are important for chromosome-to-pole (anaphase A) movement (Rath et al., 2009; Rogers et al., 2004). Specifically, in early *Drosophila* embryos KLP10A (KIF2A) localize to spindle poles and induces MT-depolymerisation at minus ends to drag chromosomes towards the poles (poleward flux model), while KLP59C (MCAK) localizes to centromeres and depolymerises MTs at plus ends so that kinetochores “chew” their way to the poles (pacman model, Figure 1-4) (Rogers et al., 2004). KLP59D (KIF2B), a kinesin-13 protein that targets to kinetochores and centrosomes, has been shown to play a role in both pacman- and flux-based chromosome movements in *Drosophila* S2 cells. At the MT plus ends which are attached to kinetochores KLP59D directly depolymerises MTs. At MT minus ends KLP59D acts indirectly by targeting KLP10A to spindle poles (Rath et al., 2009).

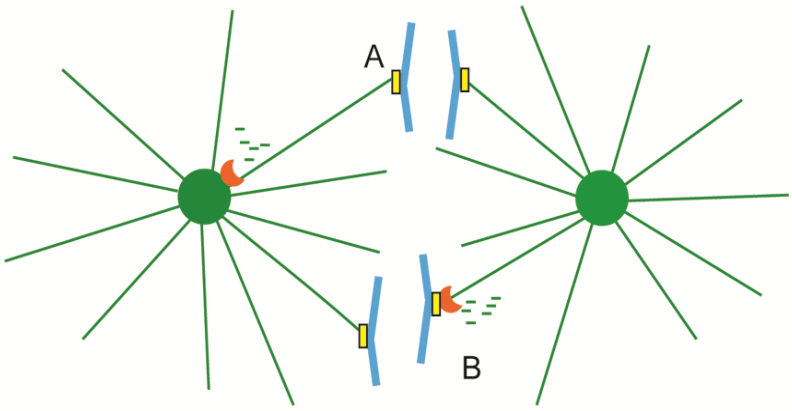

Figure 1-4 Pacman and flux models for chromosome movement during anaphase

Two models show how chromatids are moved during anaphase. These two models are not mutually exclusive. For example, both contribute to chromosome movement during anaphase A in early *Drosophila* embryos. In the poleward MT flux model (A), MTs depolymerise at the minus end and chromatids are reeled to the pole. In the pacman model (B), MTs are depolymerised at the plus end/kinetochore and chromatids move as MTs shorten (figure adapted from Moore and Wordeman, 2004). MTs are in green. Chromatids are in blue. Kinetochores are in yellow. MT-depolymerases are in orange.

Except for regulating chromosome alignment and chromosome-to-pole mobility, kinesin-13s may also be important for spindle elongation (anaphase B) [reviewed in (Walczak et al., 2013)]. In *Drosophila*, spindle elongation is driven by the sliding of anti-parallel interpolar MTs by a kinesin-5 protein. Before the onset of anaphase B, MT depolymerisation at the spindle pole, presumably by KLP10A, counters the sliding of overlapping MTs by inducing poleward flux to maintain a constant spindle-length (Brust-Mascher et al., 2004). Consistent with this idea, KLP10A inhibition results in long bipolar spindles and a reduction of flux rate

(Rogers et al., 2004). In *Xenopus* extracts a negative correlation between MCAK concentration and the length of meiotic spindles was shown (Ohi et al., 2007). More work is required to elucidate the mechanism by which individual kinesin-13s modulate spindle elongation in specific systems.

As mentioned above, kinesin-13 proteins carry out diverse cellular functions during mitosis. Most cells have multiple kinesin-13s (KIF2A, KIF2B and MCAK) and each kind of kinesin-13 exists in various subcellular places. For example, vertebrate MCAK has been reported to locate to inner centromeres, kinetochores, spindle poles, MT tips, and the cytoplasm (Andrews et al., 2004; Kline-Smith et al., 2004; Moore et al., 2005; Ohi et al., 2004; Walczak et al., 1996; Wordeman and Mitchison, 1995). These observations suggest that the mechanism of regulating kinesin-13 subcellular targeting and activity is complex.

1.3.4 Regulation of kinesin-13s

1.3.4.1 Regulation of MCAK localization and activity by Aurora kinase phosphorylation

Work in the past ten years demonstrated that the precise regulation of human and *Xenopus* MCAK localization and function occurs in part through phosphorylation by Aurora A and Aurora B serine/threonine kinases. Aurora A kinase localizes to the centrosomes and is involved in centrosome maturation and spindle assembly (Andrews et al., 2003; Chan and Botstein, 1993; Glover et al., 1995; Gopalan et al., 1997). In contrast,

Aurora B kinase localizes to the centromere to regulate chromosome segregation and cytokinesis (Lampson and Cheeseman, 2011). A subcellular division of labour for the Aurora kinases would allow independent regulation of substrates that localize to both chromatin (including chromosome arms, centromeres and kinetochores) and centrosomes.

It has been well established that Aurora B kinase inhibits MCAK MT-depolymerising activity via phosphorylation at multiple sites in the N-terminal domain and neck region (Andrews et al., 2004; Lan et al., 2004; Ohi et al., 2004). One of the key phosphorylation sites is S196 for *Xenopus* MCAK. Phosphorylation by Aurora B kinase at S196 strongly inhibits MT-depolymerising activity of centromere-located MCAK (Lan et al., 2004; Ohi et al., 2004). S196 resides in the positively charged neck region, and phosphorylation at this site may introduce a negative charge to the neck region and thus reduce MT-depolymerising efficiency (Maney et al., 2001; Ogawa et al., 2004; Ovechkina et al., 2002). S196 is a conserved Aurora B site among most kinesin-13s, indicating that a similar mechanism may be used to regulate activity of other kinesin-13 proteins [reviewed in (Ems-McClung and Walczak, 2010)].

Aurora B kinase phosphorylates MCAK not only to inhibit its MT-depolymerising activity but also to regulate MCAK localization at the chromosomes/kinetochores. For example, phospho-mimic MCAK (serine to glutamic acid substitution for multiple sites in the N-terminus and neck

region) preferentially localizes to inner centromeres while non-phosphorylatable MCAK (serine to alanine for the same sites) is concentrated at kinetochores in *Xenopus* and mammalian cell cultures (Andrews et al., 2004; Ohi et al., 2004). Furthermore, in the *Xenopus* system, MCAK binding to centromeres is increased by Aurora B mediated phosphorylation at S110, and inhibited by phosphorylation at T95. Similarly, MCAK association with chromosome arms is promoted by Aurora B-dependent phosphorylation at T95 and inhibited by phosphorylation at S196 (Figure 1-5) (Zhang et al., 2007).

More recent results by Zhang et al. revealed that MCAK localization and activity at spindle poles is regulated by phosphorylation by Aurora A kinase (Zhang et al., 2008). In *Xenopus* egg extracts, spindle-like structures can form in the absence of DNA and centrosomes, by addition of GTP-bound Ran (Carazo-Salas et al., 1999; Kalab et al., 1999; Ohba et al., 1999; Wilde and Zheng, 1999; Zhang et al., 1999). At Ran-induced asters, inhibition of MCAK MT-depolymerising activity is carried out by Aurora A phosphorylation at S196. MCAK localization at spindle poles is regulated by Aurora A phosphorylation at another site, S719. Phosphorylation of S719 is found to promote formation of bipolar spindles (Figure 1-5) (Zhang et al., 2008).

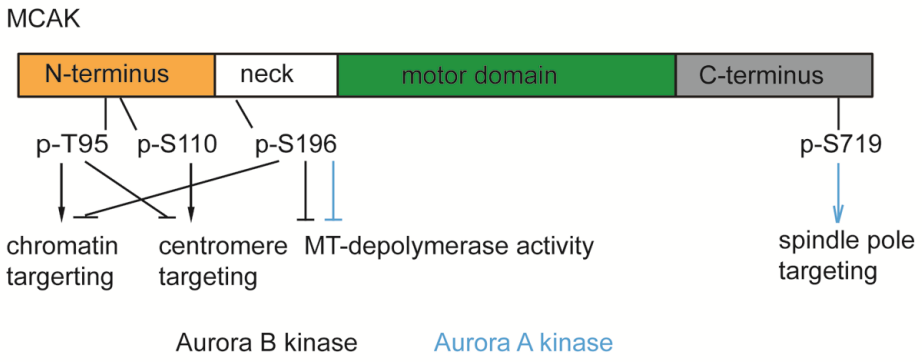

Figure 1-5 Aurora kinases phosphorylate MCAK to regulate its localization and activity

A schematic structure of MCAK is shown. Amino acid numbers are based on the sequence of *Xenopus* MCAK. Black arrows and perpendicular ends: regulation by Aurora B kinase; Cyan arrows and perpendicular ends: regulation by Aurora A kinase. Arrows represent positive regulation; perpendicular ends represent inhibitory regulation (figure adapted from Zhang et al., 2007).

Phosphorylation by Aurora kinases illustrates one mechanism to regulate MCAK localization and activity with spatial and temporal precision. Recent studies have identified MCAK as a substrate of other mitotic kinases, including cyclin-dependent kinase 1 (Cdk1), Polo-like kinase 1 (PLK1), and p21-activated kinase 1 (PAK1) (Pakala et al., 2012; Sanhaji et al., 2010; Zhang et al., 2011). Understanding the phosphorylation of MCAK by these kinases has provided more insight into the complex MCAK regulatory mechanisms during mitosis.

1.3.4.2 Phosphorylation of MCAK by Cdk1, PLK1 and PAK1 kinases

As mentioned above, MCAK is abundant at centrosomes and in the cytoplasm during mitosis, yet only a few studies have been done to reveal

how MCAK is regulated in these subcellular pools. Recent work by Sanhaji et al. showed that MCAK localization and activity at the centrosomes is regulated by Cdk1 phosphorylation in human cells. Phosphorylation of the human MCAK motor domain by Cdk1 at T537 (equivalent to T541 in *Xenopus* MCAK) releases MCAK from the centrosomes. Further, the MT-depolymerising activity of MCAK is reduced by phosphorylation at the same site, presumably via disrupting MCAK interaction with curved depolymerising MT ends. In mitotic human cells, interfering with Cdk1 mediated phosphorylation of MCAK results in defects in spindle assembly and chromosome alignment (Sanhaji et al., 2010).

Phosphorylation by Aurora kinases and Cdk1 inhibits MCAK activity. However, the MT-depolymerising activity of MCAK is positively regulated via phosphorylation by PLK1 (Zhang et al., 2011). PLK1 localizes to centrosomes and kinetochores and plays multiple essential roles during cell division, such as mitotic entry, centrosomal MT nucleation, MT-kinetochore attachment, and cytokinesis [reviewed in (Takaki et al., 2008)]. Regulation of MCAK by PLK1 phosphorylation is important for faithful chromosome alignment and segregation. In cultured human cells PLK1 phosphorylates MCAK at multiple sites in the C-terminal domain to promote MCAK MT-depolymerising activity (Zhang et al., 2011).

Other than being regulated by Aurora kinases, Cdk1 and PLK1, MCAK is also found to be a substrate of PAK1. PAK1 is a serine/threonine

protein kinase that is activated by Rac1 (Ras-related C3 botulinum toxin substrate 1) and Cdc42 (cell division cycle 42) Rho-family GTPases. It has been shown to be a key regulator of actin and MT cytoskeleton dynamics and cell mobility [reviewed in (Bokoch, 2003)]. A recent study demonstrated that PAK1 phosphorylation at S111 of human MCAK (equivalent to S125 in *Xenopus* MCAK) is required for centrosomal targeting of MCAK in cultured mammalian cells (Pakala et al., 2012). Furthermore, PAK1 phosphorylation of MCAK at S192 (S196 in *Xenopus* MCAK) inhibits MT-depolymerising activity *in vitro* (Pakala et al., 2012). *In vivo* studies demonstrated that cells expressing MCAK-S192A exhibit increased MT-polymerization after nocodazole treatment, compared with the cells expressing MCAK-WT. This result indicates that PAK1 phosphorylation of MCAK at S192 reduced MT-depolymerization. Therefore, the observations cannot be explained by a simple model in which PAK1 inhibits MCAK via phosphorylation at S192 (in this case S192A should be more efficient in depolymerizing MTs). The *in vivo* effect of phosphorylation at S192 is complicated as this site is also phosphorylated by Aurora B kinases in *Xenopus* and mammals, and by Aurora A kinase in *Xenopus*.

The above studies show that accurate control of MCAK localization and MT-depolymerising activity can be achieved by complex phosphorylation events. Interactions with regulatory proteins, such as +TIPs, provides another way for spatiotemporal regulation of MCAK.

1.3.4.3 MCAK interaction with regulatory proteins

In vitro studies have shown that MCAK accumulates at MT ends (Desai et al., 1999). MCAK moves along the MT lattice by one-dimensional diffusion (Desai et al., 1999; Helenius et al., 2006). In cultured cells MCAK tracks with the polymerising MT plus ends (Moore et al., 2005). The MT plus ends are bound with +TIPs in physiological conditions, raising the question whether MCAK tip-tracking and MT-depolymerising activity are regulated by +TIPs. It has been reported that EB1 can antagonize MCAK MT-depolymerizing activity in cells expressing low levels of MCAK (Moore et al., 2005). However, EB1 also associates with MCAK, and is required for MCAK localization to MT-tips in cultured mammalian cells (Lee et al., 2008). Therefore, the relationship between MCAK and EB1 seems complex. Further studies by Honnappa et al. demonstrated that MCAK binds to the C-terminal tails of EB proteins through an N- terminally located Serine-x-Isoleucine-Proline motif (SxIP; x for any amino acid) which are also found in several other +TIPs (Honnappa et al., 2009). Recent studies showed that EB-MCAK interactions facilitate the targeting of MCAK to the MT plus ends and makes it more effective in depolymerizing MTs (Montenegro Gouveia et al., 2010). In summary, the above findings suggest that EBs increase MCAK activity by concentrating them at MT tips; therefore, the balance between EBs and MCAK could be an important mechanism to regulate MT dynamics at the plus ends [reviewed in (Tanenbaum et al., 2011)].

Previous studies from vertebrate systems showed that MCAK localization and activity is regulated via spatial and temporal phosphorylation by several mitotic kinases, as well as interactions with other regulatory proteins. However, the *in vivo* regulatory mechanism is highly complex and is still not fully understood. For example, MCAK localizes to diverse subcellular regions, making it difficult to link the spindle assembly defects to the function of specific pools of MCAK. Also, because the same phosphorylation site can be utilized by multiple kinases (e.g. both Aurora A and Aurora B kinases phosphorylate *Xenopus* MCAK at S196; the human equivalent of this site, S192, is phosphorylated by PAK1 in cultured cells) it is hard to know contributions of individual kinases to MCAK regulation. Further, results obtained from knockdown/add-back experiments in *Xenopus* egg extracts or cultured mammalian cells should be carefully interpreted, as protein concentrations used in these experiments may not represent the physiological conditions. Finally, vertebrates have more than one kinesin-13s (KIF2A, KIF2B and MCAK), so the possibility that they have redundant functions in modulating MT dynamics cannot be ignored.

I use *Caenorhabditis elegans* (*C. elegans*) as the model organism to study the regulation and function of MCAK. *C. elegans* provides a relatively simple system as it has only one kinesin-13 protein (KLP-7). Cellular events in early divisions are relatively well characterized and are highly stereotypical in *C. elegans*, making it easier to interpret phenotypes.

In addition, in *C. elegans* embryos spindle assembly checkpoint does not completely block cell cycle progression. This allows us to determine the result of spindle MT damage on later processes such as chromosome segregation, cytokinesis (Hyman and White, 1987; Kitagawa and Rose, 1999). Further, integrated transgenes can be generated to reduce the chance of over- or mis- expression of transgenes, which are common issues in cell cultures and *Xenopus* egg extract (Frokjaer-Jensen et al., 2008; Praitis et al., 2001).

1.4 KLP-7, a kinesin-13 protein in *C. elegans*

1.4.1 *C. elegans* as a model organism

In 1974, Sydney Brenner reported the use of the nematode, *C. elegans*, as a model for genetic research (Brenner, 1974). Since then, the *C. elegans* system has been successfully utilized to address fundamental questions in all aspects of biology. These animals are small (the adults are about 1.3 mm in length and 80 microns in diameter) and easy to maintain in the laboratory using petri dishes seeded with bacteria as the food source. Worm eggs develop into fertile adults within 3 days at room temperature. *C. elegans* adults contain approximately 1000 somatic cells that form various tissue types such as hypodermis, muscles, nerves, intestine and gonad. The sexual dimorphism property of *C. elegans* is especially useful for genetic study: the self-fertilizing hermaphrodites can maintain homozygosity of alleles and males can be used for genetic crosses. Also, the *C. elegans* genome has been completely sequenced

(The *C. elegans* Sequencing Consortium, 1998). Thus, the RNA-mediated interference (RNAi) technique can be used to determine the function of particular genes by reducing their expression (Fire et al., 1998; Timmons et al., 2001).

C. elegans is not only an organism amenable to genetic analysis but also has attractive features to cell biologists. First of all, the animals are transparent throughout their life cycle, making them well suited for observing cellular events such as mitosis in live animals. Transparency also allows researchers to track fluorescent fusion-protein localization in real-time. Also, cell division events during embryogenesis and post-embryonic development are highly stereotypical in *C. elegans*. This property is important for interpreting even subtle phenotypes of mutant animals at a single-cell level.

In this study, I studied the regulation and function of the *C. elegans* MCAK protein (KLP-7, also CeMCAK). Because I focused on KLP-7's role in spindle assembly during female meiosis and the first mitotic cell division, a short description of these cellular processes is warranted.

1.4.2 Meiosis, mitosis, and spindle assembly in *C. elegans* embryos

Sexual reproduction of eukaryotic organisms requires two distinct types of cell divisions, meiosis and mitosis. Meiosis is characterized by two successive cell divisions without intervening DNA replication, ending with the creation of haploid gametes. Meiosis I is the process in which

homologous chromosomes pair, recombine, and then segregate to daughter cells. Meiosis II involves the separation of sister chromatids to generate haploid gametes. Female meiosis usually arrests at a specific meiotic stage, which differs between species, until fertilization or ovulation. The *C. elegans* oocyte arrests at prophase I and restores meiotic divisions in response to a signal from the sperm (Albertson, 1984; Miller et al., 2001; Miller et al., 2003). After fertilization, unstructured MTs can be distinguished around the female chromosomes. The MT arrays are first assembled into an elongated, pointed spindle, which is approximately 13 μm in length and parallel to the cortex. This spindle then translocates to the cortex and starts to shorten and rotate. By the end of metaphase I, the meiotic spindle is 3-4 μm in length and oriented perpendicularly to the cortex. At anaphase I, MT bundles form between the separating homologous chromosomes (Figure 1-6). After extrusion of the first polar body, the embryo goes through the second meiotic division in a similar manner to generate a second polar body (Albertson and Thomson, 1993; McNally et al., 2006).

The sperm provides not only a haploid genome but also a pair of centrioles to the embryo. After meiosis II is completed, centrioles accumulate pericentriolar material (PCM; an unstructured protein network that is critical for centrosome structure and function). In *C. elegans,* the PCM protein SPD-5, and other centrosomal protein levels increase as the cell cycle progresses (Pelletier et al., 2004). MTs start to emanate from

centrosomes in early prophase and the levels increase with the cell cycle. Once MTs grow far enough to contact the maternal nuclear envelope, the two nuclei migrate towards each other by a process that is driven by nuclear envelope bound MT-motor protein dynein (Gonczy et al., 1999; Malone et al., 2003). The pro-nuclear/centrosome complex then moves to the center of the embryo and rotates with their centrosomes orientated along the anterior-posterior axis (A-P axis). After nuclear envelope breakdown (NEB), chromosomes are aligned on the metaphase plate by the mitotic spindle apparatus (Figure 1-6). In *C. elegans* anaphase, spindle poles are pulled apart by cortical forces acting on the astral MTs, while kinetochore MTs maintain the same pole-chromosome length (Grill et al., 2003; Muller-Reichert et al., 2010). Thus, in the *C. elegans* embryo, chromosome segregation seems to utilize primarily, or exclusively, anaphase B (Labbe et al., 2004).

Meiotic and mitotic spindles show dramatic differences in their localization, size, and morphology. Like other animals, the *C. elegans* female meiotic spindle is relatively small, and it is located near the anterior cortex of the embryo. Restriction of the spindle length and cortical localization are believed to be important for unequal meiotic divisions, by which non-viable polar bodies are discarded while most of the cytoplasm remains in the oocyte. In contrast to the meiotic spindle, the first mitotic spindle is large and exhibits prominent asters that fill the cell. The spindle

aligns along the anterior-posterior axis, slightly posterior of the centre of the embryo (Figure 1-6).

Meiotic and mitotic spindles also differ in the way they are assembled. In *C. elegans* and many other animals, formation of female meiotic spindles is independent of centrosomes (Schatten, 1994). These acentrosomal spindles are assembled by an 'inside-out' mechanism, in which MTs are nucleated from chromatin and further assembled into a bipolar meiotic spindle by motor proteins (Heald and Walczak, 1999). In *C. elegans* female meiosis chromosomes are separated by a kinetochore independent mechanism. During anaphase the MT-stabilizing protein CLASP (CLS-2) generates MTs in the midzone region to push chromosomes apart (Dumont et al., 2010). In contrast to the meiotic spindles, the mitotic spindles are organized by a pair of centrosomes, which function as a MTOC to nucleate MTs. MTs emanate from centrosomes in all directions, some of which contact kinetochores (kinetochore MTs), the remainder of which, grow out to make contact with the inner cell cortex. Kinetochore-MT interaction generates force that is important for chromosome separation during mitosis. Distinctions in spindle structure and assembly suggest that different mechanisms are employed in MT regulation in meiosis and mitosis.

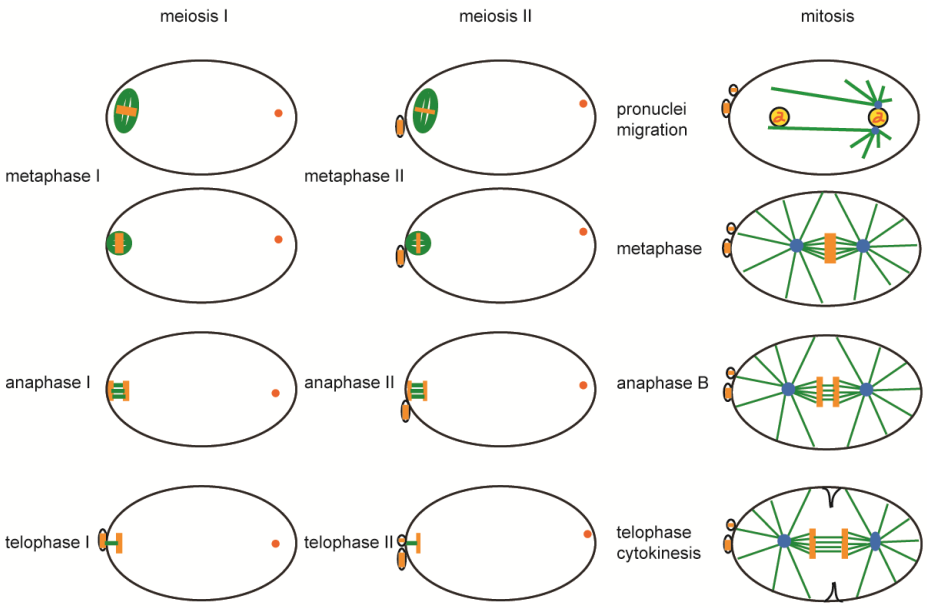

Figure 1-6 Meiosis and the first mitotic division in *C. elegans*

These schematics show the major events of meiosis (left and middle) and the first mitotic division (right). Schematics are generated based on live-imaging of *C. elegans* embryos expressing GFP: β-tubulin and GFP: histone fluorescent transgenes. MTs are in green; centrosomes are in blue; DNA is in orange (the orange dots in the meiotic embryos represents DNA from the sperm). Polar bodies are represented by small circles. Note that the distance between DNA and one spindle pole remains constant during anaphase, mitosis (anaphase B only).

1.4.3 The role for KLP-7 in *C. elegans*

In *C. elegans*, KLP-7 (CeMCAK) has been implicated in various MT-dependent processes, including meiosis and mitosis. *klp-7(RNAi)* embryos exhibit a dramatic “spindle-snap” phenotype in the first mitotic division, whereby chromatids segregate rapidly (depicted in Figure 3-6, Chapter 3). *klp-7(RNAi)* embryos appear to have fewer spindle midzone MTs in mitosis (Grill et al., 2001), and approximately 2-fold more astral

MTs (Figure 1-7A) (Schlaitz et al., 2007; Srayko et al., 2005), indicating important roles for KLP-7 in MT regulation during mitosis. KLP-7 is detected at the holocentric kinetochores and also at the centrosomes in mitotic embryos (Encalada et al., 2005; Oegema et al., 2001; Schlaitz et al., 2007), and KLP-7 localization to chromosomes requires the kinetochore components CENP-A and CENP-C (Oegema et al., 2001). Currently, it is unclear how KLP-7 functions at the chromosomes and the centrosomes to contribute to proper mitotic spindle assembly. In particular, the loss of midzone MTs associated with *klp-7(RNAi)* is not easily explained by loss of a MT depolymerizing enzyme. This issue is addressed in Chapter 4.

Work from Schlaitz et al. hypothesized that KLP-7 is regulated by the RSA (regulator of spindle assembly) complex at centrosomes. The *C. elegans* RSA complex is a PP2A phosphatase required for MT stabilization at the centrosome (Schlaitz et al., 2007). Embryos lacking RSA show a reduction of centrosomal MTs and a collapse of the mitotic spindles (centrosomes fall onto chromatin during spindle assembly, indicated by the shorter distance between centrosomes in Figure 1-7A). Since the RSA complex and KLP-7 have an opposite effect on centrosomal MTs, and they both localize to centrosomes, it could be that they participate in a common pathway, the function of which is to regulate MT dynamics and spindle stability. Indeed, *rsa-1(RNAi)* results in twice the level of KLP-7 protein at the centrosome compared to wild-type embryos

(Schlaitz et al., 2007). Furthermore, *klp-7(RNAi); rsa-1(RNAi)* embryos exhibit greater than wild-type levels of centrosomal MTs, suggesting that KLP-7 is likely to be responsible for the MT loss when RSA is depleted (Figure 1-7A) (Schlaitz et al., 2007). The above analyses were performed by using RNAi instead of null alleles. Therefore, epistasis cannot be confidently established. Overall, previous work indicates that RSA could regulate KLP-7 by inhibiting its recruitment to the centrosomes, regulating its catalytic activity, or both. But how this regulation is accomplished remains to be discovered.

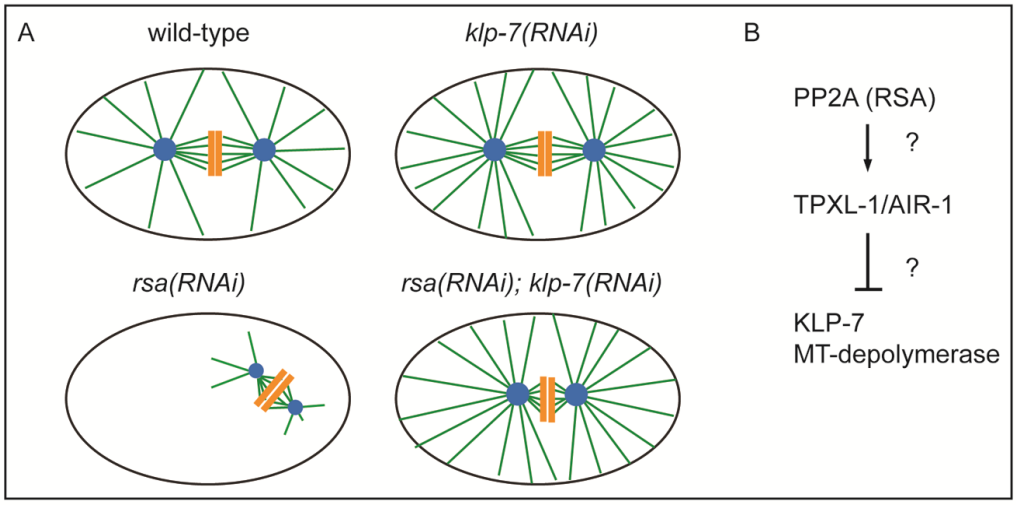

Figure 1-7 KLP-7 is regulated by the PP2A (RSA) phosphatase complex at centrosomes during *C. elegans* mitosis

(A) Phenotypes of *klp-7 (RNAi)* and *rsa (RNAi)* are shown. KLP-7 normally limits the number of astral MTs. *klp-7(RNAi)* results in an increase in astral MTs, a decrease in spindle midzone MTs, and also a spindle-snap phenotype. RSA is required for astral MT growth and spindle MT stability. *rsa (RNAi)* results in fewer MTs and a spindle-collapse phenotype. *klp-7(RNAi)*; *rsa (RNAi)* result in more astral MTs which is similar to *klp-7(RNAi)* and also a spindle-collapse phenotype. Schematics are generated based on live-imaging of *C. elegans* embryos expressing a GFP: β-tubulin transgene (Schlaitz et al., 2007). MTs are in green; centrosomes are in blue; chromosomes are in orange. (B) One potential mechanism by which KLP-7 is regulated by RSA at centrosomes.

Based on the established role for Aurora kinases in MCAK regulation, it is possible that KLP-7 is also regulated via this pathway. One intriguing link to Aurora kinase is suggested by the fact that the RSA complex interacts with and is required for the centrosomal recruitment of TPXL-1 (worm homologue for TPX2, Targeting Protein for *Xenopus* Klp2) (Figure 1-7B). TPX2, in turn, has been shown to target Aurora A kinase to

spindles in both human cells and *C. elegans* and to promote Aurora A kinase activity on histone H3 *in vitro* (Bayliss et al., 2003; Kufer et al., 2002; Ozlu et al., 2005). Moreover, AIR-1 and TPXL-1 colocalize along astral MTs, with enrichment near the centrosome (Ozlu et al., 2005). Further evidence for an involvement of TPXL-1 and RSA in the same pathway is that both *tpxl-1(RNAi)* and *rsa-1(RNAi)* result in a spindle collapse phenotype (Schlaitz et al., 2007). Together these findings suggest that RSA could negatively regulate KLP-7 localization or activity by promoting the localization or activity of TPXL-1/AIR-1 (Figure 1-7B).

Although Aurora kinases clearly influence kinesin-13 activity and localization in other systems, this has not been established for KLP-7. The *C. elegans* genome encodes both Aurora A kinase (AIR-1) and Aurora B kinase (AIR-2) (Schumacher et al., 1998a; Schumacher et al., 1998b). A simple epistasis experiment cannot be used to place KLP-7 downstream of AIR-1, because depletion of AIR-1 in *C. elegans* results in defects in centrosome maturation, including the failure to recruit of other factors important for MT formation/stability, such as ZYG-9/XMAP215 and γ-tubulin (Hannak et al., 2001). When AIR-1 is depleted from *C. elegans* embryos, centrosomal MT levels are greatly reduced (Hannak et al., 2001; Schumacher et al., 1998a). This is the opposite of *klp-7(RNAi)* embryos, which exhibit many more MTs (Figure 1-7A) (Schlaitz et al., 2007; Srayko et al., 2005), suggesting that Aurora A kinase could negatively regulate KLP-7 at the centrosome.

Goal of this thesis:

In other species, MCAK MT-depolymerizing kinesins are essential for proper spindle assembly and correcting defective microtubule-kinetochore attachments to ensure faithful chromosome segregation. Although MCAK localization and activity is regulated via phosphorylation by Aurora kinases, the precise mechanism is complex and not fully understood. Furthermore, previous studies focused on the regulation of MCAK at chromatin/kinetochores. Not much work has been done to reveal roles of MCAK at the centrosome. The major goal of this study is to determine functions of MCAK (KLP-7) in regulating MT-based events, such as spindle assembly and chromosome segregation during meiosis and mitosis by using a relatively simple system, *C. elegans*. In addition, I pursued the hypothesis that Aurora kinase is required for the localization and/or activity of KLP-7 in the *C. elegans* embryos. My work implicates Aurora kinase in the regulation of KLP-7, possibly via TPXL-1, which I show potentiates the phosphorylation of KLP-7 by Aurora kinase *in vitro*. This work provides information on how MT outgrowth at the centrosome is regulated by a MT-depolymerizing kinesin.

2 Materials and methods

2.1 Nematode culture and strains

C. elegans were cultured under standard conditions (Brenner, 1974). Worms were maintained on NGM agar [NaCl 3 g, peptone 2.5 g, agar 17 g, dH_2O 975 mL, autoclave and cool to 55°C, then add:1M $CaCl_2$ 1mL, 1M $MgSO_4$ 1mL, 1M Potassium Phosphate pH 6.0 25 mL, cholesterol (5mg/mL in EtOH) 1mL] petri dishes seeded with bacteria strain OP50 as the food source. Strains used are included in table 2-1.

Table 2-1 List of strains

Strain name	**genotype**
Bristol strain N2	wild-type
CB185	*lon-1(e185) III*
CX571	*unc-119 (ky571) III*
DP38	*unc-119(ed3) III*
EU707	*air-2(or207ts) unc-13(e51) I*
HR1185	*tbb-2(sb26) lon-1(e185) unc-119(ed4) III*
MAS7	*klp-7(tm2143) III*
MAS10	*klp-7(tm2143) unc-119(ky571) III*
MAS37	*unc-119(ed3) III; abcIs3[pie-1::EBP-2::GFP;unc-119(+)]*
MAS51	*klp-7(tm2143) III; ltIs37[pAA64; pie-1::mCherry::HIS-58; unc-119(+)] IV*; *ddIs6[tbg-1::GFP; unc-119(+)]*
MAS91	*unc-119(ed3) III; ltIs37[pAA64; pie-1::mCherry::HIS-58; unc-119(+)] IV; ojIs1[pie-1::gfp::tbb-2; unc-119(+)]*
MAS107	*unc-119(ky571) III*; *evIs111 [Prgef-1::GFP; dpy-20(+)]*
MAS108	*klp-7(tm2143) unc-119(ky571) III*; *evIs111 [Prgef-1::GFP; dpy-20(+)]*
MAS110	*klp-7(tm2143) III*; *evIs111 [Prgef-1::GFP; dpy-20(+)]*
MAS112	*klp-7(tm2143) III*; *ltIs37[pAA64; pie-1::mCherry::HIS-58;*

	unc-119(+)] IV; ojIs1[pie-1::gfp::tbb-2; unc-119(+)]
MAS127	*klp-7(tm2143) unc-119(ky571) III; abcIs3[pie-1::EBP-2::GFP;unc-119(+)]*
MAS128	*klp-7(tm2143) unc-119(ky571) III; abcIs3[pie-1::EBP-2::GFP;unc-119(+)]; [pie-1::GFP::KLP-7(WT); unc-119(+)]*
MAS161	*unc-119(ed3) ruIs32[unc-119(+) pie-1::GFP::H2B] III; [pie-1::mCherry::tubulin; unc-119(+)];*
MAS178	*klp-7(tm2143) III; [pie-1::mCherry::tubulin; unc-119(+)]*
MAS179	*klp-7(tm2143) III; [pie-1::mCherry::tubulin; unc-119(+)]; [pie-1::GFP::KLP-7(8A); unc-119(+)]*
MAS180	*klp-7(tm2143) III; [pie-1::mCherry::tubulin; unc-119(+)]; [pie-1::GFP::KLP-7(S539A); unc-119(+)]*
TH32	*unc-119(ed3) ruIs32[pie-1::GFP::H2B; unc-119(+)] III; ddIs6[tbg-1::GFP; unc-119(+)]*

klp-7(tm2143) was obtained from Dr. S. Mitani, National Bioresource Project, Japan. *klp-7*(*tm2143)* deletion was confirmed by performing genomic PCR reaction by using tm2143-f,r primers (Table 2-2). This original strain was outcrossed five times to generate MAS7. DP38 and CX571 were generously provided by Dr. Dave Pilgrim at the University of Alberta. HR1185 was a gift from Dr. Paul Mains at the University of Calgary. CB185, EU707 and TH32 were obtained from the Caenorhabditis Genetics Center (CGC, funded by NIH Office of Research Infrastructure Programs P40 OD010440). The remaining strains were generated within the Srayko laboratory. *air-2(or207)* allele was confirmed by performing genomic PCR by using or207-f, r primers followed by sequencing (Table 2-2).

The MAS37, MAS91, MAS127, MAS128, MAS161, MAS179, MAS180 and TH32 strains were maintained at 25°C, while remaining strains were maintained at 15°C. Temperature-sensitive (ts) strains, including EU707, MAS7, MAS51, MAS112, and MAS178 were upshifted to 25°C at the L4 stage 24 hours before embryos were collected.

Table 2-2 List of primers

	Primer Name	**Sequence**
1	tm2143-ex-f	CTTGTCGTCGGGATGCATGT
2	tm2143-ex-b	TCACTGTCCTGGACTTCTCA
3	T119E-f	/5phos/CTTCTGCCAACAAACGACCAGAAGGAG CTTTCACGCAGCACG
4	T119E-r	/5phos/CGTGCTGCGTGAAAGCTCCTTCTGGTC GTTTGTTGGCAGAAG
5	T119A-f	/5phos/CTTCTGCCAACAAACGACCAGCTGGAG CTTTCACGCAGCACG
6	T119A-r	/5phos/CGTGCTGCGTGAAAGCTCCAGCTGGTC GTTTGTTGGCAGAAG
7	T182E-f	/5phos/GAAGCACACTGCAAGGCGCGAAGTTGT GGTAGCTCCAGCT
8	T182E-r	/5phos/AGCTGGAGCTACCACAACTTCGCGCCTT GCAGTGTGCTTC
9	T182A-f	/5phos/AAGCACACTGCAAGGCGCGCAGTTGTG GTAGCTCCAG
10	T182A-r	/5phos/CTGGAGCTACCACAACTGCGCGCCTTG CAGTGTGCTT
11	T159ET160E-f	/5phos/CTGCACCGAAGTCTACTCGTGAAGAAG CAGCCTTCAAGCCAGATC
12	T159ET160E-r	/5phos/GATCTGGCTTGAAGGCTGCTTCTTCACG AGTAGACTTCGGTGCAG
13	T159AT160A-f	/5phos/CTGCACCGAAGTCTACTCGTGCTGCTG

		CAGCCTTCAAGCCAGATC
14	T159AT160A-r	/5phos/GATCTGGCTTGAAGGCTGCAGCAGCAC GAGTAGACTTCGGTGCAG
15	S538ES539E-f	/5phos/TCCGTGGAATGGCTCGCAACGAAGAAC ATGTCCCGTTCAGACAG
16	S538ES539E-r	/5phos/CTGTCTGAACGGGACATGTTCTTCGTTG CGAGCCATTCCACGGA
17	S538AS539A-f	/5phos/CGTGGAATGGCTCGCAACGCTGCTCAT GTCCCGTTCAGACAG
18	S538AS539A-r	/5phos/CTGTCTGAACGGGACATGAGCAGCGTT GCGAGCCATTCCACG
19	T652ET653E-f	/5phos/CTGAAAAGATCATACGCGAAGAAGAAAT TGTCCTCTCCAACG
20	T652ET653E-r	/5phos/CGTTGGAGAGGACAATTTCTTCTTCGCG TATGATCTTTTCAG
21	T652AT653A-f	/5phos/TGAAAAGATCATACGCGAAGCTGCTATT GTCCTCTCCAACGAGCC
22	T652AT653A-r	/5phos/GGCTCGTTGGAGAGGACAATAGCAGCT TCGCGTATGATCTTTTCA
23	S539E-f	/5phos/TGGAATGGCTCGCAACAGCGAACATGT CCCGTTCAGACAG
24	S539E-r	/5phos/CTGTCTGAACGGGACATGTTCGCTGTTG CGAGCCATTCCA
25	S539A-f	/5phos/GGAATGGCTCGCAACAGCGCACATGTC CCGTTCAGAC
26	S539A-r	/5phos/GTCTGAACGGGACATGTGCGCTGTTGC GAGCCATTCC
27	S546E-f	/5phos/ACATGTCCCGTTCAGACAGGAGAAGCT CACGATGGTTCTC
28	S546E-r	/5phos/GAGAACCATCGTGAGCTTCTCCTGTCTG AACGGGACATGT
29	S546A-f	/5phos/ACATGTCCCGTTCAGACAGGCGAAGCT CACGATGGTTC

30	S546A-r	/5phos/GAACCATCGTGAGCTTCGCCTGTCTGAACGGGACATGT
31	S555E-f	/5phos/CACGATGGTTCTCCGAGACGAATTCATCGGTGAGAAGTCCAG
32	S555E-r	/5phos/CTGGACTTCTCACCGATGAATTCGTCTCGGAGAACCATCGTG
33	S555A-f	/5phos/CTCACGATGGTTCTCCGAGACGCTTTCATCGGTGAGAAGTCCAGG
34	S555A-r	/5phos/CCTGGACTTCTCACCGATGAAAGCGTCTCGGAGAACCATCGTGAG
35	S472E-f	/5phos/TTCGGCAAACGCGAACTCGGAGCGTTCTCACGCCATATTC
36	S472E-r	/5phos/GAATATGGCGTGAGAACGCTCCGAGTTCGCGTTTGCCGAA
37	S264E-f	/5phos/GTGTCAACGAGAATCGGATTGAAGTTTGCGTTCGGAAGCGCC
38	S264E-r	/5phos/GGCGCTTCCGAACGCAAACTTCAATCCGATTCTCGTTGACAC
39	M13-f	GTAAAACGACGGCCAGTG
40	M13-r	GGAAACAGCTATGACCATG
41	T182sq-f	GCAGCCTTCAAGCCAGATCTTG
42	T182sq-r	TGTCATGTTGGCGATTGG
43	S472sq-f	ATAAGATGCAGAAGGTGC
44	pAZ-f	CGAGCAAATGGGATCTATGAG
45	pAZ-r	TTATCACAATTCTCTCCGTGC
46	KLP-7-5-r	GACAGCAGTTGACGCTTGAAG
47	KLP-7-3-f	AAGAGTACGATGAGATGGTCG
48	attB1-KLP-7-N	GGGGACAAGTTTGTACAAAAAAGCAGGCTTGCTTGTCGTCGGGATGCATGT
49	attB1-KLP-7-CC	GGGGACAAGTTTGTACAAAAAAGCAGGCTTCAAGGTGTGGGGCAAGTTCTC
50	attB2-KLP-7-N	GGGGACCACTTTGTACAAGAAAGCTGGGTCTCACGGAGCTGGAGCTACCACAAC

51	attB2-KLP-7-CC	GGGGACCACTTTGTACAAGAAAGCTGGGTCTC AGACGTTTTCCACGGCGACACG
52	attB1-KLP-7-CC2-f	GGGGACAAGTTTGTACAAAAAAGCAGGCTTCG AGCGAGGACAAGACACGAG
53	attB2-KLP-7-CC2-r	GGGGACCACTTTGTACAAGAAAGCTGGGTCTC ACTCTTCATCCGATTTGTCTGC
54	attB2-KLP-7-CC3-r	GGGGACCACTTTGTACAAGAAAGCTGGGTCTC ACTGTCTGAACGGGACATGTGAG
55	attB1-KLP-7-CC4-f	GGGGACAAGTTTGTACAAAAAAGCAGGCTTCG TCCCGTTCAGACAGTCGAAG
56	attB2-KLP-7-CC4-r	GGGGACCACTTTGTACAAGAAAGCTGGGTCTC ATTTGACACGATCCGCGTAGCG
57	attB1-KLP-7-C5-f	GGGGACAAGTTTGTACAAAAAAGCAGGCTTCA AAGAAATGGGAACCGACGGA
58	pDONR201-f	TCGCGTTAACGCTAGCATGGATCTC
59	pDONR201-r	GTAACATCAGAGATTTTGAGACAC
60	pDEST15-f	ATATAGCATGGCCTTTGCAG
61	pDEST15-r	TTCCTTTCGGGCTTTGTTAG
62	TPXL-N-f	GGGGACAAGTTTGTACAAAAAAGCAGGCTTGA GCAAAAGTCAAACCATTCA
63	TPXL-N-r	GGGGACCACTTTGTACAAGAAAGCTGGGTCTC ACTTGGGAAGTTGCATTTTGACC
64	TPXL-XmaI-f	TTCCCGGGATGAGCAAAAGTCAAACCATTCA
65	TPXL-XmaI-r	TTCCCGGGTCACTTGGGAAGTTGCATTTTGACC
66	KLP-7-1-T7f	TAATACGACTCACTATAGGGAGAAGCCGTGGC GAC
67	KLP-7-1-T3r	AATTAACCCTCACTAAAGGTATACCAAGGAAAT G
68	KLP-7-T3-f1	AATTAACCCTCACTAAAGGCCCGCCACTGACTA ATGTTTT
69	KLP-7-T7-r1	TAATACGACTCACTATAGGGTCAACGCGTAGAT TCCCATC
70	AIR-2-T3f	AATTAACCCTCACTAAAGGATGGAGAATAAGCC

		ACCTG
71	AIR-2-T7r	TAATACGACTCACTATAGGGTCAGTGATTCCGAAGACTTGCT
72	AIR-1-T3f	AATTAACCCTCACTAAAGGATGAGCGGAAAGGAAAATAC
73	AIR-1-T7r	TAATACGACTCACTATAGGGTTATTGATTGGCTGTAGAATT
74	klp-7-r-T7f1	TAATACGACTCACTATAGGGTCGACTTGACAAAG
75	klp-7-r-T7f2	TAATACGACTCACTATAGGGCGATCACGGTTCC
76	klp-7-r-T3r	AATTAACCCTCACTAAAGGGTAGATTCCCATCGAC
77	pGEX 5' Seq	GGGCTGGCAAGCCACGTTTGGTG
78	pGEX 3' Seq	CCGGGAGCTGCATGTGTCAGAGG
79	or207-f	GAGCAAGAGATTCTCAGAGCC
80	or207-r	TGAATGGGGTTAGACGATTGG
81	unc-119-f	AATTGCATGCCAGCACCGGTC
82	unc-119-r	TTGAACTACTGTAGGGCAGCT
83	unc-119-seq	ACACCAAATGATGTGCTAG

2.2 Microparticle bombardment in *C. elegans*

The strains expressing GFP::KLP-7-phospho-mutant transgenes were constructed by the high-pressure particle bombardment method (Praitis et al., 2001). The *klp*-7 genomic sequence (K11D9.1b.2) was cloned into a pAZ-LAP(N) Amp vector, which contains a GFP tag, the *pie-1(Pharynx and Intestine in Excess)* promoter to drive germline expression of the transgene, and a functional copy of the *unc-119 (Uncoordinated)* gene. The DNA-bound gold particles were “shot” into *unc-119(ed3)* mutant worms, which are paralyzed and cannot form dauer to survive starvation.

Successful transformants contain the wild type *unc-119* gene and are rescued in movement and dauer formation. The rescued *unc-119* animals were further selected to obtain lines with stable expression of the transgene. To express GFP::KLP-7-phospho-mutant transgenes in worms without endogenous KLP-7, MAS10 [*unc-119(ky571) klp-7(tm2143)]* worms were used instead of *unc-119(ed3)* worms. When multiple stable lines were obtained for the same DNA construct, the line with the best expression (as judged by GFP microscopy) was selected for further analysis. The strains generated by the gene bombardment method are listed in Table 2-3. All strains were maintained at 25°C.

Table 2-3 List of KLP-7 phospho-mutant transgenic strains

genotype	**strain**	**Referred to in texts and figures as**
klp-7(tm2143) unc-119(ky571); [pie-1::GFP::KLP-7(WT); unc-119(+)]	MAS42	KLP-7 WT
	MAS34	NA
klp-7(tm2143) unc-119(ky571); [pie-1::GFP::KLP-7(T119E); unc-119(+)]	MAS152	T119E
klp-7(tm2143) unc-119(ky571); [pie-1::GFP::KLP-7(T119A); unc-119(+)]	MAS149	T119A
klp-7(tm2143) unc-119(ky571); [pie-1::GFP::KLP-7(T119ET159ET160ET182E); unc-119(+)]	MAS156	N4E
	MAS125	NA
klp-7(tm2143) unc-119(ky571); [pie-1::GFP::KLP-7(T119AT159AT160AT182A); unc-119(+)]	MAS145	N4A
klp-7(tm2143) unc-119(ky571); [pie-1::GFP::KLP-7(S539E); unc-119(+)]	MAS29	S539E
	MAS28	NA

klp-7(tm2143) unc-119(ky571); [pie-1::GFP::KLP-7(S539A); unc-119(+)]	MAS86	S539A
klp-7(tm2143) unc-119(ky571); [pie-1::GFP::KLP-7(S538ES539E); unc-119(+)]	MAS148	S538ES539E
	MAS147	NA
klp-7(tm2143) unc-119(ky571); [pie-1::GFP::KLP-7(S538AS539A); unc-119(+)]	MAS143	S538AS539A
klp-7(tm2143) unc-119(ky571); [pie-1::GFP::KLP-7(S546E); unc-119(+)]	MAS31	S546E
	MAS30	NA
klp-7(tm2143) unc-119(ky571); [pie-1::GFP::KLP-7(S546A); unc-119(+)]	MAS92	S546A
klp-7(tm2143) unc-119(ky571); [pie-1::GFP::KLP-7(T182ES539ES546E); unc-119(+)]	MAS52	T182ES539E S546E
	MAS33	NA
klp-7(tm2143) unc-119(ky571); [pie-1::GFP::KLP-7(S539ES546E); unc-119(+)]	MAS126	NA
klp-7(tm2143) unc-119(ky571); [pie-1::GFP::KLP-7(T182E); unc-119(+)]	MAS25	T182E
klp-7(tm2143) unc-119(ky571); [pie-1::GFP::KLP-7(T119AT159AT160AT182AS538AS539AT652AT653A); unc-119(+)]	MAS174	8A
klp-7(tm2143) unc-119(ky571); [pie-1::GFP::KLP-7(T119ET159ET160ET182ES538ES539ES546ES555ET652ET653E); unc-119(+)]	MAS168	10E
	MAS166	NA
unc-119(ed3); [pie-1::GFP::KLP-7(WT); unc-119(+)]	MAS15	NA
unc-119(ed3); [pie-1::GFP::KLP-7(S539E); unc-119(+)]	MAS16	NA
unc-119(ed3); [pie-1::GFP::KLP-7(S546E); unc-119(+)]	MAS17	NA
unc-119(ed3); [pie-1::GFP::KLP-7(S539ES546E); unc-119(+)]	MAS19	NA

unc-119(ed3); [pie-1::GFP::KLP-7(T182ES539ES546E); unc-119(+)]	MAS18	NA

2.3 Clone generation and sequencing

2.3.1 Thermal Cycling Plasmid Mutagenesis with Pfu and Taq ligase

PCR primers for site-directed mutagenesis were designed by a web-based program PrimerX (http://www.bioinformatics.org/primerx/). Mutagenesis reactions were modified from the Stratagene Quikchange protocol. Sequences for mutagenic primers are listed in Table 2-2. The underlined nucleotide indicated the desired mutations. The mutagenesis reaction was prepared as indicated below:

17 µL PT1.1 X Master mix (56 mM KCl, 11mM Tris-HCl pH8.5, 1.7 mM $MgCl_2$, 0.01% BSA, 222 µM ea dNTPs)

1 µL 20X 10 mM NAD+ (nicotinamide adenine dinucleotide)

1 µL each 5'phosphorylated primers (200 ng/µL)

2 µL dsDNA plasmid (around 500 ng)

0.5 µL DMSO (dimethyl sulfoxide)

0.3 µL Taq ligase (New England BioLabs)

Cycling Parameters for the "Quick change Program": use "Hot Start" setting, segment 1: 95 °C 2 minutes, 1 cycle; segment 2: 95 °C 1 minutes, 55 °C 1minutes, 65 °C 1 minutes, 30 cycles.

When temperature reached 95 °C, 1 µL (2.5 U) PfuUltra High-fidelity DNA Polymerase Alternative Detergent (Agilent Technologies) was added and the program was resumed. At the end of the cycling, 0.5 µL (10 U) Dpn-1 (New England BioLabs) was added. The reaction was incubated

at 37 °C for more than 4 hours to remove the wild type plasmid. 2 µL of the reaction was used to transform DH5α *E.coli*. Mutant clones were confirmed by DNA sequencing.

2.3.2 Sequencing reaction

Sequencing reactions were carried out by incubating the reaction mix (2 µL BigDye, 6 µL 2.5 X Dilution Buffer, 200-1000ng DNA template, 3 to 5 pM sequencing primer, add dH_2O to 20 µL) with the following PCR program: 96 °C x 30 seconds; 50 °C x 15 seconds; 60 °C x 2 minutes, 25 cycles. Sequencing reactions were cleaned by the ethanol precipitation method and analyzed on an ABI 3730 DNA sequencer by the Molecular Biology Service Unit staff at the University of Alberta, Edmonton, Alberta, Canada.

2.3.3 Clone generation by restriction enzyme digestion and ligation

To generate GFP::KLP-7-phospho-mutant clones, KLP-7-phospho-mutant fragments (from a pBluescript-Cam^R vector) were subcloned into the pAZ-LAP-GFP(N)-Amp^R vector by using the Xma I enzyme and T4 DNA ligase (New England BioLabs). Xma I restriction digest reactions were assembled as below:

1 µL Xma I (10 units/ µL, NEB)
2 µL 10X NEB buffer 4
0.5 µL BSA
16 µL DNA (2-4 mg)
For pAZ vectors only: 1 µL Calf intestinal alkaline phosphatase (10 units/ µL)

Mix and incubate at 37 °C for more than 6 hours.

Desired DNA fragments were separated on 1% agarose gels and extracted by using QIAEX II Gel Extraction Kit (QIAGEN). Ligation reactions were assembled as below:

1 μL T4 ligase (400 units/ μL, NEB)
1.5 μL 10 X ligase buffer
4 μL "insert" DNA (100-200 ng)
4 μL "vector" DNA (100-200 ng)
5 μL dH_2O

Mix and incubate at 16 °C overnight. Use 2 μL of the ligation reaction to transform competent *E. coli* cells.

To create the GST-AIR-1-TPXL-1-N and the GST-AIR-1(KD)-TPXL-1-N constructs, cDNA of TPXL-1-N (a.a. 1-63, with an Xma I site at each end) was first cloned into a pGEM-T Easy vector (Promega) and confirmed by sequencing reaction. The TPXL-1-N cDNA was then subcloned into the Xma I site of GST-AIR-1 or GST-AIR-1(KD) constructs to generate in-frame fusion proteins.

2.3.4 Clone generation by using the gateway cloning technology

Constructs used for *in vitro* expression, including GST- KLP-7-N (K11D9.1b.2, a.a. 2-189), GST-KLP-7-CC (CC: a.a. 487-689, CC2: 501-620, CC3: a.a. 501-545, CC4: a.a. 541-590, C5: a.a. 590-689) and GST-TPXL-1 (a.a. 1-63) were generated by using the gateway cloning technology (Invitrogen). Briefly, the gateway PCR primers were designed by adding the "Gateway attB1, and attB2" sequences to the 5', and 3' end of gene specific PCR primers, respectively (for details on primer

sequence, see Table 2-2). To generate entry clones, the PCR amplification products are inserted into a Gateway Donor vector pDONR221 (Invitrogen) by recombination reactions catalyzed by the Gateway BP Clonase enzyme mix. The identity of entry clones were confirmed by sequencing clones with M13-f, r primers (Table 2-2). The gene fragments in the entry clones were then transferred into a Gateway Destination vector pDEST15 (Invitrogen) by using the Gateway LR Clonase enzyme mix (Invitrogen). Mutations at putative kinase sites were introduced by using a QuikChange Site-Directed Mutagenesis Kit (Stratagene) as described.

2.4 RNA-Mediated Interference (RNAi)

The *tpxl-1* RNAi feeding clone was constructed by J. Tegha Dunghu. The feeding clones used for *air-1*, *icp-1*, *rsa-1*, *ptr-2* and *gpr-1/2* were obtained from the RNAi library (Fraser et al., 2000; Kamath et al., 2003). Each clone in the RNAi library contains L4440 vector with a specific gene or fragment of interest inserted between the two inverted T7 promoters. The *E. coli* strain HT115(DE3) which has IPTG-inducible T7 polymerase and a disruption of the RNAse III gene, was used as the host of RNAi plasmids. RNAi was performed using a previously described feeding method (Fire et al., 1998; Timmons et al., 2001). Briefly, bacteria producing the desired dsRNA (double-strand RNA) were grown in LB media (Luria-Bertani: 10 mg/mL Bacto-Tryptone, 5 mg/mL Bacto-Yeast extract, 10 mg/mL NaCl) with 50 µg/mL ampicillin for 6 to 8 hours at 37°C.

RNAi plates (NGM agar supplemented with 1 mM IPTG [isopropyl β-D-1-thiogalactopyranoside] and 25 μg/mL carbenicillin) were seeded with the bacteria culture and left at room temperature overnight to induce the production of dsRNA. L4 larvae of desired worm strain were placed on RNAi plates for 22 to 26 hours at 25 °C before being examined.

RNAi against *klp-7(exon 1), klp-7(both splice forms), klp-7(RNAi-resistant cassette 1), klp-7(RNAi-resistant cassette 2)*, *air-1*, *air-2*, and *air-1 + air-2* were performed by injecting dsRNA into the syncytial gonad of L4 worms (Fire et al., 1998). RNA was *in vitro* transcribed by using the MEGAscript system (Life Technologies) and purified and annealed according to previous descriptions (Fire et al., 1998). dsRNAs were injected at 0.5 to 1.0 mg/mL for each gene. Details for RNAi targeted genes or regions are listed in Table 2-4.

Table 2-4 dsRNAs and targeted genes or regions

Targeted genes/regions	**Primers used to generate DNA template for RNA synthesis**
klp-7(exon 1)	KLP-7-1-T7f, KLP-7-1-T3r
klp-7(both splice forms)	KLP-7-T3-f1, KLP-7-T7-r1
klp-7(RNAi-resistant cassette 1)	klp-7-r-T7f1, klp-7-r-T3r
klp-7(RNAi-resistant cassette 2)	klp-7-r-T7f2, klp-7-r-T3r
air-1	AIR-1-T3f, AIR-1-T7r
air-2	AIR-2-T3f, AIR-2-T7r

2.5 Protein expression, *in vitro* kinase assays and sample preparation for Liquid chromatography-tandem mass spectrometry (LC-MS/MS) analysis

The GST-AIR-1, GST-AIR-1(KD) constructs, and poly-cistronic constructs to co-express ICP-1 and AIR-2 (or AIR-2 KD) were generously provided by Dr. Jill Schumacher (The University of Texas MD Anderson Cancer Center, Houston, TX). The *E.coli* strain Rosetta 2(DE3) (Novagen) was used as the host to express recombinant proteins. Bacteria with the desired plasmid were cultured in 500 mL LB media (with 25 µg/mL carbenicillin and 50 µg/mL chloramphenicol) at 37 °C with vigorous shaking, until the OD600 (optical density measured at a wavelength of 600 nm) reached 0.5 to 0.7. To induce protein expression, IPTG was added to 1 mM and the culture was grown for an additional 3 hours. Cells were harvested by centrifuging at 4000 X g for 20 minutes. Recombinant proteins were purified by using the Glutathione Sepharose 4B media (GE Healthcare Life Sciences) according the manufacture's instruction. Briefly, proteins were extracted by sonicating cell pellets on ice in 10 mL lysis solution (50 mM Tris-HCl pH 8.0, 50 mM NaCl, 1 mM EDTA [ethylenediaminetetraacetic acid]) supplemented with protease inhibitor cocktail (Mini-Complete, Roche Applied Science). Soluble proteins were separated from the cellular debris by centrifuging at 10,000 x g for 20 to 30 minutes at 4 °C. To bind proteins to the resin, lysates were incubated with 200 µL Glutathione Sepharose 4B media at room temperature for 1 hour.

The resin were then washed with 15 mL of lysis solution for 4 times, and eluted with 1 mL of elution solution (50 mM Tris-HCl pH 8.5, 10 mM glutathione). Purified proteins were passed through Amicon Ultra-4 (10 KDa) Centrifugal Filter Unit (Millipore) for desalting. Protein concentrations were determined by performing the Bradford assay with protein assay dye reagent (Bio-Rad Laboratories).

For each kinase assay reaction, kinase (5-10 µg) and substrate (5-10 µg) were incubated in kinase buffer (20 mM HEPES [4-(2-hydroxyethyl)-1-piperazineethanesulfonic acid] pH7.4, 25 mM beta-glycerophosphate, 10 mM $MgCl_2$, 5 mM EGTA [ethylene glycol tetraacetic acid], 2 mM DTT [dithiothreitol], and 0.01 mM ATP) including 5 µCi of γ [32P]-ATP for 30 minutes at 30 ºC. Samples were resolved by SDS-PAGE and transferred to nitrocellulose membranes (Pierce, Thermo Scientific). *In vitro* phosphorylation was analyzed by autoradiography, which was produced by exposing the nitrocellulose membranes to Kodak BioMax XAR films (Fisher Scientific). Ponceau-S staining was used to confirm that similar amounts of each substrate were added to the reaction.

To prepare samples for LC-MS/MS analysis, each kinase assay reaction was performed by using 20 µg kinase and 100 µg substrate, without adding γ [32P]-ATP (non-radioactive reaction). A similar kinase assay was performed in parallel by using γ [32P]-ATP to confirm phosphorylation (radioactive reaction). The non-radioactive reaction was sent to University of Victoria Genome BC PROTEOMICS CENTRE

(Victoria, BC Canada) for trypsin digestion of proteins followed by LC-MS/MS analysis.

2.6 Western Blotting

To perform western blot analysis on whole worm lysates, 25 to 75 young gravid hermaphrodites of the desired worm strain were picked into an eppendorf tube with 10 µL dH_2O. 10 µL of 2X sample buffer (Sigma-Aldrich) was added to each tube and the sample was boiled at 95 ºC for 5 minutes. Samples were resolved by SDS-PAGE (8% resolving gel for detection of GFP::KLP-7 in various transgenic lines, 10% resolving gel for all the other analysis). The relative molecular weight of the proteins was determined by using the prestained protein marker (7-175 kDa broad range; New England BioLabs). After the electrophoresis proteins were transferred to nitrocellulose membranes (Pierce, Thermo Scientific) at 90 V for 2 hours. The membranes were blocked in 8% skim milk in TBST (Tris buffered saline Tween 20; 20 mM Tris, pH 7.4, 150 mM NaCl, 0.05% Tween 20) for 1 hour at room temperature, followed by primary antibody incubations (1 µg/mL anti-KLP-7 or 0.2 µg/mL DM1A in 4% skim milk in TBST) at room temperature for 1 hour. Membranes were washed with TBST and then incubated with horseradish peroxidase-conjugated secondary antibodies (Bio-Rad Laboratories; 1/5000 goat anti-rabbit or goat anti-mouse antibody in 4% skim milk in TBST). ECL western blotting substrate (Pierce, Thermo Scientific) was prepared according to the

manufacturer's instructions and applied to immunoblots. Membranes were exposed to Fuji RX X-ray films (FUJIFILM) for detection.

To perform western blot analysis on embryos, 50 to 100 young gravid hermaphrodites of the desired worm strain were picked into an eppendorf tube with 50 µL of M9 buffer (22 mM KH_2PO_4, 42 mM Na_2HPO_4, 85 mM NaCl, 1 mM $MgSO_4$). To release embryos, 50 µL of a 2X bleach solution (17.5 µL Sigma-Aldrich Sodium hypochlorite solution, 5 µL 10 M NaOH, 27.5 µL H_2O) was added to each tube and vortexed for 3 minutes. 1 mL embryo wash buffer (0.1 M Tris-HCl, pH 7.4, 100 mM NaCl, 0.1% Tween 20) was then added to each tube and the mixture was centrifuged at 1000 X g for 1 minute. The wash step was repeated 2 more times, leaving the embryo pellet in 10 µL of buffer. 10 µL of 2X sample buffer (Sigma-Aldrich) was added and the sample was boiled at 95°C for 5 minutes before loading. Proteins were resolved by SDS-PAGE and transferred to nitrocellulose membranes. The resulting immunoblots were probed with the desired antibodies as described above.

2.7 Phosphatase Treatment and Phos-tag SDS-PAGE

Lambda Phosphatase (λ PPase) treatment was performed according to the manufacturer's instructions (New England BioLabs). Worm proteins were extracted in lysis buffer (50 mM HEPES pH 7.4, 1 mM EGTA, 1 mM $MgCl_2$, 100 mM KCl, 0.05% NP40, 10% glycerol) supplemented with protease inhibitor cocktail (Mini-Complete, Roche Applied Science). To dephosphorylate proteins, 20 µg of whole worm

lysate was incubated with 400 u of phosphatase (10 µL total reaction) for 60 minutes at 30 ºC. Reaction was stopped by adding 10 µL of 2X SDS-sample buffer.

Phos-tag SDS-PAGE was performed as previously described (Kinoshita et al., 2006). The relative molecular weight of the proteins was estimated by using the protein marker (10-250 kDa; New England BioLabs). Proteins were separated by a 10% polyacrylamide gel containing 25 µM Phos-tag acrylamide (NARD Institute, Ltd) and 25 µM $MnCl_2$. After electrophoresis, the gel was first soaked in transfer buffer (25 mM Tris, 192 mM glycine, 20% methanol) with 1 mM EDTA for 10 minutes, and then in transfer buffer without EDTA for another 10 minutes. Proteins were transferred to a nitrocellulose membrane (Pierce, Thermo Scientific) at 90 V for 2 hours. The resulting membrane was blocked with 8% skim milk in TBST, and probed with rabbit anti-KLP-7 antibody (1 µg/mL). The membrane was washed and incubated with a horseradish peroxidise-conjugated goat anti-rabbit antibody (Bio-Rad Laboratories). ECL western blotting substrate (Pierce, Thermo Scientific) was prepared according to the manufacturer's instructions and applied to immunoblots. The membrane was exposed to Fuji RX X-ray films (FUJIFILM) for detection.

2.8 2D gel electrophoresis

Immobiline DryStrip (7 cm; pH 7–11 NL) gels, IPG buffer (pH 7–11 NL) and DeStreak Rehydration Solution was used for 2D gel experiments

(GE Healthcare). Lysates from N2, *air-1(RNAi)* and *air-2(or207ts)* worms were extracted by sonication in sample preparation solution (8 M Urea, 4% w/v CHAPS {3-[(3-cholamidopropyl)dimethylammonio]-1-propanesulfonate hydrate}, 2% v/v IPG buffer, 40 mM DTT) supplemented with protease inhibitor cocktail (Mini-Complete, Roche Applied Science). Lysates were separated from debris by centrifuging at 8000 X g for 20 minutes. The protein concentration was determined by performing the Bradford assay with protein assay dye reagent (Bio-Rad Laboratories). 120 µg of total protein was loaded to each gel strip by rehydration at room temperature overnight. Isoelectric focusing (IEF) was performed in an Ettan IPGphor Isoelectric Focusing Unit (GE Healthcare) according to the manufacturer's instructions (Table 2-5). Protein samples were further separated on 10% polyacrylamide gels and transferred to nitrocellulose membranes. The resulting immunoblots were probed with affinity-purified anti-KLP-7 antibody as described above.

Table 2-5 Guidelines for performing IEF (GE Healthcare)

Step voltage mode	**Voltage (V)**	**Time (h:min)**	**kVh**
Step and Hold	300	0:30	0.2
Gradient	1000	1:00	0.7
Gradient	5000	1:30	4.5
Step and Hold	5000	0:20-0:55	1.6-4.6
Total		3:20-3:55	7.0-10.0

2.9 Antibody production

AIR-1 antibody was generated by immunizing one rabbit with a mixture of GST-AIR-1 protein (full length) and the BSA (Bovine Serum Albumin) coupled AIR-1 C-terminal peptide (H2N-LTKSSRNNSTANQ-COOH). Rabbits were boosted for a period of 14 weeks and final bleeds were collected. Anti-AIR-1 antiserum was purified according to standard procedures (Harlow and Lane, 2006). Briefly, antigen was reduced by mixing 4 mg of GST-AIR-1 fusion protein with 4 mL reducing buffer (50 mM Tris-HCl pH 8.5, 10 mM EDTA, 10 mM DTT) at room temperature for 30 minutes. The reduced antigen was first passed through an Amicon Ultra-4 (3 KDa) Centrifugal Filter Unit (Millipore) to remove DTT and then resuspended in 4 mL coupling buffer (50 mM Tris-HCl pH 8.5, 10 mM EDTA). Coupling was performed by recirculating the antigen solution at a speed of 1.5 mL/min through 2 mL column of SulfoLink resin (Pierce, Thermo Scientific) at room temperature for 45 minutes by using a peristaltic pump. To block nonspecific binding sites on the resin, 4 mL of quenching solution (50 mM L-Cysteine.HCl, 50 mM Tris-HCl pH 8.5,10 mM EDTA) was recirculated through the resin column at room temperature for 30 min. The column was then washed as follows: 10 mL 10 mM Tris-HCl pH 8.0, 10 mL 0.1 M glycine pH 2.0, 10 mL 10 mM Tris-HCl pH 8.0, 10 mL 0.1 M freshly prepared triethylamine pH 11.5, repeat the above cycle; and was finally washed with 50 mL phosphate-buffered saline (PBS: 137 mM NaCl, 12 mM Phosphate, 2.7 mM KCl, pH 7.4). To

prepare serum for purification, 100 mL serum was mixed with 100 mL 2 X PBS solution and NaN_3 (0.1% final concentration) and filtered using a 0.2 µm Stericup Filter Unit (Millipore). The serum was recirculated through the antigen-coupled resin column at room temperature overnight. Column was washed with 300 mL wash buffer (1 X PBS supplemented with 0.5 M NaCl, 0.1% Triton X-100) followed by 100 mL PBS solution. To elute anti-AIR-1, the column was equilibrated with 10 mM Tris-HCl pH 8.5, and eluted with 20 mL 0.1 M glycine pH 2.6 as 20 fractions (1 mL/tube). Each fraction was neutralized with 200 µL of 2 M Tris-HCl pH 8.5. Fractions that contained antibodies (A 280 $\geq$ 0.1) were pooled together and dialyzed (2L PBS for 1 hour, repeat 4 times, followed by 1L PBS with 60% glycerol for 5 hours) using a slide-A-Lyzer Dialysis Cassette, 20K MWCO (Pierce, Thermo Scientific). Purified anti-AIR-1 antibody was store at -20 °C. The column was washed with 100 mL PBS followed by 20 mL PBS with 50 % glycerol and stored at -20 °C.

To test the specificity of the anti-AIR-1 antibodies, embryos from 200 wild-type or *air-1(RNAi)* gravid hermaphrodites were collected and resolved by SDS-PAGE, transferred to nitrocellulose membranes (Pierce, Thermo Scientific) and probed with anti-AIR-1 antibody (3 µg/mL in 5 % skim milk in TBST). A protein band migrating at 37 KDa (predicted molecular weight for AIR-1) was only detected in the wild-type lysate and not in the *air-1(RNAi)* lysate.

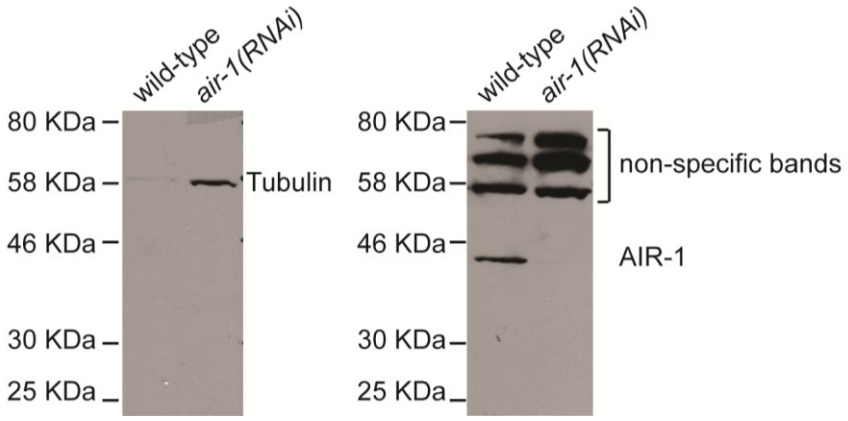

Figure 2-1 Western blot analysis demonstrating the reactivity of anti-AIR-1 antibody

Wild-type and *air-1(RNAi)* embryos were probed for tubulin (left) and AIR-1 (right). AIR-1 protein (predicted molecular weight: 37 KDa) is detected by anti-AIR-1 antibodies in wild-type, but not RNAi-treated embryos.

An attempt was also made to generate phospho-specific antibodies. Anti-phospho-antibodies against 3 putative Aurora sites on KLP-7 were generated by Pacific Immunology Company (San Diego, California, USA). The following peptide sequences were chosen for producing phospho-specific antibodies (Table 2-6). A cysteine (Table 2-6, underlined) was added to the N- or C-terminus of the peptide to allow for conjugation to the highly immunogenic KLH (keyhole limpet hemocyanin) carrier protein. Each affinity-purified anti-phospho antibody was tested by performing immunochemical staining on fixed embryos. Unfortunately, antisera generated from peptides that included pT119, pS538 and pS546 did not exhibit KLP-7 reactivity in immunostaining or Western blot experiments in

either wild-type or *klp-7(tm2143)* embryos (data not shown). None of the above antibodies were used in this study.

Table 2-6 Producing phospho-specific antibodies

Putative site	**Peptide sequence**	**Rabbits/Serum ID**
T119	C-AKGASANKRP-T(PO3)-GAFTQH	5941, 5942
S538	CIRGMARN-S(PO3)-SHVPFRQSK	5943, 5944
S546	RQ-S(PO3)-KLTMVLRDSFIGEKSR-C	5851, 5852

2.10 Indirect immunofluorescence microscopy of stained embryos

To perform immunochemical staining, embryos were processed by freeze-cracking and fixed with methanol as described (Oegema et al., 2001). 30 to 50 gravid hermaphrodites of the desired worm strain were picked into 4 µL of dH_2O on a poly-L-lysine coated glass slide (Sigma-Aldrich). An 18 X 18 mm coverslip was placed on top of the worms and pressure was applied just enough to burst the adults. The slide was placed into liquid nitrogen for more than 3 minutes. The coverslip was then removed and the slide was immediately put into 100% methanol (pre-cooled at -20 °C) for 15 minutes, followed by incubation with PBS buffer at room temperature for more than 5 minutes. For immunostaining, fixed embryos were blocked with 25% goat serum in PBS at room temperature for 1 hour in a humidified chamber. Embryos were incubated with DM1A (1 µg/mL) and anti-KLP-7 (20 µg/mL) primary antibodies in 5% goat serum in PBST (1 X PBS with 0.1% Triton X-100) at room temperature for 1 hour. The slide was washed with PBST and then incubated with 1 µg/mL

fluorescent goat-anti-mouse/rabbit secondary antibodies (Invitrogen) in 5% goat serum in PBST at room temperature for 1 hour. Embryos were stained with 1 µg/mL DAPI (4',6-diamidino-2-phenylindole), washed with PBST, and mounted in mounting medium. The slides were sealed with nail polish and stored at -20 °C. To image the meiotic embryos, 66 images were taken at a Z-spacing of 0.2 microns.

To quantify centrosomal MTs in metaphase embryos, GFP::KLP-7(S546E) or GFP::KLP-7(S546A) worms were fixed and stained under the same conditions with the wild-type control worms. DM1A (Sigma-Aldrich) and anti-γ-tubulin antibodies were used at 1 µg/mL and 8 µg/mL respectively. Alexa Fluor 594 (red) and Alexa Fluor 647 (far red) conjugated secondary antibodies were used instead of Alexa Fluor 488 (green) conjugate to avoid potential interference from GFP::KLP-7. In a single frame where the centrosome is in focus (as judged by γ-tubulin fluorescence), the centrosomal MT level was defined as the fluorescence intensity of a circular region (40 pixel diameter) at the centrosome, minus the intensity at a background cytoplasmic area. The relative intensity for each centrosome was calculated as: the integrated intensity of one centrosome/the average integrated intensity of control centrosomes) x 100.

2.11 Live imaging and Quantification

Confocal microscopy was performed with an IX81 motorized inverted microscope (Olympus) equipped with a Yokogawa CSU-10

spinning disk system. Images were collected with a 60× objective (NA 1.42) and a Hamamatsu Orca R2 camera controlled by MetaMorph software (Molecular Devices).

The spindle-snap phenotype was scored by first dissecting worms in 5 µL egg buffer (188 mM NaCl, 48 mM KCl, 2 mM $CaCl_2$, 2 mM $MgCl_2$, and 25 mM HEPES, pH 7.3). Embryos were then mounted on a thin 2% agarose pad and imaged for GFP::KLP-7(WT or mutants) from the start of mitotic metaphase to cytokinesis at 5 second intervals. The environment temperature during imaging was controlled at 25 ± 0.5 °C according to previous description (Gusnowski and Srayko, 2011). The rates of centrosome separation during the first 25 seconds of anaphase were measured using Excel (Microsoft). When the centrosome separation rate exceeded 0.130 µm/sec, the embryo was scored as having a spindle-snap phenotype.

To perform *in utero* imaging of meiotic embryos, worms expressing GFP::β-tubulin and mCherry::histone were immobilized with 4 mM tetramisole hydrochloride (Sigma-Aldrich) and mounted on a thin 2% agarose pad. Embryos within the uterus can be farther away from the coverslip (up to 100 µm) than free, dissected embryos. This can contribute to image degradation when focusing deeper into the specimen, due to refractive index mismatches between the immersion oil and the sample. To increase the resolution of *in utero* movies a 60x (NA 1.3) silicone-oil objective was used. Time-lapse images were collected at 20 second

intervals from fertilization to the end of meiosis II. At each time point, 3 images were acquired at 1 µm spacing. In this way, some 3D information on the structure of the meiotic spindles was obtained, without excessive photo-damage.

2.12 Nocodazole treatment and FRAP

To create permeabilized embryos, L4-adult worms were grown for 12-16 h at 20 ºC on *ptr-1* RNAi-feeding plates (Carvalho et al., 2011; Kamath et al., 2001). Worms were dissected in embryo buffer and mounted on agarose pads with a coverslip for imaging. To depolymerize microtubules, nocodazole was added (10 µM final concentration) just before mounting and allowed to incubate for at least 30 seconds (Bajaj and Srayko, 2013). One-cell embryos in metaphase were used for all photobleaching experiments. Only embryos that displayed a lack of anaphase pole separation after the FRAP experiment were deemed affected by nocodazole and used for analysis.

Photobleaching experiments were performed on a spinning disk confocal as described above. The bleaching laser (400 mW; Power Technology) was controlled by Metamorph Software using the Mosaic targeted illumination interface. Sufficient photobleaching of a circle (30 pixel diameter) was achieved with a targeted widefield beam at maximum laser power for 3 seconds. Confocal images were acquired at 1 second intervals both before photobleaching (5 frames), and during the recovery phase (90 frames). Fluorescence intensity of GFP::KLP-7 was measured

with Metamorph software at the centrosome and at two background locations to correct for photobleaching resulting from image acquisition. Curves were generated with easyFRAP software, using full-scale normalization and double term curve-fitting (Rapsomaniki et al., 2012).

2.13 Generation of *unc-119 klp-7* double mutant worms

unc-119 (III:5.59 +/- 0.004 cM) and *klp-7* (III:5.41 +/- 0.007 cM) are closely linked with a 0.18 cM (centimorgan) distance between them, based on mapping data (wormbase). I attempted to generate homozygous *klp-7(tm2143) unc-119(ed3), klp-7(tm2143) unc-119(ed4),* and *klp-7(tm2143) unc-119(ky571)* double-mutant worms as described in Figure 2-2. However, only *klp-7(tm2143) unc-119(ky571)* worms were viable.

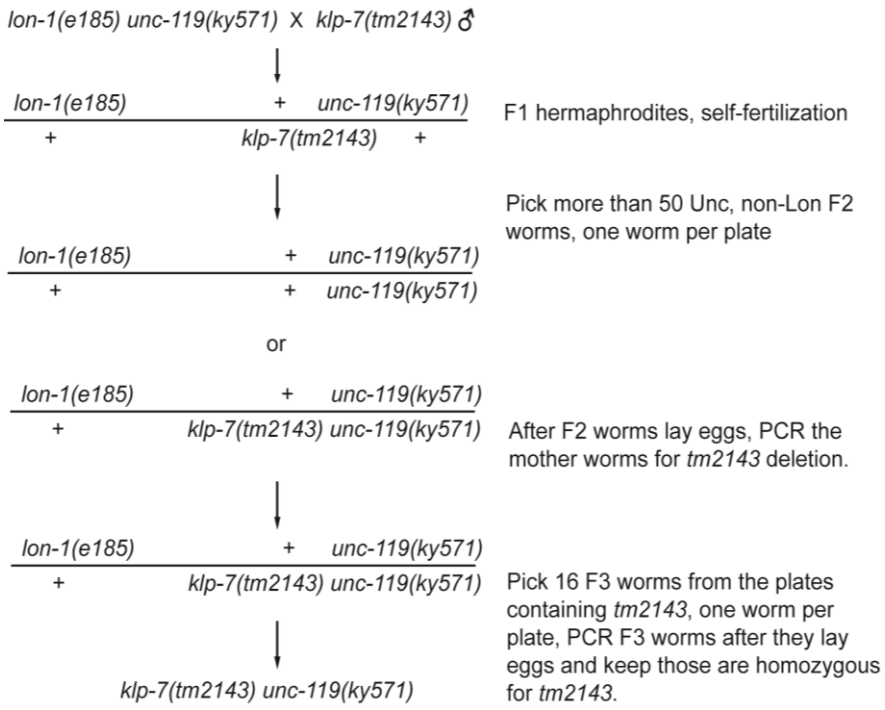

Figure 2-2 Generation of *unc-119 klp-7* double-mutant worms

2.14 Dye filling assay and imaging worms expressing pan-neuron GFP

The structural integrity of sensory cilia was tested by the ability of worms to take up a fluorescent dye (Hedgecock et al., 1985; Perkins et al., 1986; Starich et al., 1995). Vybrant DiD, DiI and DiO (Molecular Probes, Invitrogen) stock solutions (1 mM each) were diluted to make the working solutions (1/200 in M9 buffer). L3 and L4 worms of desired strains were picked into an eppendorf tubes with 50 µL fluorescent dye solution and incubated at room temperature for 20 minutes. Worms were then transferred to an NGM plate seeded with the OP50 bacteria to pass the dye out of their digestive tract. The plates were kept in a dark box at room temperature overnight before imaging.

To image dye-labeled neurons, dye-treated worms were immobilized with 30 mM NaN_3 in M9 buffer and mounted on a thin 2% agarose pad. Images were collected with a spinning-disk confocal microscope (40× objective using appropriate filters). Z-stacks (91 images at 0.5 µm spacing) were obtained to visualize head neurons.

To image pan-neuron GFP fluorescence in head and motor neurons, worms of desired strains were anesthetized with 30 mM NaN_3 in M9 buffer and mounted on a thin 2% agarose pad. Images were collected with a 60× objective (NA 1.42). 201 frames were collected at an interval of 0.2 µm for each image.

3 Results

3.1 Loss of KLP-7 results in increased MT polymer levels and spindle defects in meiosis

To characterize *klp-7* loss-of-function phenotypes, I examined the MT behaviour in *klp-7(tm2143)* embryos after fertilization through to the first mitosis. *tm2143* contains an 875 bp deletion spanning two exons (Figure 3-1). In *tm2143* worms, KLP-7 was not detected by western blot (Figure 3-2), suggesting it is a null mutation. Many progeny from *tm2143* homozygous worms survive to adulthood and are fertile. This was surprising because *klp-7* is the only gene in *C. elegans* believed to encode a kinesin-13 family member. Another surprising result was that *tm2143* lethality was temperature-sensitive, with 35% embryonic viability at permissive temperatures and 8% at the restrictive temperature (Table 3-1). This result suggested that the lethality could be due to the disruption of a process that is inherently stochastic, for example if chromosome segregation is affected but not completely abrogated by *klp-7* loss. In support of this, *klp-7(tm2143)* worms also exhibited a higher percentage of male progeny (1% at 25 °C), likely indicating meiotic defects due to nondisjunction of the X chromosome (Hodgkin et al., 1979). Also consistent with aberrant meiosis, *klp-7(tm2143)* embryos either failed to extrude polar bodies (7/18 in meiosis I and 14/18 in meiosis II, Table 3-2) or exhibited abnormally large polar bodies (4/18 in meiosis II).

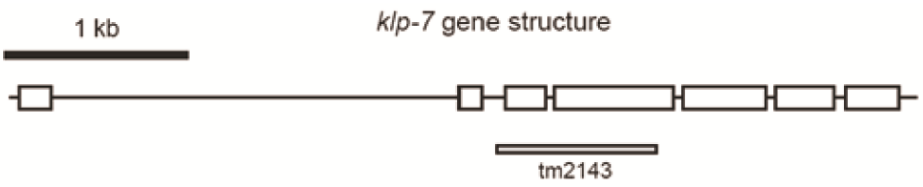

Figure 3-1 Gene structure of KLP-7

Exons are shown as white boxes. Introns are shown as solid lines. The deleted region in *klp-7(tm2143)* is underlined.

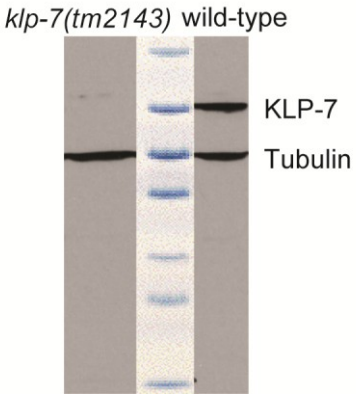

Figure 3-2 No endogenous KLP-7 is detected in *klp-7(tm2143)* worms by western blot

50 young adult worms were loaded in each lane. Proteins were resolved by 10% SDS PAGE, transferred to a nitrocellulose membrane, and blotted with anti-KLP-7 and DM1A (anti-α-tubulin) antibodies. Predicted molecular weight of KLP-7: 80 kDa. Predicted molecular weight of tubulin: 50 kDa. Molecular weights of protein marker (from top to bottom): 175 kDa, 80 kDa, 58 kDa, 46 kDa, 30 kDa, 25 kDa and 17 kDa.

Table 3-1 Temperature effects on embryonic viability of *klp-7(tm2143)*

Temperature (°C)	**Viability (%)**	**Standard error**	**# of embryos**
15	32.6	2.4	385
20	34.6	1.6	849
25	8.3	1.3	428

The number of hatched worms over total embryos (percentage of embryonic viability) was scored at each temperature. The viability of *klp-7(tm2143)* embryos was higher at permissive temperatures (15°C and 20°C) and lower at the restrictive temperature (25°C).

Table 3-2 Summary of meiotic defects of *klp-7(tm2143)*

	number of embryos (18 in total)	
meiosis I	disorganized metaphase plate	12 (66.7%)
	failure in spindle shortening	0 (0%)
	chromatin overlap with MTs at anaphase	17 (94.4%)
	abnormal anaphase spindle	8 (44.4%)
	failure to segregate chromosomes	0 (0%)
	failure to extrude polar body	7 (38.9%)
meiosis II	disorganized metaphase plate	16 (88.9%)
	failure in spindle shortening	0 (0%)
	chromatin overlap with MTs at anaphase	16 (88.9%)
	abnormal anaphase spindle	3 (16.7%)
	failure to segregate chromosomes	0 (0%)
	failure to extrude polar body	14 (77.8%)

Time-lapse images were taken to score meiosis processes in *klp-7(tm2143)* embryos expressing GFP:: β-tubulin, mCherry :: histone transgenes. Examples of defective meiotic spindles are shown in Figure 3-4.

To observe the MT cytoskeleton and chromatin during female meiosis, we examined wild-type and *klp-7(tm2143)* embryos expressing GFP::tubulin and mCherry::histone transgenes by filming one-cell embryos *in utero*. Compared to wild-type, *klp-7(tm2143)* embryos had a more extensive MT network near the cell cortex, especially surrounding the meiotic spindle (Figure 3-3). *klp-7(tm2143)* embryos also exhibited a disorganized chromosome arrangement in metaphase I and II. During

wild-type anaphase I and II, a MT bundle normally forms between the segregating chromosomes and is restricted to the midzone region (Albertson and Thomson, 1993; Dumont et al., 2010). In *klp-7(tm2143)* embryos, anaphase MTs were not restricted and often extended beyond the spindle midzone region. The chromosomes were scattered in directions orthogonal to the spindle axis, and an abnormal anaphase spindle was often observed (Table 3-2 and Figure 3-4). Despite defects in organizing meiotic spindles, chromosomes always separated during anaphase in *klp-7(tm2143)* embryos (18/18 in meiosis I and II, Table 3-2). *klp-7(tm2143)* embryos with an abnormal anaphase spindle demonstrated unequal chromosome segregation in the daughter cells (in some embryos chromosomes are separated into three groups instead of two).

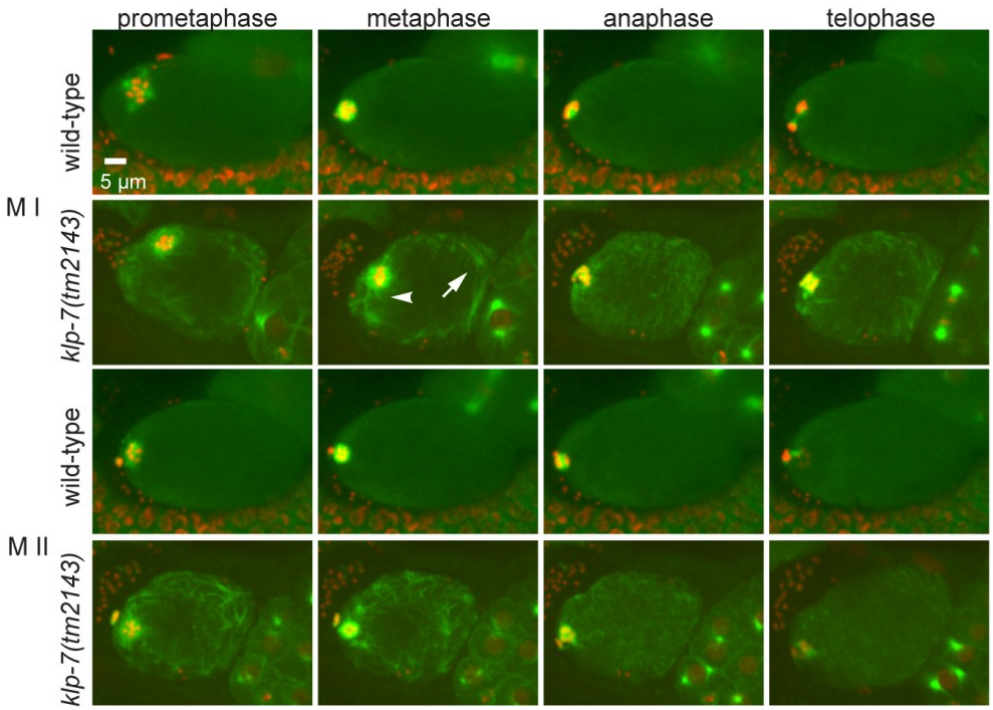

Figure 3-3 *klp-7(tm2143)* embryos has extensive MT network near the cell cortex, especially surrounding the meiotic spindle

Wild-type (upper panels) and *klp-7(tm2143)* (lower panels) embryos expressing GFP::tubulin and mCherry::histone transgenes are shown. Images of embryos at each representative stage of meiosis I and II are shown. Each image is generated by projecting three Z-stacks (Z-spacing: 1 micron). The female meiotic spindles are to the left.. Arrowhead: disorganized MT-network near the meiotic spindle; arrow: long MTs at the cortex of *klp-7(tm2143)* embryos.

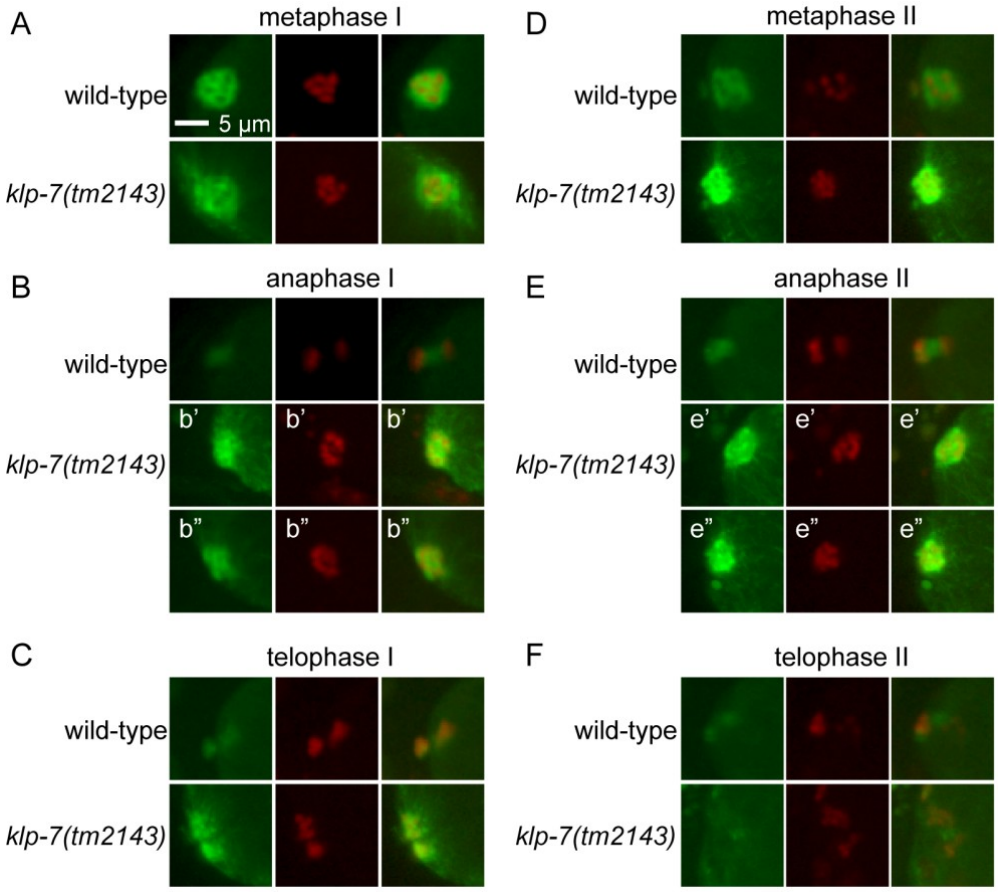

Figure 3-4 Examples of meiotic phenotypes of *klp-7(tm2143)* embryos as listed in table 3-2

Representative images of wild-type and *klp-7(tm2143)* embryos expressing GFP:: β-tubulin, mCherry:: histone transgenes are shown. Compared to wild-type, *klp-7(tm2143)* embryos exhibit a disorganized chromosome arrangement at metaphase I (A) and II (D). At anaphase I (B) and II (E), phenotypes including unrestricted MTs that extended beyond the midzone (b' and e') and formation of multipolar spindles (b" and e") were frequently observed in *klp-7(tm2143)* embryos. At telophase I (C) and II (F), *klp-7(tm2143)* embryos often failed to extrude polar bodies.

To determine the subcellular location of KLP-7 in female meiosis, I performed immunostaining using anti-KLP-7 antibody. During meiosis I

and II, KLP-7 localized to chromosomes, to the chromosomal passenger complex (CPC) region (the region in-between the chromosomes, localization pattern similar to that of Aurora B, a CPC protein), and the spindle poles in metaphase. KLP-7 remained associated with chromosomes in anaphase and telophase. During late anaphase II, KLP-7 also localized to the spindle midzone between separating chromosomes (Figure 3-5). KLP-7 immunofluorescence was also visible throughout the cytoplasm of meiotic embryos, consistent with a role of KLP-7 in regulating cytoplasmic MTs during meiosis.

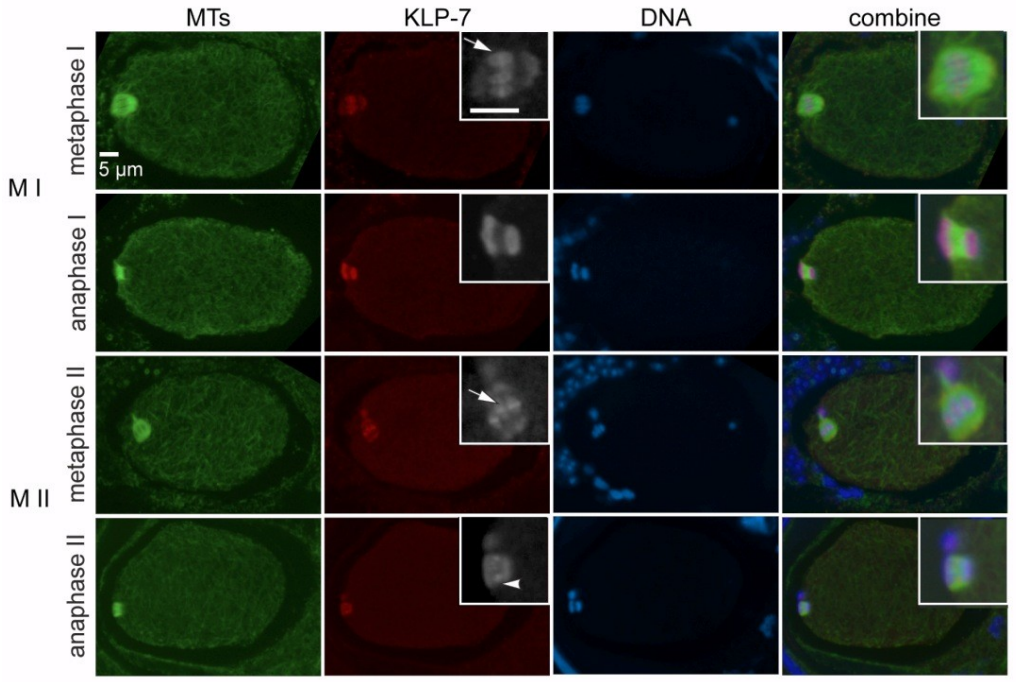

Figure 3-5 Subcellular location of KLP-7 during meiosis by immunostaining

Wild-type embryos were fixed and stained to visualize MTs (green/Alexa 488), KLP-7 (far red/Alexa 647) and DNA (blue/DAPI). KLP-7 associates with chromosomes and spindle poles. At a higher magnification (inserted images), KLP-7 located to the CPC region of meiotic chromosomes at metaphase I and II (arrows), and to the interzone between the separating chromosomes at anaphase II (arrowhead).

3.2 Loss of KLP-7 results in more centrosomal MTs and a spindle snap phenotype

Previous examination of *klp-7(RNAi)* embryos indicated three prevalent phenotypes in the first mitotic division: an approximately 2-fold increase in the number of astral MTs, an abrupt anaphase with higher than normal centrosome separation rates, and a reduction in the amount of

spindle midzone MTs during anaphase (Grill et al., 2003; Schlaitz et al., 2007; Srayko et al., 2005). I also observed similar defects with the *klp-7(tm2143)* mutant (Figure 3-6 and 3-7). I measured the centrosome separation rates in wild-type and *klp-7(tm2143)* embryos and found that although the *klp-7(tm2143)* embryos exhibited qualitatively more severe anaphase movements, both wild-type and *klp-7(tm2143)* embryos exhibited a range of pole separation rates. For wild-type embryos, pole separation rates in the first 25 seconds of anaphase were never found to be greater than 0.130 μm/sec (0.105 $\pm$ 0.007 μm/sec). Therefore, to quantify this defect I defined spindle-snap as a one-cell embryo exhibiting a minimum centrosome separation rate of 0.130 μm/sec in the first 25 seconds of anaphase (for details see material and methods). Using this method, I found that 46% (6/13) of *klp-7(tm2143)* embryos exhibited the spindle-snap phenotype. This phenotype was rescued by expressing GFP::KLP-7(WT) (7% embryos exhibited the spindle-snap; Figure 3-6 and 3-30).

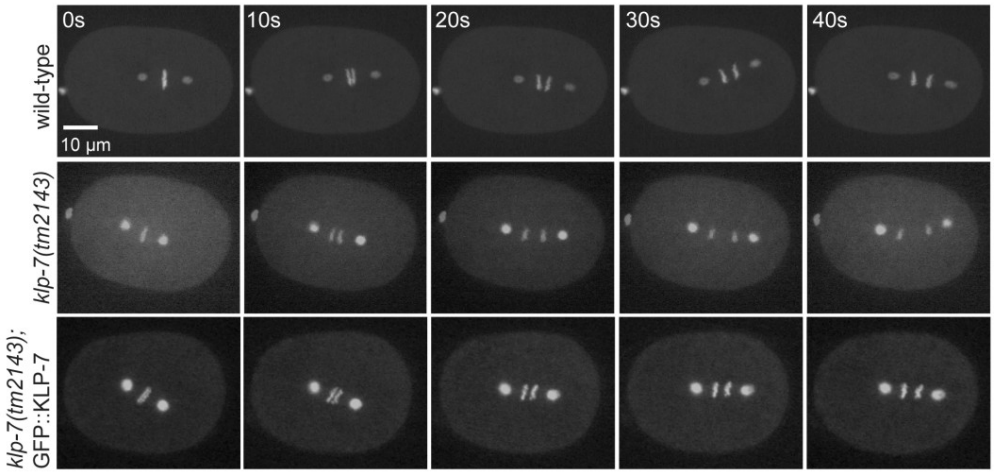

Figure 3-6 *klp-7(tm2143)* embryos exhibit a spindle-snap phenotype

Still images from time-lapse series of mitotic embryos from metaphase to anaphase. Bright dots within the embryo: centrosomes. Bright lines in-between the centrosomes: chromosomes. Top panel: wild-type embryo expressing GFP:: γ-tubulin, GFP:: histone. Middle panel: *klp-7(tm2143)* embryo expressing GFP:: γ -tubulin, mCherry:: histone. Lower panel: *klp-7(tm2143)* embryo expressing GFP:: KLP-7. Time interval: 5 seconds. At the same time point *klp-7(tm2143)* embryos exhibited greater distance between centrosomes than that of wild-type.

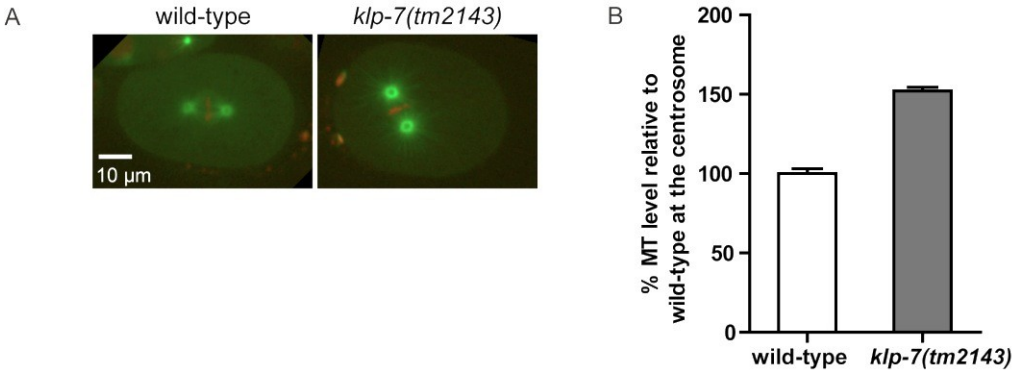

Figure 3-7 *klp-7(tm2143)* embryos have more centrosomal MTs

(A) Representative images of wild-type and *klp-7(tm2143)* embryos expressing GFP::β-tubulin, mCherry::histone at metaphase, mitosis. (B) Quantification of centrosomal MTs in wild-type and *klp-7(tm2143)* embryos. A stack of seven images were projected, with the frame that the centrosome is in focus in the middle. The integrated intensities of GFP::β-tubulin at the centrosome and background (circle diameter: 40 pixels) were measured. For each embryo, the fluorescence intensity at the centrosome is defined as: (centrosome 1 + centrosome 2)/2-background. All MT levels were compared to the average intensity of wild-type centrosomes. Wild-type: n=8; *klp-7(tm2143)*: n=12.

3.3 *gpr-1/2(RNAi)* restores mitotic spindle midzone MTs in *klp-7(tm2143)* embryos

The forces that separate chromosomes in mitotic anaphase are derived from localized force generators likely acting at the cell cortex. Modulation of the forces involves heterotrimeric G-proteins and the MT-motor protein dynein. An increase in centrosome separation rates during anaphase, as observed with *klp-7(tm2143)*, could result from increased pulling forces or from a decrease in a resistance force that opposes the

chromosome separation. In *klp-7(tm2143)*, astral MT levels are increased, but the spindle midzone MT levels are decreased compared to wild-type. Therefore, it was not clear whether the spindle-snap phenotype resulted from increased astral MT levels (causing increased cortical-pulling forces) or from decreased spindle midzone MTs (causing decreased resistance to the anaphase pulling forces) (Encalada et al., 2005; Grill et al., 2003). To distinguish between these possibilities, anaphase forces were reduced by depleting the G-protein regulators, GPR-1/2 in wild-type and *klp-7(tm2143)* embryos (Colombo et al., 2003; Gotta et al., 2003; Srinivasan et al., 2003). Consistent with previous studies, *klp-7(tm2143)* embryos showed a significant reduction in the amount of midzone MTs compared to wild-type (Figure 3-8, p=0.0007). RNAi against *gpr-1/2* in the *klp-7(tm2143)* background significantly restored midzone MTs compared with *klp-7(tm2143)* (p=0.0062). *gpr-1/2(RNAi)* embryos showed the highest level of overlapping MTs (Figure 3-8). Therefore the amount of midzone MTs was inversely correlated with the strength of the anaphase pulling force, suggesting that the extent of the midzone MT network is dependent on the rate of pole-pole separation during mitotic anaphase. I conclude that during anaphase KLP-7 influences the midzone MT levels by limiting centrosome separation rates, rather than directly regulating MT levels at the midzone.

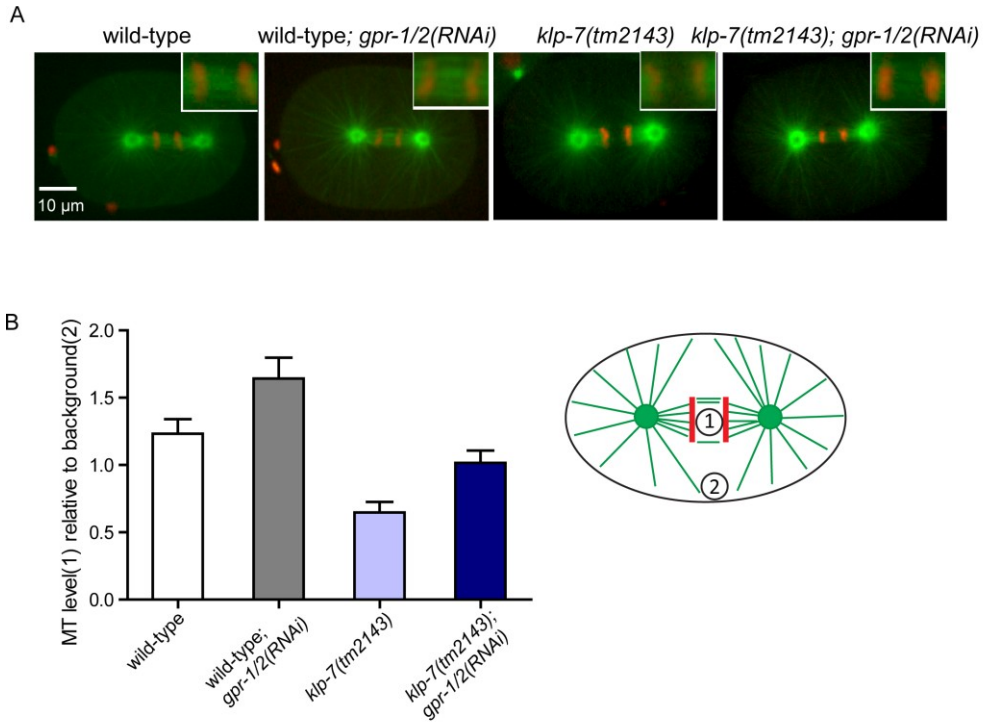

Figure 3-8 *gpr-1/2(RNAi)* restores midzone MTs in *klp-7(tm2143)* embryos

(A) Representative images of wild-type, *gpr-1/2(RNAi)*, *klp-7(tm2143)* and *klp-7(tm2143); gpr-1/2(RNAi)* embryos at anaphase, mitosis. MTs are in green and DNA is in red. (B) Quantification of GFP::β-tubulin fluorescence at the midzone from single frames of images as in Figure 3-8 A. Fluorescence intensities of a circular region (15 pixel diameter) at the midzone (1) and at the background cytoplasmic area (2) were measured. Relative fluorescence intensity values (the absolute intensity of midzone-background/background) are shown for wild-type (white, n=8), *gpr-1/2(RNAi)* (gray, n=9), *klp-7(tm2143)* (light blue, n=12) and *klp-7(tm2143); gpr-1/2(RNAi)* (dark blue, n=13) embryos.

3.4 KLP-7 protein is phosphorylated *in vivo*

Phosphorylation by Aurora kinases plays an important role in MCAK location and function. In vertebrate systems, MCAK localization to chromatin and spindle poles is regulated via phosphorylation by Aurora B

kinase and Aurora A kinase, respectively (Andrews et al., 2004; Lan et al., 2004; Ohi et al., 2004; Zhang et al., 2008; Zhang et al., 2007). Aurora B kinase phosphorylates MCAK to inhibit MT depolymerization activity at the chromatin/kinetochore in cultured cells and *Xenopus* egg extracts (Andrews et al., 2004; Lan et al., 2004; Ohi et al., 2004). Aurora A kinase phosphorylates MCAK at the spindle poles to promote Ran–dependent spindle bipolarity (Zhang et al., 2008). KLP-7 has twelve putative Aurora kinase sites, as determined by the group-based phosphorylation predicting and scoring method (Figure 3-9) (Zhou et al., 2004). Therefore, I reasoned that the Aurora kinases could be important regulators of KLP-7 in *C. elegans*. In worms, Aurora B kinase (AIR-2) is a chromosomal passenger complex protein implicated in meiotic and mitotic spindle functions and Aurora A kinase (AIR-1) is involved in centrosome maturation and mitotic spindle assembly (Hannak et al., 2001; Kaitna et al., 2002; Rogers et al., 2002; Schumacher et al., 1998a; Schumacher et al., 1998b; Severson et al., 2000; Woollard and Hodgkin, 1999). Because of the overlapping localizations of KLP-7 with AIR-1 and AIR-2 at centrosomes and chromosomes respectively, I sought to determine the role that Aurora kinases might play in either localizing or regulating KLP-7. Severe phenotypes and pleiotropy associated with *air-1(RNAi)* and *air-2(RNAi)* prevented a simple genetic experiment to determine if the Aurora kinases are in the same pathway as KLP-7. Therefore I used a more direct

structure-function analysis of KLP-7 to test the hypothesis that worm kinesin-13 is regulated by the Aurora kinases *in vivo*.

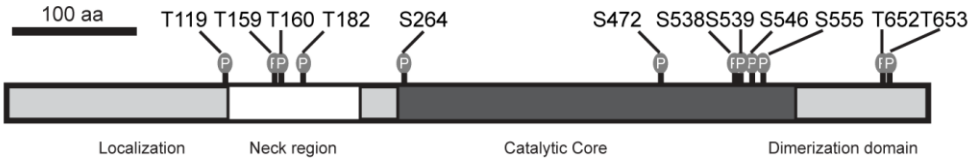

Figure 3-9 KLP-7 has multiple candidate Aurora kinase sites

Structure of the KLP-7 protein is shown. N- and C- termini are in light grey. Catalytic core (motor domain) is in dark grey. Phosphorylation sites (P) are predicted by GPS (Zhou et al, 2004).

I first looked for evidence of *in vivo* phosphorylation of KLP-7 using Phos-tag SDS-PAGE followed by immunoblotting with anti-KLP-7 antibody. Immunoblots of wild-type lysates revealed two bands that migrated more slowly than expected for KLP-7 (predicted MW of 80 KDa). Treatment of the lysate with protein phosphatase resulted in a single band at 80 KDa, which likely represents non-phosphorylated KLP-7 (Figure 3-10). I concluded that the KLP-7 protein is phosphorylated *in vivo,* possibly at multiple sites.

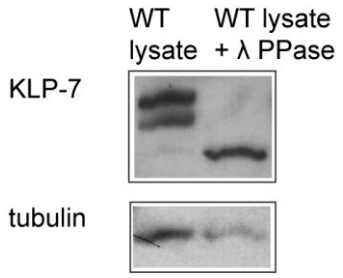

Figure 3-10 The endogenous KLP-7 protein is phosphorylated by Phos-tag SDS PAGE

Phos-tag SDS PAGE and western blot analysis of wild-type untreated lysate and phosphatase treated lysate with anti-KLP-7 antibody. Two protein bands migrating at molecular weights higher than 80 kDa were recognized by anti-KLP-7 antibody in wild-type lysate. These protein bands represent the phosphorylated forms of KLP-7. A single protein band migrating at 80 kDa (the predicted MW of KLP-7) was observed in phosphatase treated lysate. This protein band represents the non-phosphorylated form of KLP-7. Migration of tubulin protein on Phos-tag gel was not affected by phosphatase treatment.

To determine whether the mobility shift of phosphorylated KLP-7 was altered by Aurora kinase activity *in vivo*, I collected lysates from wild-type, *air-1(RNAi), air-2(RNAi)* and *air-1(RNAi);air-2(RNAi)* worms. For each RNAi experiment, expected phenotypes were observed by fluorescence microscopy, confirming effective knockdown (eg. centrosome maturation defect for *air-1(RNAi);* cytokinesis defect for *air-2(RNAi))*. Using this approach, I did not observe an obvious change in KLP-7 mobility on Phos-tag SDS PAGE (Figure 3-11). Since KLP-7 also functions in worm neurons (see Appendix 1), it is possible that any potential difference is masked by the KLP-7 protein expressed in adult neurons, which is refractory to RNAi

treatment. To rule out this possibility, I collected RNAi-treated embryos and performed Phos-tag SDS PAGE. No obvious differences in KLP-7 mobility were observed for wild-type and kinase-knockdown embryos (Figure 3-12). From the above results, I concluded that knock-down of Aurora kinases by RNAi did not significantly alter the phosphorylation state of KLP-7, or that subtle changes in phosphorylation occurred that were not detectable via the Phos-tag assay.

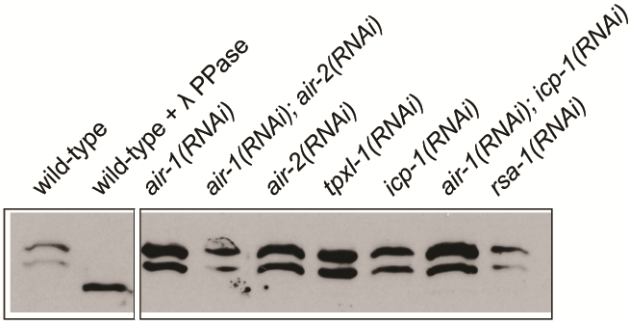

Figure 3-11 Knocking down Aurora kinases and all known kinase activators do not change KLP-7 phosphorylation in whole worms by Phos-tag SDS PAGE

Phos-tag western blotting of wild-type and kinase knockdown lysates with anti-KLP-7 antibody. 20 RNAi treated young adult hermaphrodites were loaded for each lane. Note that the lower band was only found in whole worms and not in embryos (compared to Figure 3-12).

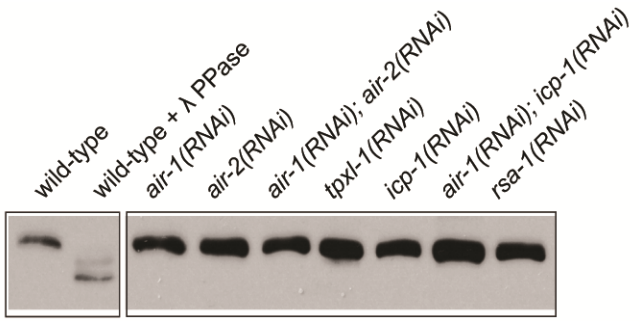

Figure 3-12 Knocking down Aurora kinases and all known kinase activators do not change KLP-7 phosphorylation in embryos by Phos-tag SDS PAGE

A Phos-tag western blot similar to Figure 3-11. Embryos from 50-70 RNAi treated young adult hermaphrodites were collected and loaded to each lane.

3.5 Aurora kinase activity has a subtle effect on the mobility of endogenous KLP-7 via 2D gel electrophoresis.

In order to resolve any differentially phosphorylated forms of KLP-7, I next looked for Aurora-dependent mobility shifts in KLP-7 via 2D gel electrophoresis. Using this approach, I observed ten distinct protein species detected by anti-KLP-7 antibody, indicating different putative phospho-isoforms of the endogenous KLP-7 protein. When compared to wild-type lysate, *air-1(RNAi)* resulted in a relative increase in at least one species of KLP-7, consistent with reduced phosphorylation (Figure 3-13; right side of isoelectric axis). *air-2(or207ts)* (a temperature sensitive loss-of-function allele of *air-2*) caused many changes in the overall pattern of KLP-7 migration, some of which could represent increased or decreased phosphorylation. Although the overall migration pattern of KLP-7 species

suggested that the protein could be post-translationally modified by other regulatory enzymes, I concluded that KLP-7 is likely a substrate of both Aurora kinases *in vivo.*

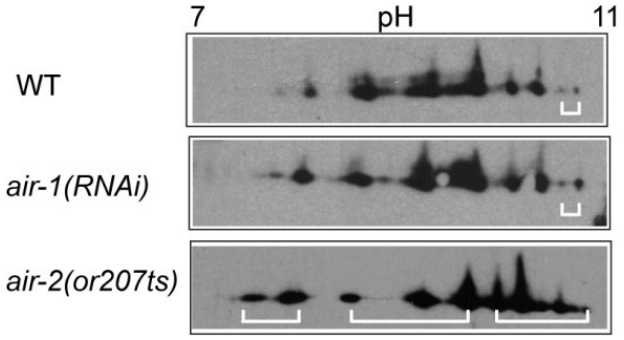

Figure 3-13 2D gel analysis of wild-type and kinase knockdown lysate

2D gel electrophoresis analysis of KLP-7 phosphorylation with wild-type (top), *air-1(RNAi)* (middle) and *air-2(or207ts)* (bottom) whole worm lysates, followed by immunoblotting with anti-KLP-7 antibody. pH gradient is indicated. Protein spots of lower pI (left): phosphorylated isoforms. Protein spots of higher pI (right): non-phosphorylated isoforms. White brackets: putative phospho-isoforms that are different in wild-type and kinase knockdown lysates.

3.6 AIR-1 and AIR-2 directly phosphorylate KLP-7 *in vitro*

In order to verify that KLP-7 is an Aurora substrate, I performed *in vitro* kinase assays on bacterially-expressed GST-KLP-7 proteins. Full-length KLP-7 was insoluble, therefore, I expressed soluble KLP-7 fragments that covered clusters of putative Aurora sites at the N-terminus and the C-terminus with part of the catalytic core domain, including KLP-7-N (a.a. 2-189), KLP-7-CC (a.a. 487-689) and KLP-7-CC2 (a.a. 501-620).

Previous work has shown that the *C. elegans* INCENP protein, ICP-1, promoted AIR-2 phosphorylation of maltose binding protein (Bishop and Schumacher, 2002). Using AIR-2-KLP-7-N and AIR-2-KLP-7-CC2 enzyme-substrate combinations in the *in vitro* kinase assay, I observed that both KLP-7-N and KLP-7-CC2 fragments were efficiently phosphorylated by AIR-2/ICP-1 enzyme complex (Figure 3-14).

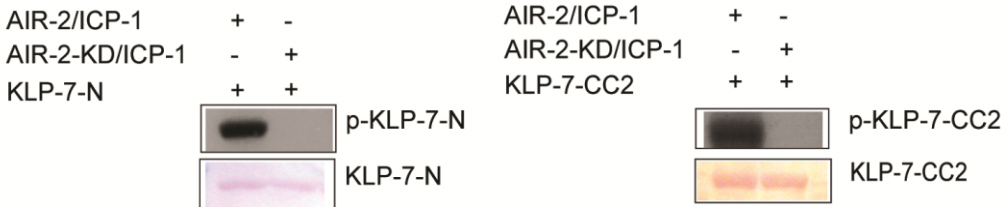

Figure 3-14 KLP-7-N and KLP-7-CC2 fragments were efficiently phosphorylated by AIR-2/ICP-1

Bacterially expressed KLP-7 fragments were purified and incubated with AIR-2 (or AIR-2-KD) and radioactive ATP. Proteins in the kinase assays were separated by SDS-PAGE. Phosphorylation was visualized by autoradiography. Ponceau-S staining was used to as the loading control.

I also tested whether AIR-1 could phosphorylate KLP-7 *in vitro*. In this case, the N-terminus and the C-terminus with part of the core domain of KLP-7 were only very weakly phosphorylated by AIR-1 (Figure 3-15). This suggested that KLP-7 is not an effective substrate for AIR-1. Aurora A may require specific activators to facilitate phosphorylation of substrates *in vitro*. This is the case for Aurora B, which requires the activator INCENP

(Inner centromere protein, which is encoded by the *icp-1* gene in *C. elegans*) for efficient phosphorylation of substrates *in vitro*. TPX2 (Targeting Protein for *Xenopus* Klp2) has been show to target Aurora A to spindles in both human cells and *C. elegans* and promote Aurora A kinase activity on histone H3 *in vitro* (Bayliss et al., 2003; Kufer et al., 2002; Ozlu et al., 2005). AIR-1 and TPXL-1 colocalize along astral MTs, with enrichment near the centrosome (Ozlu et al., 2005). Therefore, TPXL-1 could facilitate AIR-1 activity for KLP-7 phosphorylation *in vitro*. In order to test this idea, I added bacterially expressed TPXL-1 protein to the kinase assay. I found that AIR-1-TPXL-1 efficiently phosphorylated both the N-terminal and the C-terminal fragments of KLP-7 (Figure 3-15). From the above observations, I conclude that both AIR-1 and AIR-2 directly phosphorylate the N-terminus and the C-terminus with part of the catalytic core domain of KLP-7 *in vitro*, and that TPXL-1 promotes AIR-1 kinase activity on KLP-7.

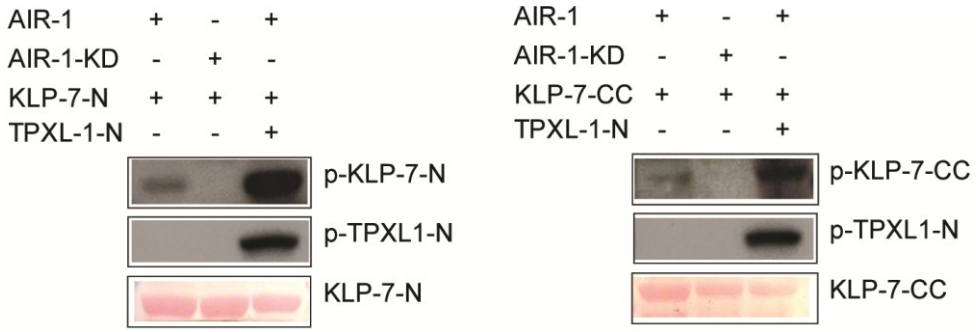

Figure 3-15 AIR-1 phosphorylates the N-terminus and Core domain with the C-terminus of KLP-7 *in vitro*, and that TPXL-1 increases AIR-1 kinase activity on KLP-7

Bacterially expressed KLP-7 fragments were purified and incubated with AIR-1 (or AIR-1-KD) and radioactive ATP in the presence or absence of TPXL-1-N. Proteins in the kinase assays were separated by SDS-PAGE. Phosphorylation was visualized by autoradiography. Ponceau-S staining was used to as the loading control.

3.7 Identification of *in vitro* Aurora kinase phosphorylation sites on KLP-7 by mass spectrometry

Based on *in vitro* kinase results and the predicted Aurora phosphorylation sites on KLP-7 (Zhou et al., 2004), I asked if all the sites are equally preferred *in vitro*. To answer this question, *in vitro* kinase assay reactions were analyzed by Liquid Chromatography with Tandem Mass Spectrometry Detection (LC-MS/MS) at UVic Genome BC PROTEOMICS CENTRE. By using this method, I identified T119 and S538 as important phosphorylation sites of Aurora B kinase at the N-

terminus and the C-terminus with part of the catalytic core domain (Table 3-3 and 3-4).

Table 3-3 Phosphorylation sites identified by LC-MS/MS analysis of the AIR-2/ICP-1 and KLP-7-N kinase-substrate combination

Protein	**Phosphorylation sites**
KLP-7	K.RPTGAFTQHVPVR.M (T119)
ICP-1	R.NAAYSGTPR.R (S167)
	R.MQQMSISK.K (S150)
	K.RGSSAVWK.K (S598, S599)
	R.NIFSSTPGR.M (S189, S190)
	K.SPSTLNTSSR.T (S612)
	K.VEILIGSDGQK.T (S337)
	K.KSPSTLNTSSR.T (S607, T608, T611)
	K.IFPTAESTSTPGR.G (S317, S319)
	K.TPPPAAYEMTPPR.T (T504, Y510)
	K.ISSIFDEVSEAHDDAAAK.V (S27, S28, S34)
	R.AGSVATDGDFEEDILPVTLKR.M (S127)
	K.NDYGLNDLNSDDETDQEDDPRK.D (Y526)
	R.SAHAASSSTSNVEAAAALAALQEQQR.I (S393, S398, S400, S402)
	K.AKPAQPSSSSHRGDDDMETDEVETDQAGPITPR.A (T110)

Phosphorylated peptides are listed. Phosphorylation sites are underlined.

Table 3-4 Phosphorylation sites identified by LC-MS/MS analysis of the AIR-2/ICP-1 and KLP-7-CC2 kinase-substrate combination

Protein	**Phosphorylation sites**
KLP-7	R.N<u>S</u>SHVPFR.Q (S538)
ICP-1	R.NAAY<u>S</u>GTPR.R (S167)
	R.MQQM<u>S</u>ISK.K (S150)
	K.RG<u>SS</u>AVWK.K (S598, S599)
	R.NIF<u>SS</u>TPGR.M (S189, S190)
	K.KSP<u>S</u>TLNT<u>S</u>SR.T (S607, S612)
	K.VEILIG<u>S</u>DGQK.T (S337)
	K.IFPTAE<u>S</u>T<u>S</u>TPGR.G (S317, S319)
	K.<u>T</u>PPPAA<u>Y</u>EMTPPR.T (T504, Y510)
	K.I<u>SS</u>IFDEVSEAHDDAAAK.V (S27, S28)
	R.AG<u>S</u>VATDGDFEEDILPVTLK.R (S127)
	K.ND<u>Y</u>GLNDLNSDDETDQEDDPRK.D (Y526)
	R.<u>S</u>AHAA<u>S</u>S<u>STS</u>NVEAAAALAALQEQQR.I (S393, S398, S400, T401, S402)
	R.T<u>Y</u>QNNSKNDYGLNDLNSDDETDQEDDPRK.D (Y518)
	K.AKPAQPSSSSHRGDDDME<u>T</u>DEVETDQAGPITPR.A (T110)

Phosphorylated peptides are listed. Phosphorylation sites are underlined.

I also attempted to identify critical Aurora A sites on KLP-7 *in vitro*. Even though phosphorylation was observed by autoradiography, no Aurora A-dependent phosphorylation site on KLP-7 was identified by LC-MS/MS analysis (Table 3-5). However, this experiment did not yield complete sequence coverage with peptides derived from trypsin digestion (Figure 3-16). Several peptides with putative kinase sites (eg. T159, T160

and T182 at the N-terminus; S546 and S555 at the core domain) were not recovered in above LC-MS/MS analysis.

Table 3-5 A phosphorylation site on TPXL-1 was identified by LC-MS/MS analysis of the TPXL-1, AIR-1 and KLP-7-N kinase assay reaction

Protein	**Phosphorylation site**
TPXL-1	DYSRL<u>S</u>SSPSR (S30)

One phosphorylated peptide was identified. The phosphorylation site is underlined.

A
AIR-2/ICP-1 and KLP-7-N kinase-substrate combination
Sequence Coverage: 122/188
KLP-7-N:
1 LVVGMHVEI KRSDGR**IHGA VIAEVK**SNGR **FMVEWYEKGE TKGKESSLEE**
51 **LLTLNPSLQA PKPTPPPQPP QKTLQASTAV NRQNGIHAQS MILDDEDTFL**
101 **LDHINMIPAK GASANKRPTG AFTQHVPVRM APPSEKPLPT RR**APSPKEDA
151 APAPKSTRTT AAFKPDLDST AITVPKHTAR RTVVVAPAP

B
AIR-2/ICP-1 and KLP-7-CC2 kinase-substrate combination
Sequence Coverage: 72/120
KLP-7-CC2:
501 ERGQDTRECD RDTR**KEGANI NTSLLALK**EC IRGMAR**NSSH VPFR**QSKLTM
551 VLRDSFIGEK SR**TVMISMIS PGISSSDHTL NTLR**YADR**VK EMGTDGSGEA**
601 **TPIRDEELFL PPSADK**SDEE

C
AIR-1, TPXL-1 and KLP-7-N kinase-substrate combination
Sequence Coverage: 120/188
KLP-7-N:
1 LVVGMHVEI KRSDGR**IHGA VIAEVK**SNGR **FMVEWYEKGE TK**GK**ESSLEE**
51 **LLTLNPSLQA PKPTPPPQPP QKTLQASTAV NRQNGIHAQS MILDDEDTFL**
101 **LDHINMIPAK GASANKRPTG AFTQHVPVRM APPSEKPLPT RR**APSPKEDA
151 APAPKSTRTT AAFKPDLDST AITVPKHTAR RTVVVAPAP

Figure 3-16 Sequence coverage yielded by LC-MS/MS analysis

The sequences of KLP-7 truncations used in kinase assays followed by LC-MS/MS analyses are shown. Matched peptides are in bold. Putative Aurora kinase motifs are underlined.

3.8 Identification of *in vitro* Aurora kinase phosphorylation sites on KLP-7 by *in vitro* kinase assays

Since I was unable to confirm many of the putative Aurora sites on KLP-7 by LC-MS/MS analysis, I decided to mutate each site within the N-terminus and the C-terminus and compare the phosphorylation signal with

wild-type substrates in the *in vitro kinase* assays. Four putative sites are in the N-terminus and the neck region of KLP-7 (T119, T159, T160, and T182). Because both AIR-1 and TPXL-1 are efficient substrates of AIR-1, I fused the N-terminus of TPXL-1 (a.a. 1-63) (Ozlu et al., 2005) to AIR-1 to enhance AIR-1 activity and limit the background phosphorylation to a single TPXL-1-AIR-1 band on the protein gel. I found that, as with the individually added proteins, the TPXL-1-AIR-1 fusion also efficiently phosphorylated KLP-7-N protein (Figure 3-17). By performing the *in vitro* kinase assay I found that an equivalent mass of the T119A mutant form of KLP-7 exhibited a lower level of phosphorylation by AIR-1-TPXL-1 and AIR-2/ICP-1, based on autoradiography exposure (Figure 3-17 and 3-18). In contrast, the single T182A mutant and the double T159A160A mutant were still phosphorylated to levels similar to wild type, suggesting that T119 had a major effect on Aurora phosphorylation *in vitro*. Since T119A was still weakly phosphorylated in the kinase assays, I considered the possibility that the other three consensus sites were also phosphorylated by Aurora kinases, albeit at low efficiency. To test this possibility, I generated a KLP-7 mutant protein with all four residues changed to alanines (KLP-7-N4A). The KLP-7-N4A protein was not phosphorylated by AIR-1-TPXL-1 or AIR-2/ICP-1 (Figure 3-17 and 3-18). Therefore, I concluded that *in vitro* phosphorylation of the N-terminus of KLP-7 by AIR-1 and AIR-2 is primarily dependent on the T119 residue, but that T159,

T160 and T182 together facilitate efficient phosphorylation of the N-terminus of KLP-7.

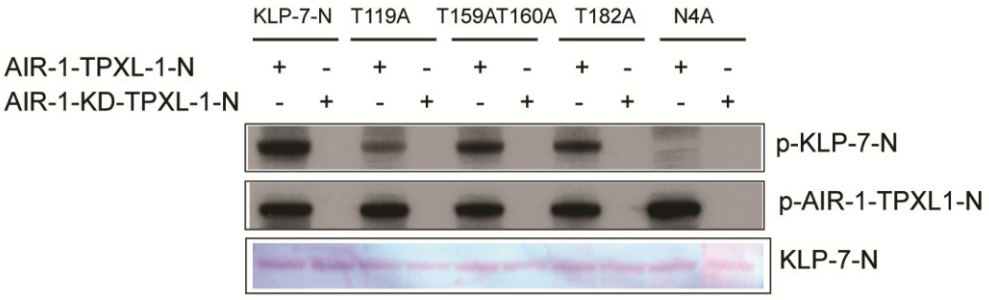

Figure 3-17 AIR-1-TPXL-1-N phosphorylates KLP-7 N-terminus primarily at T119, and weakly at T159, T160 and T182 *in vitro*

In vitro phosphorylation of KLP-7 N-terminus by AIR-1-TPXL-1 is reduces by T119A mutation, and eliminated by N4A mutations. Phosphorylation was visualized by autoradiography.

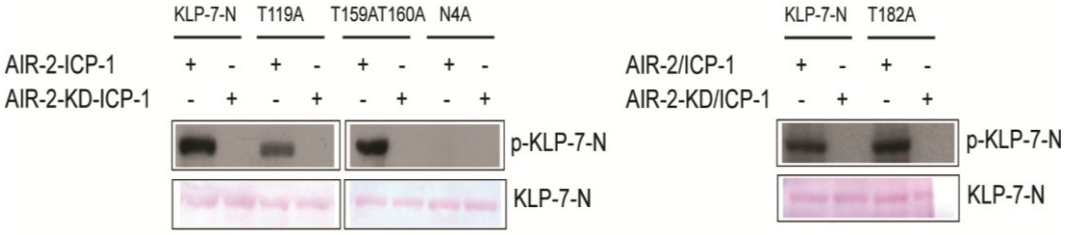

Figure 3-18 AIR-2/ICP-1 phosphorylates KLP-7 N-terminus primarily at T119, and weakly at T159, T160 and T182 *in vitro*

An *in vitro* kinase assay similar to Figure 3-17. Phosphorylation was visualized by autoradiography.

Despite the fact that there are six candidate sites in the C-terminus with part of the core domain fragment of KLP-7, the phosphorylation

efficiency was low compared to the N-terminus (Figure 3-15). In order to identify the phosphorylation sites at the C-terminus with the core domain, KLP-7 was split into three regions: CC3 (a.a. 501-545), CC4 (a.a. 541-590) and C5 (a.a. 590-689) (Figure 3-19). I found that KLP-7-CC3 (a.a. 501-545) was efficiently phosphorylated by AIR-1-TPXL-1 and AIR-2/ICP-1 *in vitro*. Mutating the two putative Aurora sites S538 and S539 to alanines eliminated phosphorylation of KLP-7-CC3 by AIR-1 and AIR-2 (Figure 3-20). From these observations, I concluded that AIR-1 and AIR-2 phosphorylate the C-terminus with part of the core domain of KLP-7 at S538 and/or S539 *in vitro*.

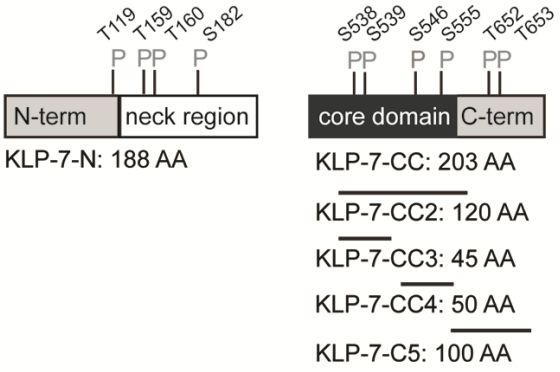

Figure 3-19 KLP-7 fragments used in *in vitro* kinase assays

Each putative Aurora kinase site is marked as a “P”.

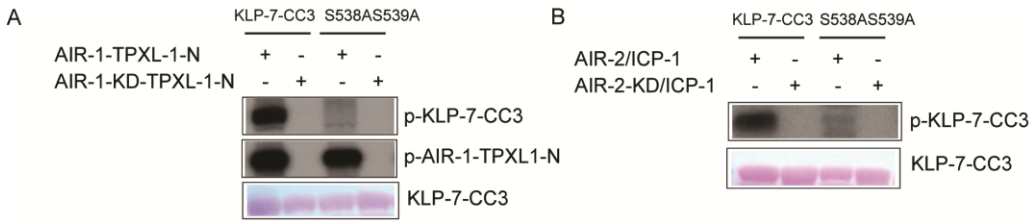

Figure 3-20 AIR-1-TXPL-1-N and AIR-2/ICP-1 kinases phosphorylates KLP-7 CC3 fragment at S538 and/or S539 *in vitro*

KLP-7-CC3 fragment is phosphorylated by AIR-1-TPXL-1(A) and AIR-2/ICP-1(B). S538AS539A mutations abolish phosphorylation of KLP-7-CC3.

Similar kinases assays were performed using the KLP-7-CC4 (a.a. 541-590) and KLP-7-C5 (a.a. 590-689) proteins. I found that KLP-7-CC4 and KLP-7-C5 were phosphorylated only very weakly by AIR-1-TXPL-1-N or AIR-2/ICP-1 kinases *in vitro* (Figure 3-21 and 3-22). Mutating the two putative Aurora sites (T652 and T653 to alanines) in KLP-7-C5 did not alter its phosphorylation status by AIR-1 and AIR-2 (Figure 3-21). However, mutating the two putative Aurora kinases sites (S546 and S555 to alanines) in KLP-7-CC4 resulted in an increase in phosphorylation signal as judged by autoradiography (Figure 3-22). This unexpected result is discussed in Chapter 4.

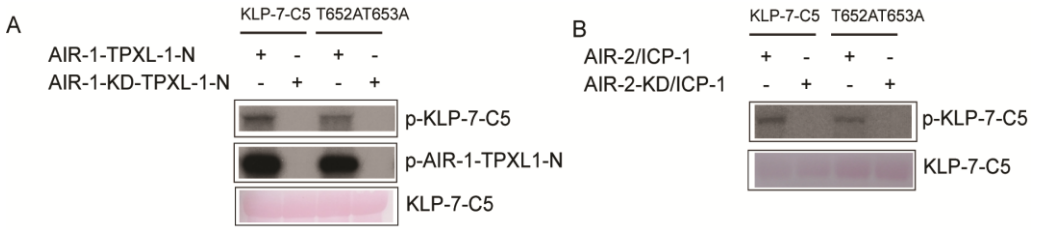

Figure 3-21 KLP-7-C5 protein is not phosphorylated by AIR-1-TXPL-1-N or AIR-2/ICP-1 kinases *in vitro*

Neither KLP-7-C5 nor KLP-7-T652AT653A is phosphorylated by AIR-1 or AIR-2. Phosphorylation was visualized by autoradiography.

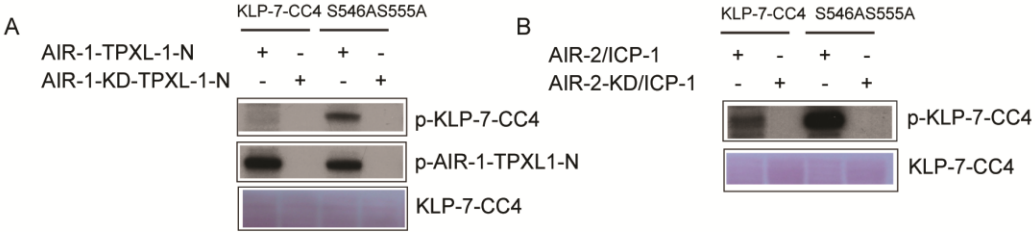

Figure 3-22 KLP-7-CC4 is not phosphorylated by AIR-1-TXPL-1-N or AIR-2/ICP-1 kinases *in vitro*

KLP-7-S546AS555A is phosphorylated by AIR-1 or AIR-2 *in vitro*. Phosphorylation was visualized by autoradiography.

From the above observations, I concluded that *in vitro* phosphorylation of the N-terminus of KLP-7 by AIR-1 and AIR-2 occurs primarily on the T119 residue, and weakly on the other three residues, including T159, T160 and T182. For the six sites clustered within the core domain and the C-terminus, only residue S538 and/or S539 was phosphorylated by AIR-1 and AIR-2 *in vitro* (Figure 3-23).

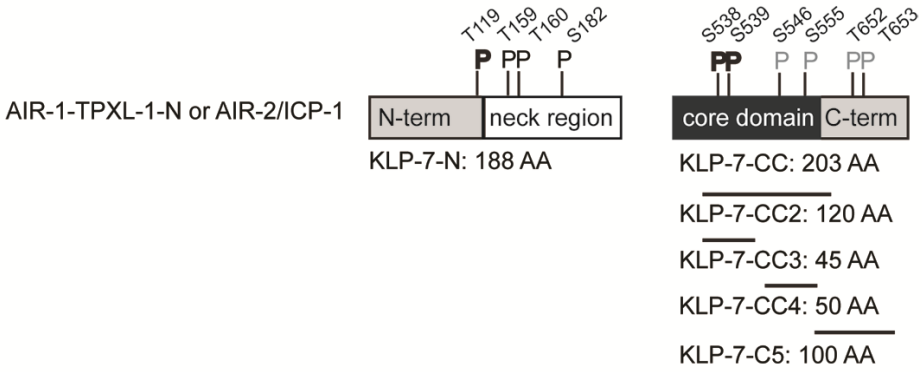

Figure 3-23 Summary of *in vitro* kinase assay results

Substrates used in the *in vitro* kinase assays are shown. Each putative Aurora kinase site is marked as a "P". Black bold: strong phosphorylation; Black regular: weak phosphorylation; Grey regular: no phosphorylation.

3.9 Mutational analysis of putative Aurora kinase sites reveals a role for S546 in KLP-7 function *in vivo*

3.9.1 A structure-function analysis to reveal role of putative Aurora kinases sites in KLP-7 function *in vivo*

Previous work established that Aurora kinases phosphorylate MCAK to regulate its activity with spatial and temporal precision. In the chromatin region, Aurora B kinase phosphorylates MCAK at S196 to inhibit its MT depolymerization activity, and at T95 and S110 to regulate its localization to chromatin (Andrews et al., 2004; Lan et al., 2004; Ohi et al., 2004; Zhang et al., 2007). In *Xenopus* egg extracts without chromatin and centrosomes, Aurora A kinase phosphorylates MCAK at S196 to promote pole focusing and at S719 to promote its localization to spindle poles for

bipolar spindle formation (Zhang et al., 2008). In order to test the putative Aurora phosphorylation sites for their role in KLP-7 function *in vivo*, I used site-directed mutagenesis to create GFP-tagged KLP-7 transgenes that mimic non-phosphorylation (serine or threonine to alanine, S/T to A) and constitutive phosphorylation (serine or threonine to glutamic acid, S/T to E). I then tested their ability to rescue the *klp-7* deletion mutant. The GFP-tagged KLP-7 allowed an assessment of changes in the intracellular location of the mutated proteins (Figure 3-24).

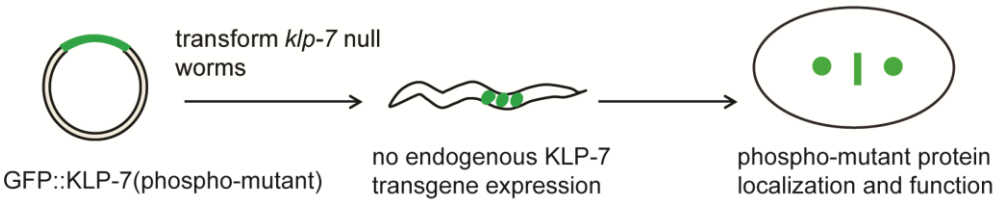

Figure 3-24 Scheme of a structure-function analysis to reveal roles of Aurora phosphorylation of KLP-7 *in vivo*

Phospho-mutant KLP-7 transgenes are expressed in worms without the endogenous protein. The localization and function of each transgene is examined.

3.9.2 Considerations in expressing the GFP::KLP-7 transgene

There are two putative splice isoforms of *klp-7*, both of which were confirmed by cDNAs (Figure 3-25). The two isoforms differ in that exon-1 was only included in the “a” isoform (the longer isoform). I decided to use a genomic sequence encoding the “b” isoform (the shorter isofrom) to generate GFP::KLP-7 for the following reasons: 1) previous work had

success in expressing this transgene in worms and the localization pattern of the protein produced by this transgene is consistent with immunostaining results by using anti-KLP-7 antibody (Oegema et al., 2001; Schlaitz et al., 2007); 2) this DNA fragment is shorter and more convenient for the subsequent molecular cloning work. Since GFP::KLP-7 transgenes will be used in the following structure-function studies, I wanted to know whether the shorter isoform was sufficient for KLP-7 function. To answer this question, I performed RNAi against exon-1, which is unique to the longer isoform. I found that RNAi directed against the longer isoform of *klp-7* caused no reduction in embryonic viability. This indicating that, either the RNAi was not effective, or that the longer isoform is not required for KLP-7 function (Table 3-6). RNAi against a region common to both isoforms resulted in a 34% reduction in embryonic viability (Table 3-6). This result suggested that the shorter isoform is likely sufficient for KLP-7 function in *vivo*.

Table 3-6 Knocking down the long isoform of *klp-7* does not reduce embryonic viability at 20°C

RNAi target	Viability (%)	Standard error	# of embryos
exon-1	98.6	0.8	1060
both splice forms	65.7	3.5	1235
wild-type	99.7	0.2	2210
klp-7(tm2143)	34.6	4.1	849

Percentage of embryonic viability indicates the number of hatched worms over total embryos. RNAi against the exon specific to the long isoform of *klp-7* does not reduce embryonic viability. RNAi against a region which is common to both isoforms reduces embryonic viability.

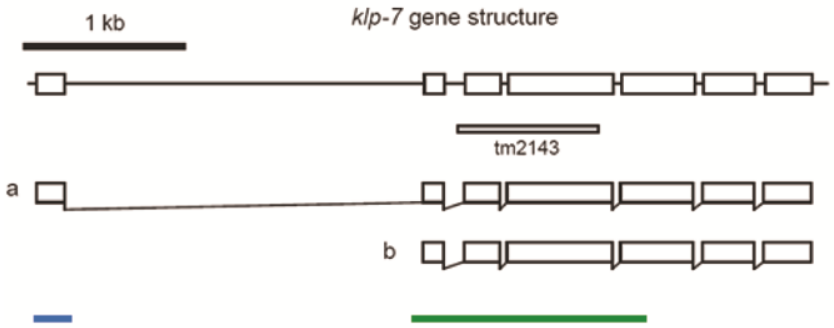

Figure 3-25 Two splice isoforms of KLP-7

There are the two splice isoforms for *klp-7* gene, a and b. Both are confirmed by cDNAs (http://legacy.wormbase.org/). Blue line: a dsRNA fragment targeting exon 1. Green line: a dsRNA fragment targeting both splice forms of *klp-7*.

3.9.3 Experiments to determine whether Aurora kinases influence KLP-7 localization

Previous studies suggested that MCAK localization was regulated by phosphorylation by Aurora A and B kinases in vertebrates (Andrews et al., 2004; Lan et al., 2004; Ohi et al., 2004; Zhang et al., 2007). To test whether KLP-7 localization is regulated by Aurora kinase phosphorylation, I assessed KLP-7 localization in *air-1(RNAi)*, *air-2(or207)* and *air-1(RNAi); air-2(or207)* embryos by using anti-KLP-7 antibody. I found that KLP-7 localized to centrosomes and kinetochores in kinase knockdown embryos, similar to that in wild-type embryos (Figure 3-26). Live imaging of *air-1(RNAi)* and *air-2(RNAi)* embryos expressing mCherry::tubulin; GFP::KLP-7 also indicated that KLP-7 could still locate to centrosomes and kinetochores (Figure 3-27). GFP::KLP-7 fluorescence was reduced at the centrosomes in *air-1(RNAi)* embryos in mitosis. However, this observation may not reflect a specific role of AIR-1 in KLP-7 localization, as *air-1(RNAi)* embryos are defective in the recruitment of all other centrosome components (Hannak et al., 2001).

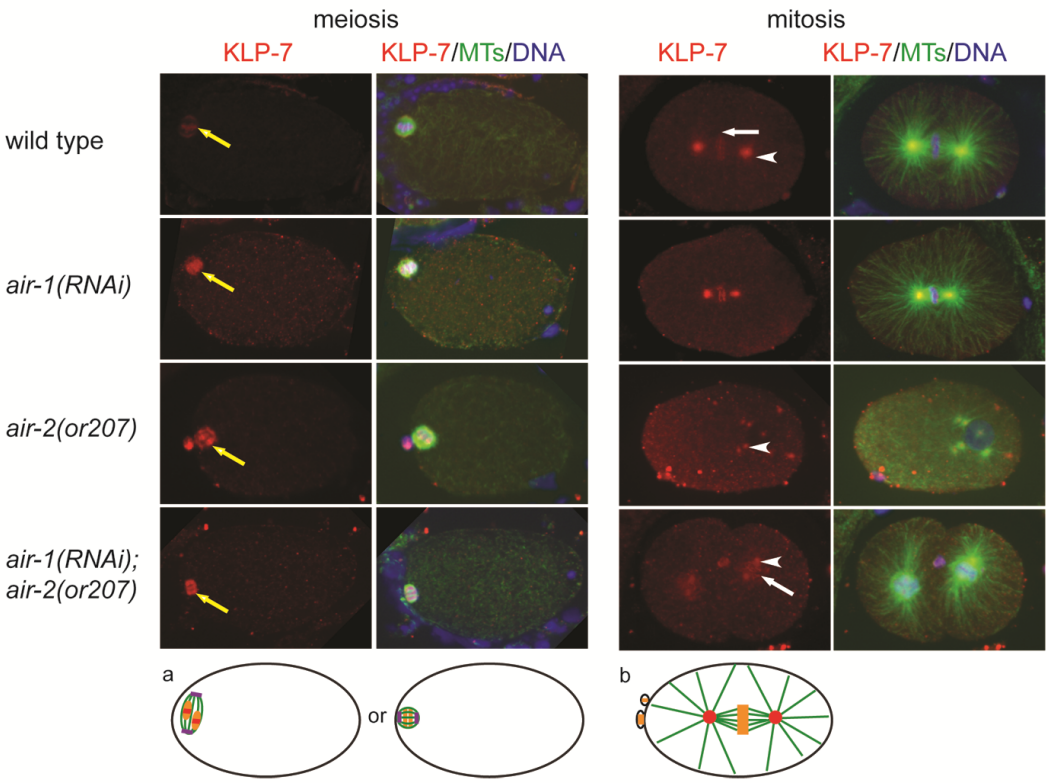

Figure 3-26 KLP-7 immunofluorescence at centrosomes and kinetochores in Aurora kinase knockdown embryos

Wild-type, *air-1(RNAi)*, *air-2(or207)* and *air-1(RNAi); air-2(or207)* embryos were fixed and stained for MTs (green), KLP-7 (red) and DNA (blue). Meiotic (left) and mitotic (right) embryos were imaged. Yellow arrow: KLP-7 localization during meiosis; White arrow: kinetochore localization of KLP-7 during mitosis; White arrow head: centrosome localization of KLP-7 during mitosis. Schematics show KLP-7 immunofluorescence in meiotic (a) and mitotic (b) embryos. In meiotic embryos (a), KLP-7 immunofluorescence was found at spindle poles (purple), chromosomes (orange), and the chromosomal passenger complex region (red). In mitotic embryos (b), KLP-7 immunofluorescence was found at kinetochores (orange) and centrosomes (red). KLP-7 localization in kinase knockdown embryos is similar to that of wild-type embryos.

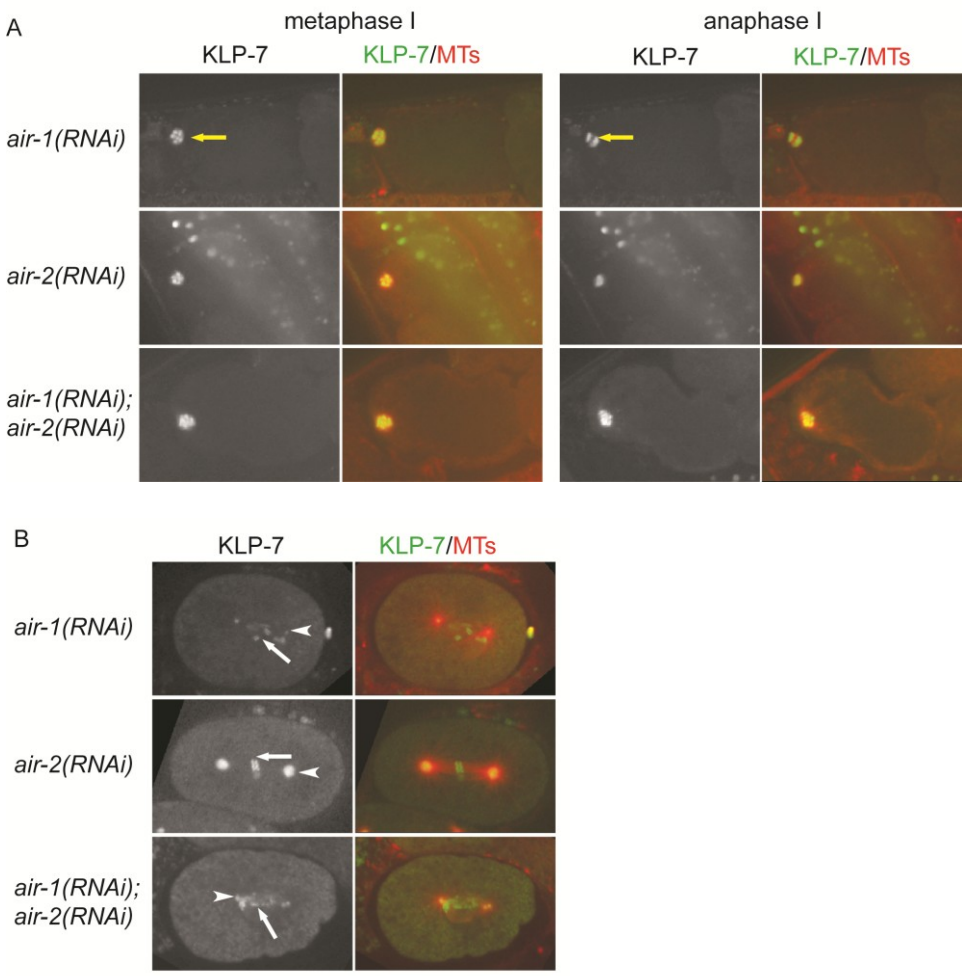

Figure 3-27 GFP::KLP-7 localization in Aurora kinase knockdown embryos

Meiotic (A) and mitotic (B) embryos were treated with *air-1(RNAi)*, *air-2(RNAi)* or *air-1(RNAi); air-2(RNAi)*. MTs are in red and KLP-7 is in green. GFP::KLP-7(S539A) was used instead of GFP::KLP-7(WT), as GFP::KLP-7(WT) was linked to the mCherry::tubulin transgene so that it is difficult to generate a strain with both transgenes. GFP::KLP-7(S539A) and GFP::KLP-7(WT) rescued *klp-7(tm2143)* embryonic lethality to a similar level (Table 3-7). Yellow arrow: chromosomes in meiotic embryos; white arrow: chromosomes in mitotic embryos; arrow head: centrosomes.

To determine the essential Aurora sites for KLP-7 regulation *in vivo*, I generated a series of phospho-mutant *klp-7* transgenic worms. I was unable to obtain every possible mutant combination; however, I tested multiple residues in regions with clusters of kinase sites for both non-phosphorylation and constitutive phosphorylation (Table 2-3 and Table 3-7). Fluorescence microscopy indicated that the intracellular location of transgenes with mutations in individual Aurora kinase sites and groups of up to 8 sites was not obviously different from the pattern displayed by GFP::KLP-7(WT) (Figure 3-28). One mutant transgene with mutations in 10 putative Aurora kinase sites (10E) resulted in loss of intracellular location of KLP-7 (Figure 3-28). Western blots of lysates from KLP-7 (10E) transgenic animals probed with anti-KLP-7 revealed that the fusion proteins were expressed, suggesting that the loss of localization was not due to a lack of protein expression (Figure 3-29).

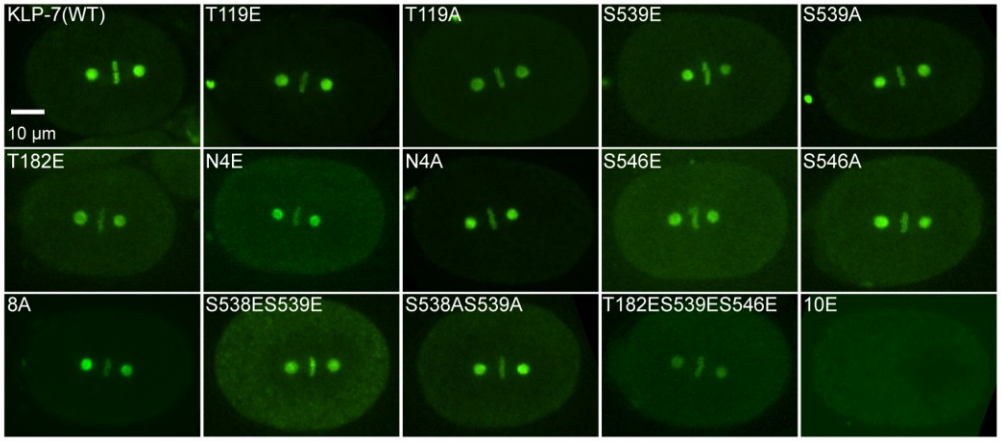

Figure 3-28 Mutating individual putative Aurora kinase sites and groups of up to 8 sites does not affect KLP-7 localization in *C. elegans* embryos

Phospho-mutant KLP-7 proteins localize at centrosomes and kinetochores. Images of metaphase embryos expressing GFP::KLP-7(WT) or GFP::KLP-7(phospho-mutant) transgenes are shown.

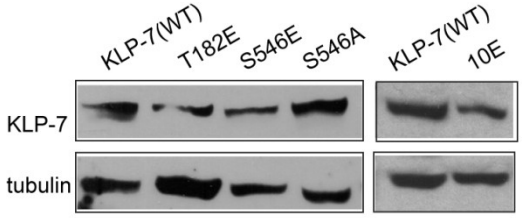

Figure 3-29 Western blot analysis to assess GFP::KLP-7(S546E), GFP::KLP-7(S546A) and GFP::KLP-7(10E) transgene expression

The expression level of GFP::KLP-7(S546E), GFP::KLP-7(S546A) and GFP::KLP-7(10E) transgenes is determined by western blotting transgenic worms with DM1A and anti-KLP-7 antibodies. 70 young adult hermaphrodites were loaded for each lane.

3.9.4 GFP::KLP-7 (S546E) and GFP::KLP-7 (S546A) transgenes fail to rescue *klp-7* loss-of-function phenotypes

Since mutating individual putative Aurora sites and groups of up to 8 sites did not alter KLP-7 localization, I next determined whether any of these sites were essential for KLP-7 function. First, I scored each of the stable transgenic lines for viability. At 25 ºC, *klp-7(tm2143)* worms exhibited low viability (15.9 $\pm$ 4.1% survival). Compared to *klp-7(tm2143),* transgenic worms, including KLP-7(WT), T119A, T119E, T182E, N4A, N4E, S539A, S539E, S538A539A, S538ES539E and 8A showed increased viability, ranging from 40% to 90% (Table 3-7). This suggested that these transgenes retained at least some functionality. In contrast, four worm strains exhibited very low viability (16-30%; Table 3-7). In all of these strains, the S546 residue was mutated (S546A, S546E, T182ES539ES546E and 10E). Protein expression was confirmed for the mutated KLP-7 protein via western blot analyses (Figure 3-29).

Table 3-7 Embryonic viability of phospho-mutant KLP-7 transgenic worms at 25 ºC

genotype	viability(%)	SE(%)	# of embryos
klp-7 (tm2143)	15.9	4.1	768
KLP-7 WT	84.6	7.0	511
T119E	62.0	2.3	508
T119A	87.7	3.7	547
N4E	44.3	5.8	331
N4A	76.0	3.2	481
S538ES539E	49.5	7.0	476
S538AS539A	48.6	3.8	240
S539E	65.3	2.4	677
S539A	84.1	3.1	994
S546E	27.5	3.1	1392
S546A	17.6	1.8	464
T182ES539ES546E	15.7	2.7	548
T182E	53.7	3.7	597
8A	74.3	6.6	361
10E	30.0	1.9	861

Percentage of embryonic viability is the number of hatched worms over total embryos. Expression of GFP::KLP-7(WT) or several GFP-KLP-7(phospho-mutant) transgenes increases embryonic viability of *klp-7(tm2143)* worms. Transgenes which contain mutations in S546 fail to increase embryonic viability of *klp-7(tm2143)* worms.

The rescue experiments indicated that residue S546 was important for the function of KLP-7. Because KLP-7 activity inversely correlates with MT outgrowth and spindle pole separation rates in anaphase, I tested

whether these parameters were specifically affected by the S546 mutations. I found that neither GFP::KLP-7(S546A) nor GFP::KLP-7(S546E) mutations rescued the *klp-7(tm2143)* spindle-snap phenotype (Figure 3-30). Furthermore, neither mutation rescued the increase in microtubule levels at the centrosome characteristic of *klp-7(tm2143)* (Figure 3-31). Based on the fact that GFP::KLP-7(S546E/A) localizes properly but does not rescue viability or the early embryonic phenotypes such as spindle-snap and excessive MTs in mitosis, I concluded that the S546 residue is essential for KLP-7 activity.

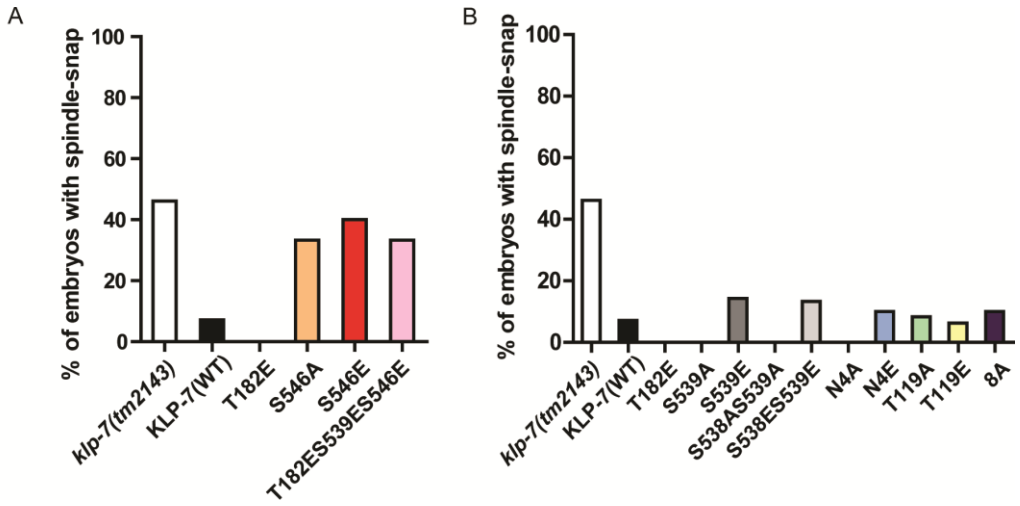

Figure 3-30 GFP::KLP-7(S546E) and GFP::KLP-7(S546A) transgenes fail to rescue spindle-snap phenotype of *klp-7(tm2143)*

Spindle snap was scored as described in Chapter 2. More than 6 embryos were scored for each strain. 40% *klp-7(tm2143)* embryos exhibited spindle-snap at 25 ºC. Similar phenotype was observed when GFP::KLP-7(S546E) or GFP::KLP-7(S546A) transgenes were expressed in *klp-7(tm2143)* background.

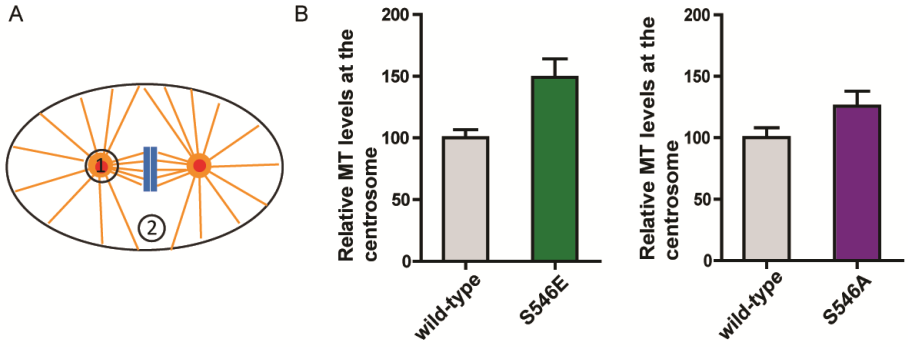

Figure 3-31 GFP::KLP-7(S546E) and GFP::KLP-7(S546A) embryos exhibited an increase in centrosomal MTs

(A) Quantification of centrosomal MTs in fixed embryos stained to reveal α-tubulin (orange) and γ-tubulin (red). The single frame with one centrosome in focus was determined by γ-tubulin fluorescence. The centrosomal MT level is defined as the fluorescence intensity of a circular region (40 pixel diameter) at the centrosome (1) subtracting the intensity at a background cytoplasmic area (2). Relative MT levels are shown. More than 14 centrosomes were analyzed for each strain.

3.9.5 Frap analysis revealed that S546 is essential for dynamic properties of KLP-7

Although the S546 mutants did not alter the localization of KLP-7, it was possible that these sites were critical for dynamic properties of the protein not revealed with conventional microscopy. Therefore, we used fluorescence recovery after photobleaching (FRAP) to measure the turnover of KLP-7 at the centrosome (Figure 3-32). Using this approach, we found similar recovery rates for GFP::KLP-7(WT) and GFP::KLP-7(S546A) (T1/2 = 24.1 and 25.0, respectively) and a slightly faster

recovery for GFP::KLP-7(S546E) (T1/2 = 18.8, Figure 3-32). Because KLP-7 is expected to interact with MTs as part of its depolymerizing function, we next tested KLP-7 protein recovery at the centrosomes in embryos pre-treated with the MT-depolymerizing drug nocodazole. In the nocodazole-treated embryos, GFP::KLP-7(WT) and GFP::KLP-7(S546A) exhibited similar, but much slower recovery rates (T1/2 = 52.2 and 58.1, respectively), suggesting that KLP-7 turnover was at least partially dependent on centrosomal MTs. Interestingly, GFP::KLP-7(S546E) embryos exhibited a recovery rate similar to untreated embryos (T1/2 = 18.2, Figure 3-32). This result suggests that the turnover rates for both WT and S546A forms of KLP-7 are dependent on MTs, and that phosphorylation of S546 may interfere with a phase of KLP-7 loading onto MTs at the centrosome (see Chapter 4 for discussion).

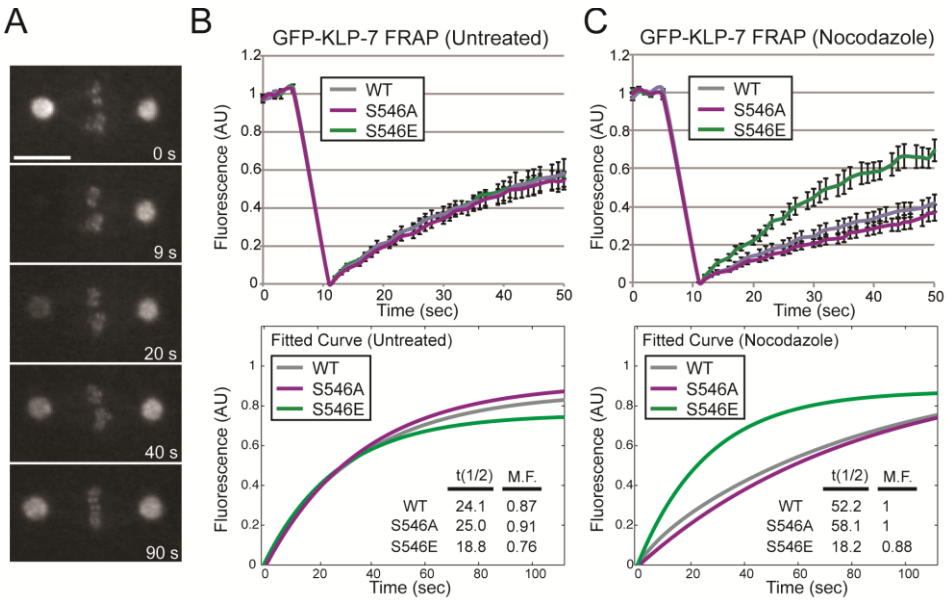

Figure 3-32 Fluorescence recovery after photobleaching of centrosomal GFP::KLP-7

(A) An example of fluorescence recovery of GFP::KLP-7 at the centrosome is shown. One centrosome was photobleached and the fluorescence intensity was measured from images acquired at one second intervals. Bar: 10 µm. (B) Mean centrosomal recovery rates (in arbitrary units) are displayed for the first 50 seconds for WT, S546A and S546E versions of GFP::KLP-7. All embryos were derived from worms grown on *ptr-1(RNAi)* feeding plates to permeabilize the eggshell (refer to Materials and Methods). Bars are SEM (WT untreated: n=5; S546E untreated: n=5; S546A untreated: n=6). (C) Pre-treatment of the embryos with nocodazole reveals a slower recovery time for GFP::KLP-7(WT) and GFP::KLP-7(S546A), compared to untreated embryos. GFP::KLP-7(S546E) recovery is similar in nocodazole treated and untreated samples. Normalized fitted recovery curves (WT nocodazole: n=6; S546E nocodazole: n=6; S546A nocodazole: n=5) are shown below. Insets display the calculated t(1/2) and mobile fractions (M.F.).

4 Discussion and future directions

4.1 KLP-7, a MT-depolymerase in *C. elegans* embryos

4.1.1 Roles of KLP-7 in chromosome segregation during meiosis and mitosis

Vertebrate MCAK proteins play an essential role in chromosome segregation in both meiotic and mitotic divisions. For example, inhibition of MCAK causes defects in chromosome alignment in meiotic *Xenopus* egg extracts and mouse oocytes, as well as chromosome segregation defects resulting from increased MT-kinetochore attachment errors during mitosis (Illingworth et al., 2010; Kline-Smith et al., 2004; Ohi et al., 2004). In my studies I found that loss of KLP-7 resulted in an unequal segregation of chromosomes during meiosis, which likely is responsible for the higher frequency of male progeny and also reduced viability of *klp-7(tm2143)*. I did not however detect chromosome segregation errors in the mitotic embryos of *klp-7(tm2143)*. These observations raise an interesting question: why KLP-7 contributes to faithful chromosome segregation in meiosis but not in mitosis? Differences in the spindle assembly pathways may provide one answer. In the *C. elegans* one-cell embryo, mitotic spindle assembly seems largely dependent on centrosomal MT outgrowth and a “search and capture” mechanism (Kirschner and Mitchison, 1986) to establish MT-kinetochore attachment (Muller-Reichert et al., 2010). The acentrosomal meiotic spindle is assembled by an “inside-out” mechanism, in which MTs initially form around the chromosomes, and then organize to

form a bipolar spindle. Therefore, it is possible that chromatin-based pathways of spindle assembly, such as female meiosis, are more likely to generate MT-kinetochore attachment errors and thus rely more on kinesin-13 activity for proper MT-kinetochore attachments (Figure 4-1). Consistent with this, in *klp-7(tm2143)* embryos meiotic chromosomes were not lined up properly in metaphase I and II spindles. Some *klp-7(tm2143)* embryos exhibited mis-segregation of chromosomes in anaphase I and II. On the contrary, no chromosome alignment errors were observed at metaphase of the first mitotic division in *klp-7(tm2143)* embryos.

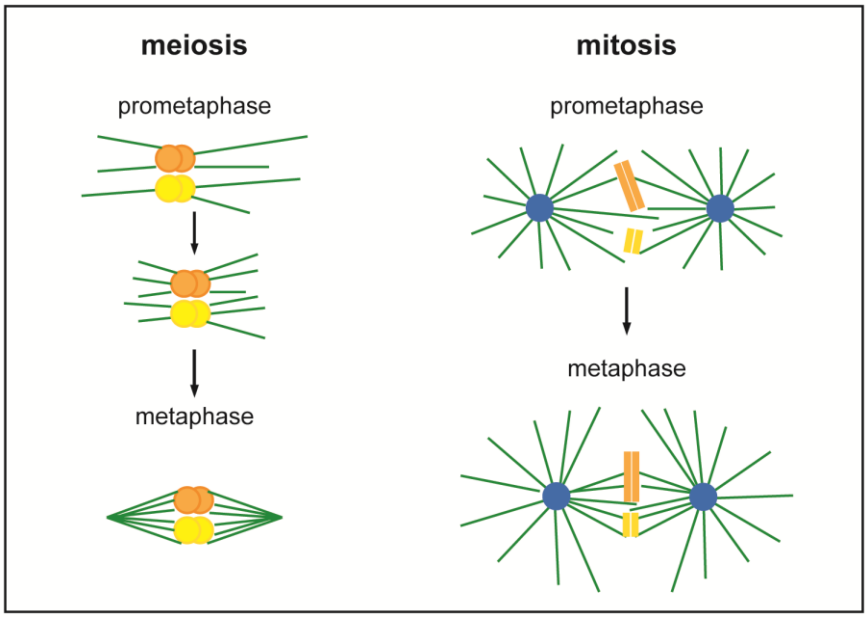

Figure 4-1 Chromatin and centrosome based pathways of spindle assembly

During *C. elegans* female meiosis (left), MTs initially form around the chromosomes and are organized into the meiotic spindle (Srayko et al., 2006). In mitosis (right), MTs grow from the centrosomes and MT-kinetochore attachment is established by a "search and capture" mechanism (Kirschner and Mitchison, 1986). Orange and Yellow: chromosomes, Green: MTs, Blue: centrosomes.

Another possibility as to why KLP-7 is only important in meiotic chromosome segregation is that KLP-7 is just essential during meiotic spindle assembly. *klp-7(tm2143)* embryos showed an increase in cortical MTs and a disorganization of female meiosis I and II spindles. However, in mitosis the morphology of metaphase spindles is relatively normal in *klp-7(tm2143)* embryos. These two possibilities may not be mutually exclusive: more MT-kinetochore attachment errors and disorganized

spindle structures could both contribute to the chromosome segregation defects in *klp-7(tm2143)* embryos during meiosis.

4.1.2 Midzone MTs are inversely correlated with anaphase pulling force

MT-dependent forces are important for chromosomes segregation during anaphase. In vertebrates and *Drosophila*, chromosome to pole movement (anaphase A) is at least in part mediated by depolymerising MTs at the minus end (poleward flux) (Desai et al., 1998; Maddox et al., 2003). In *Drosophila* embryos, spindle elongation (anaphase B) can be driven by pushing forces generated via sliding of antiparallel interpolar MT bundles by kinesin-5 motors [reviewed in (Brust-Mascher and Scholey, 2011)]. Spindle elongation can also be mediated by pulling forces transmitted by astral MTs from contacting the cell cortex. *C. elegans* embryos do not undergo anaphase A in mitosis (Oegema et al., 2001). Thus pole-pole separation is the major mechanism by which chromosomes segregate. Spindle cutting experiments revealed a role of midzone MTs in limiting spindle elongation in *C. elegans* embryos (Grill et al., 2001). Furthermore, no significant poleward flux was observed for spindle MTs in anaphase B, indicating that chromosomes are not “reeled in” to the spindle poles by MT depolymerisation at their minus ends (Labbe et al., 2004). Together, these findings suggest that forces, most likely transmitted by astral MTs, pull the centrosomes away from each other to facilitate chromosome segregation in *C. elegans* embryos.

klp-7(RNAi) embryos exhibit a “spindle-snap” phenotype during anaphase of mitosis (Grill et al., 2003; Schlaitz et al., 2007), which is also observed in *klp-7(tm2143)*. Considering the location of KLP-7 at the kinetochore and the centrosome, there are several possible explanations for how KLP-7 mediates pole-pole separation. One mechanism is that KLP-7 could contribute to the formation of midzone MTs. Loss of KLP-7 could cause midzone MT defects and the formation of a mechanically unstable spindle, which has a weakened resistance to anaphase pulling force. Alternatively, the spindle-snap phenotype could be due to increased numbers of astral MTs contacting cortical force generators to generate excessive pulling forces during anaphase (Srayko et al., 2005). The latter explanation for the loss of midzone MTs implies that the midzone MT array requires a slow, regulated separation of the poles for its assembly. Consistent with this idea, I found that midzone MTs can be restored in the *klp-7(tm2143)* background by reducing anaphase forces via *gpr-1/2(RNAi)*. This observation supports a model whereby KLP-7 is not directly involved in forming midzone MTs. The amount of midzone MTs is dependent on the pole-pole separation rates during anaphase (Figure 4-2).

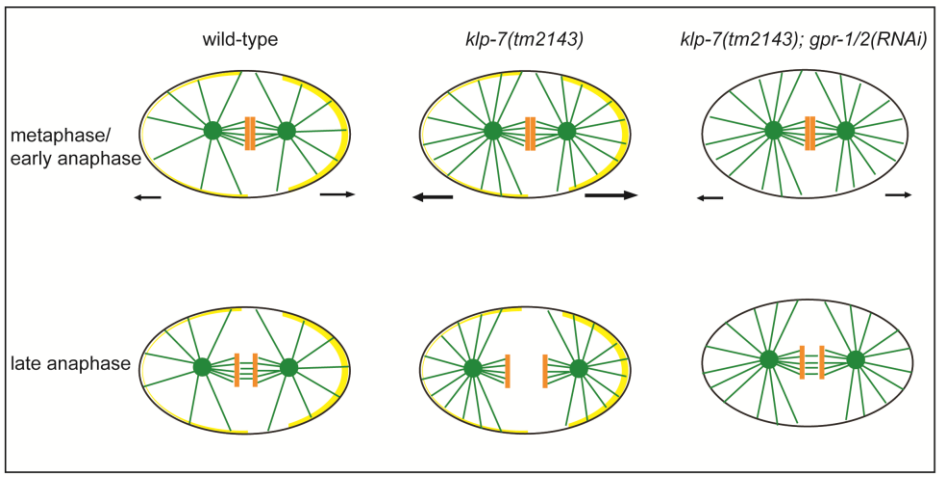

Figure 4-2 Midzone MTs are inversely correlated with pole-pole separation rates during anaphase

Anaphase pulling force is regulated by both force generators (eg. *gpr-1/2*) and the number of astral MTs that contact force generators. *klp-7(tm2143)* embryos had more astral MTs and thus increased anaphase pulling force, which likely causes the spindle-snap phenotype and failure in midzone MTs formation. Anaphase pulling force can be reduced by knocking down *gpr-1/2* in *klp-7(tm2143)* embryos. The spindle-snap phenotype was rescued in these embryos and bundles of midzone MTs formed in-between the separating chromosomes. Green: MTs, Orange: chromosomes, Yellow: GPR-1/2, Black arrows: anaphase pulling force.

4.2 Phosphorylation of KLP-7 by Aurora kinases

4.2.1 Knocking down Aurora kinases resulted in subtle changes of KLP-7 phosphorylation status *in vivo*

The Phos-tag SDS-PAGE analysis shows that endogenous KLP-7 proteins are phosphorylated *in vivo*, possibly at multiple sites. By 2D gel electrophoresis I found that knocking down AIR-1 resulted in a consistent but subtle change of KLP-7 phosphorylation status *in vivo*. One possibility

for the absence of a drastic change in KLP-7 phosphorylation with the loss of AIR-1 could be that only a subset of KLP-7 (*i.e*., the population at the centrosomes) is directly phosphorylated by AIR-1 *in vivo*. Alternatively, of the potential phosphorylation sites predicted on KLP-7, perhaps only one or a few are utilized by AIR-1 to regulate the protein, in which case only subtle mobility shifts would be expected via 2D gel analysis. This is consistent with our data that implicated only S546 in KLP-7 function *in vivo*. In addition, other kinases have been shown to phosphorylate MCAK and regulate its localization and/or activity in mammalian cells, including Cdk1 (Cyclin-dependent kinase 1), PLK1 (Polo-like kinase 1), and PAK1 (p21 activated kinase) (Pakala et al., 2012; Sanhaji et al., 2010; Zhang et al., 2011). Worm homologues exist for all three kinases and they may also regulate KLP-7. If KLP-7 is phosphorylated by multiple kinases in worms, knocking down one of them may not result in an obvious change in the overall charge of KLP-7.

Loss of AIR-2 resulted in a more complex change in KLP-7 mobility, some of which could represent increased or decreased phosphorylation. Loss of a kinase is not expected to result in an increase in phosphorylation, but the effect of AIR-2 loss on KLP-7 may not be direct. It is possible that AIR-2 regulates KLP-7 via direct phosphorylation and also indirect mechanisms such as by activating a phosphatase that dephosphorylates KLP-7, or by inactivating a kinase that phosphorylates KLP-7. In this case subsets of KLP-7 that are directly phosphorylated by AIR-2 will show

decreased phosphorylation in *air-2(or207)* lysates, while subsets of KLP-7 dephosphorylated by a AIR-2-dependent phosphatase will show increased phosphorylation in *air-2(or207)* lysates.

4.2.2 Phosphorylation of KLP-7 by Aurora kinases *in vitro*

Kinase assays performed herein demonstrated that KLP-7 is a direct substrate of AIR-1 and AIR-2 kinases *in vitro*. AIR-1 on its own exhibited weak kinase activity on KLP-7, however, the addition of TPXL-1 resulted in efficient phosphorylation of KLP-7 by AIR-1. Previous work has demonstrated that TPX2 (the vertebrate homologue of worm TPXL-1) stimulates Aurora A kinase activity as judged by phosphorylation of histone H3 or Aurora A autophosphorylation (Eyers et al., 2003; Ozlu et al., 2005; Trieselmann et al., 2003; Tsai et al., 2003). My results from 2D gel electrophoresis analysis and *in vitro* kinase assays, together with the fact that KLP-7, AIR-1 and TPXL-1 all locate at the centrosomes (Ozlu et al., 2005), suggest that KLP-7 is a physiological substrate of the active AIR-1/TPXL-1 complex.

To identify critical Aurora kinases sites on KLP-7 *in vitro*, I first performed LC-MS/MS analysis of *in vitro* kinase assay reactions. By using this approach I identified T119 and S538 as critical Aurora B kinase sites on KLP-7 *in vitro*. No phosphorylation site on KLP-7 was identified in the AIR-1 kinase assay by LC-MS/MS analysis, possibly due to low abundance of phosphopeptide in the AIR-1 reaction. Another challenge with this approach is incomplete sequence coverage with peptides derived

from trypsin digestion. Several peptides containing putative kinase sites (*i.e.* T159, T160 and T182 at the N-terminus; S546 and S555 at the core domain) were not recovered in my LC-MS/MS analysis. Given that almost identical sequence coverage were obtained for two independent LC-MS/MS analyses (AIR-1 KLP-7-N and AIR-2 KLP-7-N), it is likely that phosphorylation site determination by mass spectrometry is very dependent on the particular peptide sequence.

To identify all critical Aurora kinases sites *in vitro*, I next performed site-directed mutagenesis on putative Aurora sites followed by *in vitro* kinase assays. Consistent with results from LC-MS/MS analysis, T119 and S538 and/or S539 are identified as critical *in vitro* phosphorylation sites on KLP-7 for both AIR-1 and AIR-2 kinases. Three putative sites at the N-terminus of KLP-7 (T159, T160, and T182) are weakly phosphorylated by AIR-1 and AIR-2 kinases, while four sites at the C-terminus (S546, S555, T652, and T653) are not phosphorylated in *in vitro* kinase assays. One unexpected result was obtained from the *in vitro* phosphorylation of the core domain fragment KLP-7-CC4 (a.a. 541-590). The wild type protein for this fragment was neither phosphorylated by AIR-1 nor AIR-2 *in vitro*. However, when all putative Aurora sites (S546 and S555) were mutated to alanines (non-phosphorylation), this fragment was efficiently phosphorylated by both AIR-1 and AIR-2 kinases. One possible explanation is that mutating these two amino acids resulted in conformation changes in KLP-7-CC4, so that Aurora kinases can

phosphorylate S/T residues that are not in the canonical phosphorylation motif (6 serine and 4 threonine residues). Testing this idea could require mutating all theses residues to alanines or multiple residues in various combinations.

Although *in vitro* kinase assays have generated very interesting results, there are still potential caveats in these studies. First, all *in vitro* kinase assays were performed by using truncated fragments of KLP-7, due to the insolubility of the full-length protein. Phosphorylation sites that are dependent on phosphorylation/dephosphorylation at other residues will not be identified in above analyses. Furthermore, some phosphorylation sites were identified for both AIR-1 and AIR-2 kinases in *in vitro* kinase assays. It is likely that *in vivo* the substrate specificity of each kinase is determined by the subcellular localization of the kinase or interaction with specific regulators. These factors are not taken into account in the *in vitro* system where only a few purified proteins are included. A better approach for understanding KLP-7 phosphorylation by Aurora kinases is to perform a structure-function analysis to test the role of putative Aurora sites *in vivo.*

4.3 Regulation of KLP-7 by Aurora kinases phosphorylation

4.3.1 KLP-7 localization is not regulated by Aurora kinase phosphorylation

Previous studies suggested that MCAK localization was regulated by phosphorylation by Aurora A and B kinases in *Xenopus* and cultured

cells (Andrews et al., 2004; Lan et al., 2004; Ohi et al., 2004; Zhang et al., 2007). However, the precise mechanism for this regulation can be highly complex and is still not fully understood. For example, centromere localization of *Xenopus* MCAK is increased by Aurora B mediated phosphorylation at S110, and is inhibited by phosphorylation by the same kinase at T95. Similarly, MCAK association with chromosome arms is promoted by Aurora B-dependent phosphorylation at T95 and inhibited by phosphorylation at S196 (Zhang et al., 2007).

In this study I found that individual Aurora kinase sites and groups of up to 8 sites could be altered without affecting the localization of KLP-7 in *C. elegans* embryos. Furthermore, I showed that KLP-7 is detected at centrosomes and kinetochores when the function of either or both Aurora kinases is reduced. GFP::KLP-7 fluorescence was reduced at the centrosomes in *air-1(RNAi)* embryos in mitosis. However, *air-1(RNAi)* embryos are defective in the recruitment of all other centrosome components making it difficult to make conclusions about the role of phosphorylation of KLP-7 specifically (Hannak et al., 2001). The GFP::KLP-7 protein that contained 10 mutated Aurora sites (10E) failed to localize to kinetochores and centrosomes. Although I could not rule out the possibility of incorrect folding of the 10E protein *in vivo*, it is possible that dephosphorylation of KLP-7 at multiple Aurora sites is required for proper localization in mitosis.

Since I could not test all combinations in my structure-function analysis, I could not rule out the possibility that proper KLP-7 localization requires more complex phosphorylation events (*i.e.* phosphorylation at some putative sites and non-phosphorylation at other sites). However, my present data are most consistent with the idea that the *C. elegans* system may use a different mechanism to regulate KLP-7 localization compared to *Xenopus*. The inconsistency between results from vertebrates and *C. elegans* could be caused by the differences between organisms. For example, in vertebrates the kinetochore is assembled on a constricted region on each chromosome and serves as the primary attachment site for spindle MTs (monocentric). Forces on chromosomes are powered by MT interactions with both kinetochores and chromosome arms. A force for poleward movement is generated by MT interaction with kinetochore, and a repulsive force for moving away from the spindle pole is generated by MT interaction with chromosome arms [for review, see (Rieder and Salmon, 1998)]. Thus it is possible MCAK localization at the kinetochore, centromere and chromosome arms needs to be precisely regulated for proper mitotic force generation in vertebrates. In nematodes such as *C. elegans*, the kinetochore is not assembled in a constricted region on a chromosome during mitosis. The kinetochore structure is diffused along the entire chromosome (holocentric) [for review, see (Maddox et al., 2004)]. The differences in chromosome architectures could explanation why distinct mechanisms are used to regulate MCAK localization.

Alternatively, the different results from *Xenopus* and *C. elegans* could be due to the cell-free extract and *in vivo* systems. *Xenopus* extract is a very powerful system for biochemical studies of protein functions and has led to numerous important discoveries in cell cycle research. However, there are also limitations and may not reveal all *in vivo* mechanisms.

4.3.2 Regulation of KLP-7 function by Aurora kinase phosphorylation

Despite localizing normally, four GFP::KLP-7 phospho-mutant transgenes failed to rescue embryonic lethality in *klp-7(tm2143)* embryos, indicating that these transgenes have compromised functionality compared to GFP::KLP-7(WT). All four transgenes contain mutations in one putative Aurora kinase site, S546. Further analysis confirmed that GFP::KLP-7(S546E) or GFP::KLP-7(S546A) transgenes also failed to recue other *klp-7(lf)* phenotypes, including spindle-snap and excessive centrosomal MTs in mitosis. I was unable to verify phosphorylation of S546 by Aurora kinases *in vitro*, possibly due to problems with the KLP-7 substrate (for details, see 4.2.2). However, my structure-function analysis identified S546 site as an essential site for KLP-7 function *in vivo*. This predicted Aurora kinase site lies within the catalytic core and is well conserved among *C. elegans*, *Xenopus*, mouse and human (Figure 4-3). S546 is located in the α-helix 5 of the catalytic core domain, which is likely important for kinesin-MT binding (Ogawa et al., 2004; Woehlke et al.,

1997). Phosphorylation at S546 may introduce a negative charge to this region and thus interfere with KLP-7's interaction with MTs.

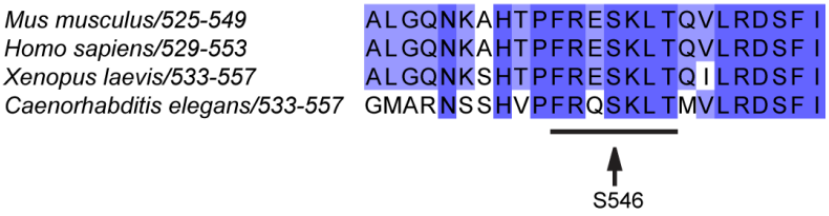

Figure 4-3 S546 is a conserved site of Aurora kinases

Sequence alignment of the region which contains S546 is shown. Color indicates amino acid percent identities. Aurora kinase motif is underlined.

Although it is well established that precise control of the location and function of kinesin-13 family proteins are regulated via phosphorylation, few reports have identified phosphorylation sites in the core domain (Andrews et al., 2004; Lan et al., 2004; Mennella et al., 2009; Ohi et al., 2004; Zhang et al., 2008; Zhang et al., 2007). One *Drosophila* kinesin-13 protein, KLP10A is phosphorylated by casein kinase 1α in the core domain (*Drosophila* S573, which is equivalent to *C. elegans* S555). Phosphorylation at this site alters KLP10A association with the MT lattice (Mennella et al., 2009). One Cdk1 phosphorylation site (T537) has also been identified in the vicinity of S542 (the human equivalent of the worm S546 site) in mamalian cells (Sanhaji et al., 2010). Phosphorylation of this site by Cdk1 is required for proper mitotic spindle formation, likely by

attenuating MCAK MT-depolymerizing activity and promoting the release of MCAK from the spindle poles (Sanhaji et al., 2010). Although *C. elegans* KLP-7 does not have an equivalent *cdk-1* site, S546 seems to perform a similar function, suggesting that this form of regulation may occur through different regulatory pathways in different systems.

My structure-function analysis indicated that putative Aurora kinase phosphorylation sites, except S546, either have no biological functions or unidentified roles in KLP-7 regulation. Among the twelve putative Aurora kinase sites, four (T119, S472, S546 and S555) are conserved among *C. elegans*, *Xenopus*, mouse and human. Nine sites (T119, T182, S264, S472, S538, S539, S546, S555 and T652) are conserved among four *Caenorhabditis* nematode species (*C. brenneri*, *C. briggsae*, *C. elegans*, and *C. remanei*). It is likely that MCAK regulation is conserved within nematode species.

4.3.3 A model for Aurora-dependent loading of KLP-7 onto MTs at the centrosome

The FRAP results revealed a distinct difference in the behavior of GFP::KLP-7(S546A) and GFP::KLP-7(S546E) mutants. When MTs were depolymerized with nocodazole, GFP::KLP-7(S546A) and GFP::KLP-7(WT) turnover at the centrosome was 2-fold slower, whereas the GFP::KLP-7(S546E) mutant embryos showed no change from untreated embryos. These results suggest that the recovery of KLP-7 was dependent on both MTs and the phosphorylation state of S546. One

explanation is that phosphorylation of S546, presumably by Aurora A kinase alters KLP-7 MT-binding properties. We suggest that there are two phases of KLP-7 behaviour that contribute to the observed recovery rates (Figure 4-4). A pool of phosphorylated KLP-7 could be exchanged between the cytoplasm and the centrosome, exhibiting the observed fast recovery rates and upon dephosphorylation of S546, KLP-7 loads onto MTs at the centrosome. In this model cycles of KLP-7 phosphorylation would be required for proper function, which would explain why both GFP::KLP-7(S546A) and GFP::KLP-7(S546E) mutants were unable to rescue the *klp-7* deletion mutant. It is possible that the GFP::KLP-7(S546E) mutant protein is locked into the first phase of the cycle, able to localize to the centrosome but unable to load onto MTs, explaining why the recovery of GFP::KLP-7(S546E) was unaffected by the loss of MTs. Further work will focus on the precise mechanism by which phosphorylation at S546 changes KLP-7 function.

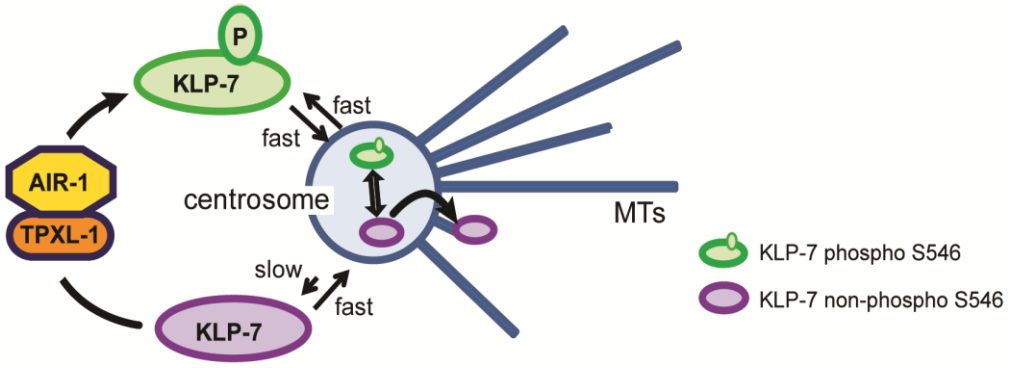

Figure 4-4 A model for two phases of KLP-7 behaviour

A model for two phases of KLP-7 behaviour related to the phosphorylation state of S546. Phosphorylated KLP-7 exchanges rapidly between centrosomes and cytoplasm by a MT-independent mechanism. Once dephosphorylated, KLP-7 can load onto MTs at the centrosome and its turnover is dependent on MTs. The relevant phosphorylation of KLP-7 at the centrosome likely occurs via TPXL-1-activated Aurora kinase A (AIR-1), based on *in vitro* data presented and data from Ozlü et al., 2005.

4.4 Future Directions

4.4.1 Regulation of KLP-7 via phosphorylation by other mitotic kinases

Previous studies on human MCAK have identified multiple phosphorylation sites by several mitotic kinases, including Cdk1, Plk1 and PAK1. Sequence alignment analysis revealed that none of the published phosphorylation sites are conserved between human MCAK and worm KLP-7 with one exception. A Plk1 site, S595 of human MCAK, was found to be the equivalent of S597 in KLP-7. Computational prediction of

phosphorylation sites by using a group-based prediction system (Xue et al., 2008) have identified multiple candidate phosphorylation sites in KLP-7 by *cdk-1*, *plk-1* and *pak-1* (Table 4-1, 4-2 and 4-3). Furthermore, results from my Phos-tag SDS-PAGE and 2D gel analyses showed that knocking down Aurora kinases only resulted in subtle changes in the overall phosphorylation status of KLP-7 *in vivo*. Overall these findings suggest that KLP-7 might be regulated by phosphorylation by *cdk-1*, *plk-1* or *pak-1* in *C. elegans*. To address this possibility, Phos-tag SDS-PAGE analysis will be performed by using worm lysates in which individual kinase is depleted by RNAi. If a mobility shift of KLP-7 proteins is observed in the absence of a specific kinase, it is very likely that KLP-7 is directly phosphorylated by that kinase *in vivo*. Further studies will focus on whether KLP-7 localization and activity are regulated by phosphorylation by this kinase (i.e. any change in subcellular localization of the GFP::KLP-7 transgene in kinase knockdown embryos).

Table 4-1 KLP-7 contains multiple candidate CDK-1 phosphorylation sites

amino acid	peptide	score
S57	ELLTLNPSLQAPKPT	2.82
T64	SLQAPKPTPPPQPPQ	9.317
S134	PVRMAPPSEKPLPTR	2.453
T140	PSEKPLPTRRAPSPK	2.345
S145	LPTRRAPSPKEDAAP	8.187
T178	AITVPKHTARRTVVV	2.043
T182	PKHTARRTVVVAPAP	3
T201	APPIANMTSQRAPSP	2.245
S207	MTSQRAPSPVARVPS	5.741
S214	SPVARVPSPKNVPRS	5.698
T457	LELINKGTLVRTAGT	2.079
S570	TVMISMISPGISSSD	3.432
T601	TDGSGEATPIRDEEL	5.827
T653	EKIIRETTIVLSNEP	2.043

Phosphorylation sites are predicted based on the GPS system (Xue et al., 2008).

Table 4-2 Candidate KLP-7 phosphorylation sites by PLK-1

amino acid	peptide	score
T41	EWYEKGE<u>T</u>KGKESSL	1.17
S47	ETKGKES<u>S</u>LEELLTL	1.191
S57	ELLTLNP<u>S</u>LQAPKPT	1.149
T64	SLQAPKP<u>T</u>PPPQPPQ	1.106
T73	PPQPPQK<u>T</u>LQASTAV	1.106
T98	MILDDED<u>T</u>FLLDHIN	1.277
S145	LPTRRAP<u>S</u>PKEDAAP	1.638
T157	AAPAPKS<u>T</u>RTTAAFK	1.681
S169	AFKPDLD<u>S</u>TAITVPK	1.617
T182	PKHTARR<u>T</u>VVVAPAP	1.34
S207	MTSQRAP<u>S</u>PVARVPS	1.851
S214	SPVARVP<u>S</u>PKNVPRS	1.064
T305	PQTRVDL<u>T</u>KYLDNQK	1.085
S367	HTMGGDF<u>S</u>GKKQNAS	1.298
T465	LVRTAGT<u>T</u>SANANSS	1.085
T506	GNERGQD<u>T</u>RECDRDT	1.617
S570	TVMISMI<u>S</u>PGISSSD	1.191
T653	EKIIRET<u>T</u>IVLSNEP	1.319
S661	IVLSNEP<u>S</u>AAQKAEC	1.021

Phosphorylation sites are predicted based on the GPS system (Xue et al., 2008).

Table 4-3 Candidate KLP-7 phosphorylation sites by PAK-1

amino acid	peptide	score
S47	ETKGKES<u>S</u>LEELLTL	4.893
T119	ASANKRP<u>T</u>GAFTQHV	4.857
T182	PKHTARR<u>T</u>VVVAPAP	6.429
S264	GVNENRI<u>S</u>VCVRKRP	4.679
S538	IRGMARN<u>S</u>SHVPFRQ	6.214
S546	SHVPFRQ<u>S</u>KLTMVLR	4.357
S555	LTMVLRD<u>S</u>FIGEKSR	4.464
T563	FIGEKSR<u>T</u>VMISMIS	4.607

Phosphorylation sites are predicted based on the GPS system (Xue et al., 2008).

4.4.2 Identifying proteins that interact with KLP-7

To better understand the mechanisms of KLP-7 regulation, it is important to identify genes that interact with KLP-7. This aim can be achieved by both genetic and biochemical approaches. An RNAi feeding library targeting ~90% of predicted genes allows the genome-wide RNAi screening to identify genes required for KLP-7 localization (Fraser et al., 2000; Kamath et al., 2003). Using this approach, worms expressing GFP::KLP-7 could be fed with individual dsRNA-expressing bacteria strains and examined by fluorescence microscopy for any changes in KLP-7 subcellular localization. This is a very powerful approach to identify genes regulating KLP-7, but going through more than 16000 genes can be very laborious and time-consuming. Alternatively, the identification of physical interaction partners for KLP-7 could provide insight into how the protein is regulated in the cell. For example, biochemical approaches such

as co-immunoprecipitation assays followed by mass spectrometry may be more efficient in rapid identification of proteins that bind to KLP-7.

In a previous IP experiment, KLP-7 and several unknown proteins were pulled down from worm lysate by the anti-KLP-7 antibody but not by the control IgG antibody (Srayko, unpublished, Figure 4-5). To identify these candidate interacting proteins, the Co-IP experiment will be repeated and the immunoprecipitated proteins will be separated by SDS-PAGE and characterized by Matrix Assisted Laser Desorption /Ionization-Time Of Flight (MALDI-TOF) spectrometric strategy. All identified candidate genes will be tested for their genetic interaction with KLP-7, meaning the enhancement or suppression of *klp-7(lf)* lethality. Whether depletion of these genes changes KLP-7 localization at the centrosomes or activity on MT depolymerization will also be analyzed as previously described.

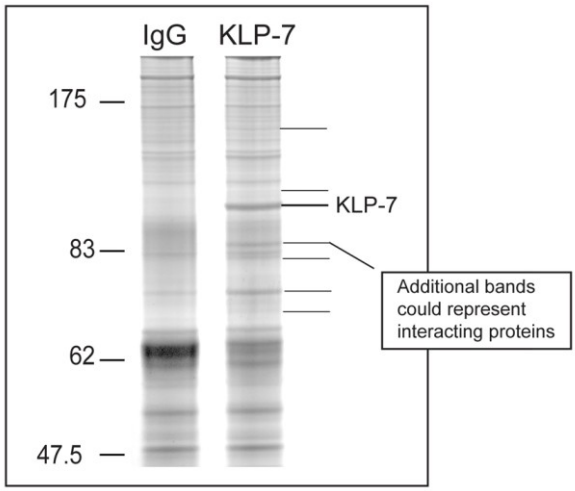

Figure 4-5 Immunoprecipitates from IgG and anti-KLP-7 antibodies

Protein A-bound antibodies against random IgG or KLP-7 were incubated with worm lysate, washed, and the eluted proteins separated via SDS-PAGE; gel was silver stained (Srayko, unpublished).

5 Bibliography

Akhmanova, A., and Steinmetz, M.O. (2008). Tracking the ends: a dynamic protein network controls the fate of microtubule tips. Nat Rev Mol Cell Biol 9, 309-322.

Albertson, D.G. (1984). Formation of the first cleavage spindle in nematode embryos. Dev Biol 101, 61-72.

Albertson, D.G., and Thomson, J.N. (1993). Segregation of holocentric chromosomes at meiosis in the nematode, Caenorhabditis elegans. Chromosome research : an international journal on the molecular, supramolecular and evolutionary aspects of chromosome biology 1, 15-26.

Allen, C., and Borisy, G.G. (1974). Structural polarity and directional growth of microtubules of Chlamydomonas flagella. J Mol Biol 90, 381-402.

Amos, L., and Klug, A. (1974). Arrangement of subunits in flagellar microtubules. J Cell Sci 14, 523-549.

Andrews, P.D., Knatko, E., Moore, W.J., and Swedlow, J.R. (2003). Mitotic mechanics: the auroras come into view. Curr Opin Cell Biol 15, 672-683.

Andrews, P.D., Ovechkina, Y., Morrice, N., Wagenbach, M., Duncan, K., Wordeman, L., and Swedlow, J.R. (2004). Aurora B regulates MCAK at the mitotic centromere. Dev Cell 6, 253-268.

Bajaj, M., and Srayko, M. (2013). Laulimalide Induces Dose-Dependent Modulation of Microtubule Behaviour in the C. elegans Embryo. PLoS One 8, e71889.

Bayliss, R., Sardon, T., Vernos, I., and Conti, E. (2003). Structural basis of Aurora-A activation by TPX2 at the mitotic spindle. Mol Cell 12, 851-862.

Bishop, J.D., and Schumacher, J.M. (2002). Phosphorylation of the carboxyl terminus of inner centromere protein (INCENP) by the Aurora B Kinase stimulates Aurora B kinase activity. J Biol Chem 277, 27577-27580.

Bobinnec, Y., Fukuda, M., and Nishida, E. (2000). Identification and characterization of Caenorhabditis elegans gamma-tubulin in dividing cells and differentiated tissues. J Cell Sci 113 Pt 21, 3747-3759.

Bokoch, G.M. (2003). Biology of the p21-activated kinases. Annu Rev Biochem 72, 743-781.

Brenner, S. (1974). The genetics of Caenorhabditis elegans. Genetics 77, 71-94.

Brouhard, G.J., Stear, J.H., Noetzel, T.L., Al-Bassam, J., Kinoshita, K., Harrison, S.C., Howard, J., and Hyman, A.A. (2008). XMAP215 is a processive microtubule polymerase. Cell 132, 79-88.

Brust-Mascher, I., Civelekoglu-Scholey, G., Kwon, M., Mogilner, A., and Scholey, J.M. (2004). Model for anaphase B: role of three mitotic motors in a switch from poleward flux to spindle elongation. Proc Natl Acad Sci U S A 101, 15938-15943.

Brust-Mascher, I., and Scholey, J.M. (2011). Mitotic motors and chromosome segregation: the mechanism of anaphase B. Biochem Soc Trans 39, 1149-1153.

Carazo-Salas, R.E., Guarguaglini, G., Gruss, O.J., Segref, A., Karsenti, E., and Mattaj, I.W. (1999). Generation of GTP-bound Ran by RCC1 is required for chromatin-induced mitotic spindle formation. Nature 400, 178-181.

Carvalho, A., Olson, S.K., Gutierrez, E., Zhang, K., Noble, L.B., Zanin, E., Desai, A., Groisman, A., and Oegema, K. (2011). Acute drug treatment in the early C. elegans embryo. PLoS One 6, e24656.

Chan, C.S., and Botstein, D. (1993). Isolation and characterization of chromosome-gain and increase-in-ploidy mutants in yeast. Genetics 135, 677-691.

Colombo, K., Grill, S.W., Kimple, R.J., Willard, F.S., Siderovski, D.P., and Gonczy, P. (2003). Translation of polarity cues into asymmetric spindle positioning in Caenorhabditis elegans embryos. Science 300, 1957-1961.

Desai, A., Maddox, P.S., Mitchison, T.J., and Salmon, E.D. (1998). Anaphase A chromosome movement and poleward spindle microtubule flux occur At similar rates in Xenopus extract spindles. J Cell Biol 141, 703-713.

Desai, A., Verma, S., Mitchison, T.J., and Walczak, C.E. (1999). Kin I kinesins are microtubule-destabilizing enzymes. Cell 96, 69-78.

Dumont, J., Oegema, K., and Desai, A. (2010). A kinetochore-independent mechanism drives anaphase chromosome separation during acentrosomal meiosis. Nat Cell Biol 12, 894-901.

Ems-McClung, S.C., Hertzer, K.M., Zhang, X., Miller, M.W., and Walczak, C.E. (2007). The interplay of the N- and C-terminal domains of MCAK control microtubule depolymerization activity and spindle assembly. Mol Biol Cell 18, 282-294.

Ems-McClung, S.C., and Walczak, C.E. (2010). Kinesin-13s in mitosis: Key players in the spatial and temporal organization of spindle microtubules. Semin Cell Dev Biol 21, 276-282.

Encalada, S.E., Willis, J., Lyczak, R., and Bowerman, B. (2005). A spindle checkpoint functions during mitosis in the early Caenorhabditis elegans embryo. Mol Biol Cell 16, 1056-1070.

Evans, L., Mitchison, T., and Kirschner, M. (1985). Influence of the centrosome on the structure of nucleated microtubules. J Cell Biol 100, 1185-1191.

Eyers, P.A., Erikson, E., Chen, L.G., and Maller, J.L. (2003). A novel mechanism for activation of the protein kinase Aurora A. Curr Biol 13, 691-697.

Fire, A., Xu, S., Montgomery, M.K., Kostas, S.A., Driver, S.E., and Mello, C.C. (1998). Potent and specific genetic interference by double-stranded RNA in Caenorhabditis elegans. Nature 391, 806-811.

Fraser, A.G., Kamath, R.S., Zipperlen, P., Martinez-Campos, M., Sohrmann, M., and Ahringer, J. (2000). Functional genomic analysis of C. elegans chromosome I by systematic RNA interference. Nature 408, 325-330.

Frokjaer-Jensen, C., Davis, M.W., Hopkins, C.E., Newman, B.J., Thummel, J.M., Olesen, S.P., Grunnet, M., and Jorgensen, E.M. (2008). Single-copy insertion of transgenes in Caenorhabditis elegans. Nat Genet 40, 1375-1383.

Ganem, N.J., and Compton, D.A. (2004). The KinI kinesin Kif2a is required for bipolar spindle assembly through a functional relationship with MCAK. J Cell Biol 166, 473-478.

Gard, D.L., and Kirschner, M.W. (1987). A microtubule-associated protein from Xenopus eggs that specifically promotes assembly at the plus-end. J Cell Biol 105, 2203-2215.

Gardner, M.K., Zanic, M., Gell, C., Bormuth, V., and Howard, J. (2011). Depolymerizing kinesins Kip3 and MCAK shape cellular microtubule architecture by differential control of catastrophe. Cell 147, 1092-1103.

Glover, D.M., Leibowitz, M.H., McLean, D.A., and Parry, H. (1995). Mutations in aurora prevent centrosome separation leading to the formation of monopolar spindles. Cell 81, 95-105.

Gonczy, P., Pichler, S., Kirkham, M., and Hyman, A.A. (1999). Cytoplasmic dynein is required for distinct aspects of MTOC positioning, including centrosome separation, in the one cell stage Caenorhabditis elegans embryo. J Cell Biol 147, 135-150.

Gopalan, G., Chan, C.S., and Donovan, P.J. (1997). A novel mammalian, mitotic spindle-associated kinase is related to yeast and fly chromosome segregation regulators. J Cell Biol 138, 643-656.

Gorbsky, G.J. (2004). Mitosis: MCAK under the aura of Aurora B. Curr Biol 14, R346-348.

Gotta, M., Dong, Y., Peterson, Y.K., Lanier, S.M., and Ahringer, J. (2003). Asymmetrically distributed C. elegans homologs of AGS3/PINS control spindle position in the early embryo. Curr Biol 13, 1029-1037.

Grill, S.W., Gonczy, P., Stelzer, E.H., and Hyman, A.A. (2001). Polarity controls forces governing asymmetric spindle positioning in the Caenorhabditis elegans embryo. Nature 409, 630-633.

Grill, S.W., Howard, J., Schaffer, E., Stelzer, E.H., and Hyman, A.A. (2003). The distribution of active force generators controls mitotic spindle position. Science 301, 518-521.

Gusnowski, E.M., and Srayko, M. (2011). Visualization of dynein-dependent microtubule gliding at the cell cortex: implications for spindle positioning. J Cell Biol 194, 377-386.

Hannak, E., Kirkham, M., Hyman, A.A., and Oegema, K. (2001). Aurora-A kinase is required for centrosome maturation in Caenorhabditis elegans. J Cell Biol 155, 1109-1116.

Hannak, E., Oegema, K., Kirkham, M., Gonczy, P., Habermann, B., and Hyman, A.A. (2002). The kinetically dominant assembly pathway for centrosomal asters in Caenorhabditis elegans is gamma-tubulin dependent. J Cell Biol 157, 591-602.

Harlow, E., and Lane, D. (2006). Immunoprecipitation: purifying the immune complexes. CSH Protoc 2006.

Heald, R., and Walczak, C.E. (1999). Microtubule-based motor function in mitosis. Curr Opin Struct Biol 9, 268-274.

Hedgecock, E.M., Culotti, J.G., Thomson, J.N., and Perkins, L.A. (1985). Axonal guidance mutants of Caenorhabditis elegans identified by filling sensory neurons with fluorescein dyes. Dev Biol 111, 158-170.

Helenius, J., Brouhard, G., Kalaidzidis, Y., Diez, S., and Howard, J. (2006). The depolymerizing kinesin MCAK uses lattice diffusion to rapidly target microtubule ends. Nature 441, 115-119.

Hertzer, K.M., Ems-McClung, S.C., Kline-Smith, S.L., Lipkin, T.G., Gilbert, S.P., and Walczak, C.E. (2006). Full-length dimeric MCAK is a more efficient microtubule depolymerase than minimal domain monomeric MCAK. Mol Biol Cell 17, 700-710.

Hirokawa, N., Noda, Y., Tanaka, Y., and Niwa, S. (2009). Kinesin superfamily motor proteins and intracellular transport. Nat Rev Mol Cell Biol 10, 682-696.

Hirokawa, N., and Takemura, R. (2004). Kinesin superfamily proteins and their various functions and dynamics. Exp Cell Res 301, 50-59.

Hodgkin, J., Horvitz, H.R., and Brenner, S. (1979). Nondisjunction Mutants of the Nematode CAENORHABDITIS ELEGANS. Genetics 91, 67-94.

Holmfeldt, P., Stenmark, S., and Gullberg, M. (2004). Differential functional interplay of TOGp/XMAP215 and the Kinl kinesin MCAK during interphase and mitosis. EMBO J 23, 627-637.

Honnappa, S., Gouveia, S.M., Weisbrich, A., Damberger, F.F., Bhavesh, N.S., Jawhari, H., Grigoriev, I., van Rijssel, F.J., Buey, R.M., Lawera, A., et al. (2009). An EB1-binding motif acts as a microtubule tip localization signal. Cell 138, 366-376.

Hunter, A.W., Caplow, M., Coy, D.L., Hancock, W.O., Diez, S., Wordeman, L., and Howard, J. (2003). The kinesin-related protein MCAK is a microtubule depolymerase that forms an ATP-hydrolyzing complex at microtubule ends. Mol Cell 11, 445-457.

Hyman, A., and Karsenti, E. (1998). The role of nucleation in patterning microtubule networks. J Cell Sci 111 (Pt 15), 2077-2083.

Hyman, A.A., and White, J.G. (1987). Determination of cell division axes in the early embryogenesis of Caenorhabditis elegans. J Cell Biol 105, 2123-2135.

Illingworth, C., Pirmadjid, N., Serhal, P., Howe, K., and Fitzharris, G. (2010). MCAK regulates chromosome alignment but is not necessary for preventing aneuploidy in mouse oocyte meiosis I. Development 137, 2133-2138.

Jessus, C., Thibier, C., and Ozon, R. (1985). Identification of microtubule-associated proteins (MAPs) in Xenopus oocyte. FEBS Lett 192, 135-140.

Kaitna, S., Pasierbek, P., Jantsch, M., Loidl, J., and Glotzer, M. (2002). The aurora B kinase AIR-2 regulates kinetochores during mitosis and is required for separation of homologous Chromosomes during meiosis. Curr Biol 12, 798-812.

Kalab, P., Pu, R.T., and Dasso, M. (1999). The ran GTPase regulates mitotic spindle assembly. Curr Biol 9, 481-484.

Kallio, M.J., McCleland, M.L., Stukenberg, P.T., and Gorbsky, G.J. (2002). Inhibition of aurora B kinase blocks chromosome segregation, overrides the spindle checkpoint, and perturbs microtubule dynamics in mitosis. Curr Biol 12, 900-905.

Kamath, R.S., Fraser, A.G., Dong, Y., Poulin, G., Durbin, R., Gotta, M., Kanapin, A., Le Bot, N., Moreno, S., Sohrmann, M., et al. (2003). Systematic functional analysis of the Caenorhabditis elegans genome using RNAi. Nature 421, 231-237.

Kamath, R.S., Martinez-Campos, M., Zipperlen, P., Fraser, A.G., and Ahringer, J. (2001). Effectiveness of specific RNA-mediated interference through ingested double-stranded RNA in Caenorhabditis elegans. Genome Biol 2, RESEARCH0002.

Kinoshita, E., Kinoshita-Kikuta, E., Takiyama, K., and Koike, T. (2006). Phosphate-binding tag, a new tool to visualize phosphorylated proteins. Mol Cell Proteomics 5, 749-757.

Kirschner, M., and Mitchison, T. (1986). Beyond self-assembly: from microtubules to morphogenesis. Cell 45, 329-342.

Kitagawa, R., and Rose, A.M. (1999). Components of the spindle-assembly checkpoint are essential in Caenorhabditis elegans. Nat Cell Biol 1, 514-521.

Kline-Smith, S.L., Khodjakov, A., Hergert, P., and Walczak, C.E. (2004). Depletion of centromeric MCAK leads to chromosome congression and segregation defects due to improper kinetochore attachments. Mol Biol Cell 15, 1146-1159.

Kline-Smith, S.L., and Walczak, C.E. (2002). The microtubule-destabilizing kinesin XKCM1 regulates microtubule dynamic instability in cells. Mol Biol Cell 13, 2718-2731.

Kufer, T.A., Sillje, H.H., Korner, R., Gruss, O.J., Meraldi, P., and Nigg, E.A. (2002). Human TPX2 is required for targeting Aurora-A kinase to the spindle. J Cell Biol 158, 617-623.

Kull, F.J., Sablin, E.P., Lau, R., Fletterick, R.J., and Vale, R.D. (1996). Crystal structure of the kinesin motor domain reveals a structural similarity to myosin. Nature 380, 550-555.

Labbe, J.C., McCarthy, E.K., and Goldstein, B. (2004). The forces that position a mitotic spindle asymmetrically are tethered until after the time of spindle assembly. J Cell Biol 167, 245-256.

Lampson, M.A., and Cheeseman, I.M. (2011). Sensing centromere tension: Aurora B and the regulation of kinetochore function. Trends Cell Biol 21, 133-140.

Lan, W., Zhang, X., Kline-Smith, S.L., Rosasco, S.E., Barrett-Wilt, G.A., Shabanowitz, J., Hunt, D.F., Walczak, C.E., and Stukenberg, P.T. (2004). Aurora B phosphorylates centromeric MCAK and regulates its localization and microtubule depolymerization activity. Curr Biol 14, 273-286.

Lawrence, C.J., Dawe, R.K., Christie, K.R., Cleveland, D.W., Dawson, S.C., Endow, S.A., Goldstein, L.S., Goodson, H.V., Hirokawa, N., Howard, J., et al. (2004). A standardized kinesin nomenclature. J Cell Biol 167, 19-22.

Ledbetter, M.C., and Porter, K.R. (1964). Morphology of Microtubules of Plant Cell. Science 144, 872-874.

Lee, T., Langford, K.J., Askham, J.M., Bruning-Richardson, A., and Morrison, E.E. (2008). MCAK associates with EB1. Oncogene 27, 2494-2500.

Maddox, P., Straight, A., Coughlin, P., Mitchison, T.J., and Salmon, E.D. (2003). Direct observation of microtubule dynamics at kinetochores in Xenopus extract spindles: implications for spindle mechanics. J Cell Biol 162, 377-382.

Maddox, P.S., Oegema, K., Desai, A., and Cheeseman, I.M. (2004). "Holo"er than thou: chromosome segregation and kinetochore function in C. elegans. Chromosome Res 12, 641-653.

Malone, C.J., Misner, L., Le Bot, N., Tsai, M.C., Campbell, J.M., Ahringer, J., and White, J.G. (2003). The C. elegans hook protein, ZYG-12, mediates the essential attachment between the centrosome and nucleus. Cell 115, 825-836.

Maney, T., Hunter, A.W., Wagenbach, M., and Wordeman, L. (1998). Mitotic centromere-associated kinesin is important for anaphase chromosome segregation. J Cell Biol 142, 787-801.

Maney, T., Wagenbach, M., and Wordeman, L. (2001). Molecular dissection of the microtubule depolymerizing activity of mitotic centromere-associated kinesin. J Biol Chem 276, 34753-34758.

McNally, K., Audhya, A., Oegema, K., and McNally, F.J. (2006). Katanin controls mitotic and meiotic spindle length. J Cell Biol 175, 881-891.

Mennella, V., Tan, D.Y., Buster, D.W., Asenjo, A.B., Rath, U., Ma, A., Sosa, H.J., and Sharp, D.J. (2009). Motor domain phosphorylation and regulation of the Drosophila kinesin 13, KLP10A. The Journal of cell biology 186, 481-490.

Miller, M.A., Nguyen, V.Q., Lee, M.H., Kosinski, M., Schedl, T., Caprioli, R.M., and Greenstein, D. (2001). A sperm cytoskeletal protein that signals oocyte meiotic maturation and ovulation. Science 291, 2144-2147.

Miller, M.A., Ruest, P.J., Kosinski, M., Hanks, S.K., and Greenstein, D. (2003). An Eph receptor sperm-sensing control mechanism for oocyte meiotic maturation in Caenorhabditis elegans. Genes Dev 17, 187-200.

Mitchison, T., and Kirschner, M. (1984). Dynamic instability of microtubule growth. Nature 312, 237-242.

Montenegro Gouveia, S., Leslie, K., Kapitein, L.C., Buey, R.M., Grigoriev, I., Wagenbach, M., Smal, I., Meijering, E., Hoogenraad, C.C., Wordeman, L., et al. (2010). In vitro reconstitution of the functional interplay between MCAK and EB3 at microtubule plus ends. Curr Biol 20, 1717-1722.

Moore, A., and Wordeman, L. (2004). C-terminus of mitotic centromere-associated kinesin (MCAK) inhibits its lattice-stimulated ATPase activity. Biochem J 383, 227-235.

Moore, A.T., Rankin, K.E., von Dassow, G., Peris, L., Wagenbach, M., Ovechkina, Y., Andrieux, A., Job, D., and Wordeman, L. (2005). MCAK associates with the tips of polymerizing microtubules. J Cell Biol 169, 391-397.

Moores, C.A., Cooper, J., Wagenbach, M., Ovechkina, Y., Wordeman, L., and Milligan, R.A. (2006). The role of the kinesin-13 neck in microtubule depolymerization. Cell Cycle 5, 1812-1815.

Moores, C.A., and Milligan, R.A. (2006). Lucky 13-microtubule depolymerisation by kinesin-13 motors. J Cell Sci 119, 3905-3913.

Moores, C.A., Yu, M., Guo, J., Beraud, C., Sakowicz, R., and Milligan, R.A. (2002). A mechanism for microtubule depolymerization by KinI kinesins. Mol Cell 9, 903-909.

Moritz, M., and Agard, D.A. (2001). Gamma-tubulin complexes and microtubule nucleation. Curr Opin Struct Biol 11, 174-181.

Muller-Reichert, T., Greenan, G., O'Toole, E., and Srayko, M. (2010). The elegans of spindle assembly. Cell Mol Life Sci 67, 2195-2213.

Musacchio, A., and Salmon, E.D. (2007). The spindle-assembly checkpoint in space and time. Nat Rev Mol Cell Biol 8, 379-393.

Newton, C.N., Wagenbach, M., Ovechkina, Y., Wordeman, L., and Wilson, L. (2004). MCAK, a Kin I kinesin, increases the catastrophe frequency of steady-state HeLa cell microtubules in an ATP-dependent manner in vitro. FEBS Lett 572, 80-84.

Nicklas, R.B. (1997). How cells get the right chromosomes. Science 275, 632-637.

Noda, Y., Sato-Yoshitake, R., Kondo, S., Nangaku, M., and Hirokawa, N. (1995). KIF2 is a new microtubule-based anterograde motor that transports membranous organelles distinct from those carried by kinesin heavy chain or KIF3A/B. J Cell Biol 129, 157-167.

Nogales, E., Wolf, S.G., and Downing, K.H. (1998). Structure of the alpha beta tubulin dimer by electron crystallography. Nature 391, 199-203.

O'Toole, E., Greenan, G., Lange, K.I., Srayko, M., and Muller-Reichert, T. (2012). The role of gamma-tubulin in centrosomal microtubule organization. PLoS One 7, e29795.

Oegema, K., Desai, A., Rybina, S., Kirkham, M., and Hyman, A.A. (2001). Functional analysis of kinetochore assembly in Caenorhabditis elegans. J Cell Biol 153, 1209-1226.

Oegema, K., Wiese, C., Martin, O.C., Milligan, R.A., Iwamatsu, A., Mitchison, T.J., and Zheng, Y. (1999). Characterization of two related Drosophila gamma-tubulin complexes that differ in their ability to nucleate microtubules. J Cell Biol 144, 721-733.

Ogawa, T., Nitta, R., Okada, Y., and Hirokawa, N. (2004). A common mechanism for microtubule destabilizers-M type kinesins stabilize curling of the protofilament using the class-specific neck and loops. Cell 116, 591-602.

Ohba, T., Nakamura, M., Nishitani, H., and Nishimoto, T. (1999). Self-organization of microtubule asters induced in Xenopus egg extracts by GTP-bound Ran. Science 284, 1356-1358.

Ohi, R., Burbank, K., Liu, Q., and Mitchison, T.J. (2007). Nonredundant functions of Kinesin-13s during meiotic spindle assembly. Curr Biol 17, 953-959.

Ohi, R., Sapra, T., Howard, J., and Mitchison, T.J. (2004). Differentiation of cytoplasmic and meiotic spindle assembly MCAK functions by Aurora B-dependent phosphorylation. Mol Biol Cell 15, 2895-2906.

Olmsted, J.B. (1986). Microtubule-associated proteins. Annu Rev Cell Biol 2, 421-457.

Ovechkina, Y., Wagenbach, M., and Wordeman, L. (2002). K-loop insertion restores microtubule depolymerizing activity of a "neckless" MCAK mutant. J Cell Biol 159, 557-562.

Ozlu, N., Srayko, M., Kinoshita, K., Habermann, B., O'Toole E, T., Muller-Reichert, T., Schmalz, N., Desai, A., and Hyman, A.A. (2005). An essential function of the C. elegans ortholog of TPX2 is to localize activated aurora A kinase to mitotic spindles. Dev Cell 9, 237-248.

Pakala, S.B., Nair, V.S., Reddy, S.D., and Kumar, R. (2012). Signaling-dependent phosphorylation of mitotic centromere-associated kinesin regulates microtubule depolymerization and its centrosomal localization. J Biol Chem 287, 40560-40569.

Pelletier, L., Ozlu, N., Hannak, E., Cowan, C., Habermann, B., Ruer, M., Muller-Reichert, T., and Hyman, A.A. (2004). The Caenorhabditis elegans centrosomal protein SPD-2 is required for both pericentriolar material recruitment and centriole duplication. Curr Biol 14, 863-873.

Perkins, L.A., Hedgecock, E.M., Thomson, J.N., and Culotti, J.G. (1986). Mutant sensory cilia in the nematode Caenorhabditis elegans. Dev Biol 117, 456-487.

Praitis, V., Casey, E., Collar, D., and Austin, J. (2001). Creation of low-copy integrated transgenic lines in Caenorhabditis elegans. Genetics 157, 1217-1226.

Rapsomaniki, M.A., Kotsantis, P., Symeonidou, I.E., Giakoumakis, N.N., Taraviras, S., and Lygerou, Z. (2012). easyFRAP: an interactive, easy-to-use tool for qualitative and quantitative analysis of FRAP data. Bioinformatics 28, 1800-1801.

Rath, U., Rogers, G.C., Tan, D., Gomez-Ferreria, M.A., Buster, D.W., Sosa, H.J., and Sharp, D.J. (2009). The Drosophila kinesin-13, KLP59D, impacts Pacman- and Flux-based chromosome movement. Mol Biol Cell 20, 4696-4705.

Rieder, C.L., and Salmon, E.D. (1998). The vertebrate cell kinetochore and its roles during mitosis. Trends Cell Biol 8, 310-318.

Roberts, A.J., Kon, T., Knight, P.J., Sutoh, K., and Burgess, S.A. (2013). Functions and mechanics of dynein motor proteins. Nat Rev Mol Cell Biol 14, 713-726.

Rogers, E., Bishop, J.D., Waddle, J.A., Schumacher, J.M., and Lin, R. (2002). The aurora kinase AIR-2 functions in the release of chromosome cohesion in Caenorhabditis elegans meiosis. The Journal of cell biology 157, 219-229.

Rogers, G.C., Rogers, S.L., Schwimmer, T.A., Ems-McClung, S.C., Walczak, C.E., Vale, R.D., Scholey, J.M., and Sharp, D.J. (2004). Two mitotic kinesins cooperate to drive sister chromatid separation during anaphase. Nature 427, 364-370.

Sack, S., Muller, J., Marx, A., Thormahlen, M., Mandelkow, E.M., Brady, S.T., and Mandelkow, E. (1997). X-ray structure of motor and neck domains from rat brain kinesin. Biochemistry 36, 16155-16165.

Sanhaji, M., Friel, C.T., Kreis, N.N., Kramer, A., Martin, C., Howard, J., Strebhardt, K., and Yuan, J. (2010). Functional and spatial regulation of mitotic centromere-associated kinesin by cyclin-dependent kinase 1. Mol Cell Biol 30, 2594-2607.

Schatten, G. (1994). The centrosome and its mode of inheritance: the reduction of the centrosome during gametogenesis and its restoration during fertilization. Dev Biol 165, 299-335.

Schlaitz, A.L., Srayko, M., Dammermann, A., Quintin, S., Wielsch, N., MacLeod, I., de Robillard, Q., Zinke, A., Yates, J.R., 3rd, Muller-Reichert, T., et al. (2007). The C. elegans RSA complex localizes protein

phosphatase 2A to centrosomes and regulates mitotic spindle assembly. Cell 128, 115-127.

Schumacher, J.M., Ashcroft, N., Donovan, P.J., and Golden, A. (1998a). A highly conserved centrosomal kinase, AIR-1, is required for accurate cell cycle progression and segregation of developmental factors in Caenorhabditis elegans embryos. Development 125, 4391-4402.

Schumacher, J.M., Golden, A., and Donovan, P.J. (1998b). AIR-2: An Aurora/Ipl1-related protein kinase associated with chromosomes and midbody microtubules is required for polar body extrusion and cytokinesis in Caenorhabditis elegans embryos. J Cell Biol 143, 1635-1646.

Severson, A.F., Hamill, D.R., Carter, J.C., Schumacher, J., and Bowerman, B. (2000). The aurora-related kinase AIR-2 recruits ZEN-4/CeMKLP1 to the mitotic spindle at metaphase and is required for cytokinesis. Current biology : CB 10, 1162-1171.

Srayko, M., Kaya, A., Stamford, J., and Hyman, A.A. (2005). Identification and characterization of factors required for microtubule growth and nucleation in the early C. elegans embryo. Dev Cell 9, 223-236.

Srayko, M., O'Toole E, T., Hyman, A.A., and Muller-Reichert, T. (2006). Katanin disrupts the microtubule lattice and increases polymer number in C. elegans meiosis. Curr Biol 16, 1944-1949.

Srinivasan, D.G., Fisk, R.M., Xu, H., and van den Heuvel, S. (2003). A complex of LIN-5 and GPR proteins regulates G protein signaling and spindle function in C elegans. Genes Dev 17, 1225-1239.

Starich, T.A., Herman, R.K., Kari, C.K., Yeh, W.H., Schackwitz, W.S., Schuyler, M.W., Collet, J., Thomas, J.H., and Riddle, D.L. (1995). Mutations affecting the chemosensory neurons of Caenorhabditis elegans. Genetics 139, 171-188.

Stout, J.R., Rizk, R.S., Kline, S.L., and Walczak, C.E. (2006). Deciphering protein function during mitosis in PtK cells using RNAi. BMC Cell Biol 7, 26.

Strome, S., Powers, J., Dunn, M., Reese, K., Malone, C.J., White, J., Seydoux, G., and Saxton, W. (2001). Spindle dynamics and the role of gamma-tubulin in early Caenorhabditis elegans embryos. Mol Biol Cell 12, 1751-1764.

Su, L.K., Burrell, M., Hill, D.E., Gyuris, J., Brent, R., Wiltshire, R., Trent, J., Vogelstein, B., and Kinzler, K.W. (1995). APC binds to the novel protein EB1. Cancer Res 55, 2972-2977.

Takaki, T., Trenz, K., Costanzo, V., and Petronczki, M. (2008). Polo-like kinase 1 reaches beyond mitosis--cytokinesis, DNA damage response, and development. Curr Opin Cell Biol 20, 650-660.

Tanenbaum, M.E., Medema, R.H., and Akhmanova, A. (2011). Regulation of localization and activity of the microtubule depolymerase MCAK. Bioarchitecture 1, 80-87.

Tilney, L.G., Bryan, J., Bush, D.J., Fujiwara, K., Mooseker, M.S., Murphy, D.B., and Snyder, D.H. (1973). Microtubules: evidence for 13 protofilaments. J Cell Biol 59, 267-275.

Timmons, L., Court, D.L., and Fire, A. (2001). Ingestion of bacterially expressed dsRNAs can produce specific and potent genetic interference in Caenorhabditis elegans. Gene 263, 103-112.

Tirnauer, J.S., and Bierer, B.E. (2000). EB1 proteins regulate microtubule dynamics, cell polarity, and chromosome stability. J Cell Biol 149, 761-766.

Tournebize, R., Popov, A., Kinoshita, K., Ashford, A.J., Rybina, S., Pozniakovsky, A., Mayer, T.U., Walczak, C.E., Karsenti, E., and Hyman, A.A. (2000). Control of microtubule dynamics by the antagonistic activities of XMAP215 and XKCM1 in Xenopus egg extracts. Nat Cell Biol 2, 13-19.

Trieselmann, N., Armstrong, S., Rauw, J., and Wilde, A. (2003). Ran modulates spindle assembly by regulating a subset of TPX2 and Kid activities including Aurora A activation. Journal of cell science 116, 4791-4798.

Tsai, M.Y., Wiese, C., Cao, K., Martin, O., Donovan, P., Ruderman, J., Prigent, C., and Zheng, Y. (2003). A Ran signalling pathway mediated by the mitotic kinase Aurora A in spindle assembly. Nat Cell Biol 5, 242-248.

Vale, R.D., and Fletterick, R.J. (1997). The design plan of kinesin motors. Annu Rev Cell Dev Biol 13, 745-777.

Verhey, K.J., and Hammond, J.W. (2009). Traffic control: regulation of kinesin motors. Nat Rev Mol Cell Biol 10, 765-777.

Voter, W.A., and Erickson, H.P. (1984). The kinetics of microtubule assembly. Evidence for a two-stage nucleation mechanism. J Biol Chem 259, 10430-10438.

Walczak, C.E., Gan, E.C., Desai, A., Mitchison, T.J., and Kline-Smith, S.L. (2002). The microtubule-destabilizing kinesin XKCM1 is required for chromosome positioning during spindle assembly. Curr Biol 12, 1885-1889.

Walczak, C.E., Gayek, S., and Ohi, R. (2013). Microtubule-depolymerizing kinesins. Annu Rev Cell Dev Biol 29, 417-441.

Walczak, C.E., Mitchison, T.J., and Desai, A. (1996). XKCM1: a Xenopus kinesin-related protein that regulates microtubule dynamics during mitotic spindle assembly. Cell 84, 37-47.

Weisenberg, R.C., Deery, W.J., and Dickinson, P.J. (1976). Tubulin-nucleotide interactions during the polymerization and depolymerization of microtubules. Biochemistry 15, 4248-4254.

Wiese, C., and Zheng, Y. (2006). Microtubule nucleation: gamma-tubulin and beyond. J Cell Sci 119, 4143-4153.

Wilde, A., and Zheng, Y. (1999). Stimulation of microtubule aster formation and spindle assembly by the small GTPase Ran. Science 284, 1359-1362.

Woehlke, G., Ruby, A.K., Hart, C.L., Ly, B., Hom-Booher, N., and Vale, R.D. (1997). Microtubule interaction site of the kinesin motor. Cell 90, 207-216.

Woollard, A., and Hodgkin, J. (1999). Stu-7/air-2 is a C. elegans aurora homologue essential for chromosome segregation during embryonic and post-embryonic development. Mech Dev 82, 95-108.

Wordeman, L., and Mitchison, T.J. (1995). Identification and partial characterization of mitotic centromere-associated kinesin, a kinesin-related protein that associates with centromeres during mitosis. J Cell Biol 128, 95-104.

Wordeman, L., Wagenbach, M., and Maney, T. (1999). Mutations in the ATP-binding domain affect the subcellular distribution of mitotic centromere-associated kinesin (MCAK). Cell Biol Int 23, 275-286.

Xue, Y., Ren, J., Gao, X., Jin, C., Wen, L., and Yao, X. (2008). GPS 2.0, a tool to predict kinase-specific phosphorylation sites in hierarchy. Mol Cell Proteomics 7, 1598-1608.

Zhang, C., Hughes, M., and Clarke, P.R. (1999). Ran-GTP stabilises microtubule asters and inhibits nuclear assembly in Xenopus egg extracts. J Cell Sci 112 (Pt 14), 2453-2461.

Zhang, L., Shao, H., Huang, Y., Yan, F., Chu, Y., Hou, H., Zhu, M., Fu, C., Aikhionbare, F., Fang, G., et al. (2011). PLK1 phosphorylates mitotic centromere-associated kinesin and promotes its depolymerase activity. J Biol Chem 286, 3033-3046.

Zhang, X., Ems-McClung, S.C., and Walczak, C.E. (2008). Aurora A phosphorylates MCAK to control ran-dependent spindle bipolarity. Mol Biol Cell 19, 2752-2765.

Zhang, X., Lan, W., Ems-McClung, S.C., Stukenberg, P.T., and Walczak, C.E. (2007). Aurora B phosphorylates multiple sites on mitotic centromere-associated kinesin to spatially and temporally regulate its function. Mol Biol Cell 18, 3264-3276.

Zheng, Y., Wong, M.L., Alberts, B., and Mitchison, T. (1995). Nucleation of microtubule assembly by a gamma-tubulin-containing ring complex. Nature 378, 578-583.

Zhou, F.F., Xue, Y., Chen, G.L., and Yao, X. (2004). GPS: a novel group-based phosphorylation predicting and scoring method. Biochem Biophys Res Commun 325, 1443-1448.

Appendix 1

Genetic interactions between *klp-7* and *unc-119* were indentified in the preceding section of this work, indicating a potential role of KLP-7 in *C. elegans* neurons. Preliminary results related to this finding are included here.

Introduction

A general introduction to the neuronal MTs

MTs can undergo rapid assembly and disassembly cycles. This intrinsic dynamic instability allows MTs to efficiently search cellular space to reach their target, even at the cell periphery. According to the selective MT stabilization model proposed by Kirschner and Mitchison, a population of dynamic MTs are stabilized in specialized regions in response to signals from the cell cortex or from outside of the cell. Selective stabilization of MTs results in reorientation of MT arrays and contributes to the polarization of many cell types, such as neurons (Kirschner and Mitchison, 1986). Such polarization of the MT cytoskeleton could then lead to morphological changes and cell asymmetry.

Neurons are highly polarized cells with a single long axon to transmit signals and multiple shorter dendrites to receive signals (Craig and Banker, 1994). Both axons and dendrites contain dense MT arrays. However, the organization of MTs is different in axons and dendrites. Axonal MTs are orientated with their plus ends directed to the axon tip,

whereas, in dendrites, some MTs have their plus ends directed towards the dendritic tip, while others have their plus end directed to the cell body. Also, axons and dendrites contain different MAPs. For example, Tau proteins (microtubule-associated proteins that modulate stability of microtubules in axons) are only found in axons, while MAP2 (Microtubule-associated protein 2, a MT stabilizer) is dendrite specific [reviewed in (Conde and Caceres, 2009)]. The distinct morphologies and functions of dendrites and axons within one cell indicate neuron polarization. In early neuronal development one neurite with a higher ratio of stable to dynamic MTs is selected as the future axon (Witte et al., 2008). Furthermore, MT stabilization is sufficient to induce axon formation. Multiple axons formed when hippocampal neurons were treated with low concentrations of MT stabilizing drug taxol (Witte et al., 2008). Overall, these findings indicate that regulation of MT dynamics is essential for proper neuron polarization and/or neuronal morphology.

Individual MTs within a single axon also exhibit distinct dynamic properties. MTs in the proximal region of the axon are enriched in detyrosinated (Glu-tubulin) and acetylated α-tubulin and are more stable, while MTs at the neuritic tips are concentrated with tyrosinated α-tubulin and are more dynamic [reviewed in (Conde and Caceres, 2009)]. The highly dynamic MTs at the distal region play a critical role in the navigation, extension and branching behaviours of a developing axon.

KIF2A suppresses axon branching by destabilizing MTs in mouse neurons

A developing neuron cell extends a single long axon to make connections with its target. In some neurons, secondary collateral branches form *de novo* from the primary axon to allow individual neurons to reach multiple targets [reviewed in (Gallo, 2011)]. The growth cone, an actin-supported structure at the tip of a developing axon plays an important role in forming proper axon structures. While the primary growth cone is still extending, secondary growth cones which form future collateral branches are suppressed and remain short (Kalil et al., 2000; O'Leary and Terashima, 1988). Secondary growth cones extend in response to environmental cues, such as the Rho family of GTPases [reviewed in (Gallo, 2011)]. Axon branching is a complex morphological process that involves rapid changes in the organization of cytoskeletal components, such as actin filaments and MTs. Axon branching is initiated by the protrusion of actin-based structures, such as lamellipodia (thin, but broad actin projections at the edge of a migrating cell) or filopodia (thin and long actin projections that extend beyond the leading edge of a migrating cell). The actin-based protrusions are subsequently invaded by MTs which allow the sprouting branches to mature and extend [reviewed in (Gallo, 2011)]. Previous studies have demonstrated that MTs are reorganized and fragmented into smaller MTs at sprouting branches (Yu et

al., 1994). The reorganization of MT arrays at the site of branching is mediated by MT-associated and MT-severing proteins (Gallo, 2011).

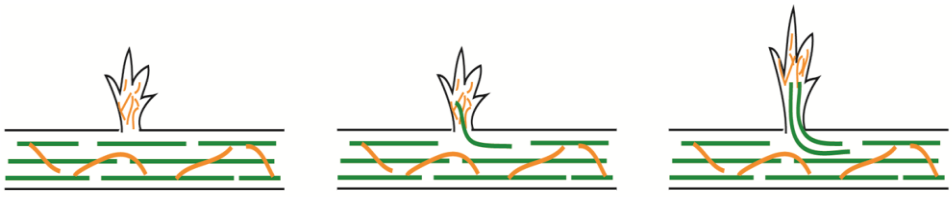

Figure A-1 Organization of cytoskeleton structures during collateral branching

Collateral branching is initiated by the protrusion of actin filament based structures from the axon shaft (left). Axon MTs invade the protrusions and form the sprouting branches (middle). More MTs and cellular organelles enter the sprouting branches and result in the formation of mature branches (right). MTs are in green; actin filaments are in orange. This figure is adapted from Gallo 2010.

One kinesin13 protein, KIF2A, is found to suppress the extension of collateral axon branches. KIF2A is predominately expressed at the growth cone of neurons in the brain tissue (Noda et al., 1995). Loss of KIF2A resulted in an increase in the lengths of collateral branches, which delayed the migration of cortical neurons in the mouse brain (Homma et al., 2003). Furthermore, MT depolymerizing activity was found to be decreased in the growth cones of cultured Kif2a mutant neurons. Fluorescence microscopy imaging of individual MTs revealed that MT tips stopped growing and began to depolymerise upon reaching the cell periphery in wild-type

neurons. However, in Kif2a mutant neurons MTs continued to grow even after they reached the cell edge. As a result some MTs were observed to curl at the cell edge and run along the plasma membrane. This may lead them to push against the growth cone and cause the overextension of axon branches (Homma et al., 2003). The above findings indicate that KIF2A inhibits collateral branching by destabilizing MTs at the cell periphery of the growth cone.

UNC-119 suppresses axon branching in *C. elegans* motor neurons

unc-119 (Uncoordinated) was originally identified by its locomotory defect in *C. elegans* (Maduro and Pilgrim, 1995). In *C. elegans* and *Drosophila* UNC-119 is pan-neuronally expressed from early development (i.e. comma stage in *C. elegans*, approximately 560 cells) to adulthood (Maduro et al., 2000). Expression of mammalian *unc-119* homologues, such as HRG4 (human UNC119) and RRG4 (rat UNC119) were only found in the photoreceptor cells in the retina (Higashide et al., 1996; Swanson et al., 1998). The *C. elegans unc-119* mutant phenotype can be fully rescued by the expression of *Drosophila* or human *unc-119* transgenes, indicating functional conservation of UNC-119 proteins. Although these proteins are highly conserved at the sequence level, UNC-119 does not contain known structural domains and the molecular functions of UNC-119 proteins are poorly understood (Maduro et al., 2000). Work by Knobel et al demonstrated that UNC-119 plays an important role in stabilizing the architecture of the *C. elegans* nerve

system. In *unc-119(ed3)* worms, axons of many motor neurons are ectopically branched. After the original growth cone has migrated to its destination, many secondary growth cones form from the shaft and cell body of the neuron and develop into new branches (Knobel et al., 2001). Improper location of synapses was also observed in *unc-119(ed3)* worms. Ectopic synapses were found at the dendritic regions in addition to their normal location at the tip of the axon. Overall, these findings suggested that UNC-119 has an important function in inhibiting axon branching and restricting the distribution of synapses in *C. elegans* neurons (Knobel et al., 2001).

KLP-7 regulates MT growth in axon regeneration in *C. elegans* sensory neurons

Mature axons are frequently capable of regrowth after injury. The regeneration of an injured axon requires the assembly of a new growth cone at the cut axon stump. Since axonal MTs exhibit different dynamic properties in a region-specific manner (i.e. MTs at the proximal part of an axon are stable, while MTs near the growth cone at the axon tip are highly dynamic), the regeneration process involves converting a stable MT cytoskeleton into one that is more dynamic [reviewed in (Bradke et al., 2012)]. However, the mechanisms by which MTs are remodeled remain poorly understood. Several neuron types in *C. elegans* display robust regenerative responses after injury, including motor and sensory neurons [reviewed in (Ghosh-Roy and Chisholm, 2010)]. Previous work has

identified two MAPK (Mitogen-activated protein kinases) pathways which are essential for axon regeneration (Ghosh-Roy et al., 2010; Nix et al., 2011).

A more recent study demonstrated that the MT depolymerase KLP-7 and post-translational modification of α-tubulin are also involved in remodeling the MT cytoskeleton in axon regrowth. By performing *in vivo* live imaging in *C. elegans* axons, Ghosh-Roy et al found that in *klp-7(tm2143)* worms touch sensory neurons, including PLM (posterior lateral microtubule) and ALM (anterior lateral microtubule), often extend ectopic neurites from their cell bodies. This phenotype can be rescued by expressing a transgene containing *klp-7(+)* genomic DNA in early touch cell lineages but not by expressing the same transgene in differentiated touch sensory neurons. This result indicates a role of KLP-7 in early neuronal development in ensuring that one single axon is extended from a touch neuron via an unknown mechanism. In mature sensory neurons the majority of axonal MTs are stable, while a small pool of growing MTs also exists and is maintained by KLP-7. Ghosh-Roy et al demonstrated that axonal injury triggers an up-regulation of MT growth and a down-regulation of KLP-7 by the DLK (Dual-Leucine zipper Kinase) pathway at the injured axon tip. Overall, these results suggested that in the steady state KLP-7 maintains a low number of growing MTs in axons of a mature neuron. Upon axonal injury, KLP-7 is locally removed from the injured axon tip to

allow an increase in growing MTs for axon regeneration (Ghosh-Roy et al., 2012).

Results and Discussion

Synthetic lethal genetic interactions between *klp-7* and *unc-119*

As mentioned in the preceding section, the structure-function analysis required the expression of KLP-7-phospho-mutant transgenes in worms without the endogenous protein. Germline transgenic animals were generated by a previously described high-pressure particle bombardment method (Praitis et al., 2001). Briefly, GFP::KLP-7-phospho-mutant transgenes that contain a functional copy of the *unc-119* gene were used to transform *unc-119 (lf)* worms. Transformants were selected based on the rescue of the *unc-119* mutant phenotypes, such as restoration in locomotion and formation of dauers (worms that are developmentally arrested since the second molt to survive harsh environments) (for more details, see 2.2 and 2.13).

I attempted to generate *klp-7 unc-119* double-mutant worms for the transgenic rescue experiments. However, *klp-7(tm2143) unc-119(ed3)* and *klp-7(tm2143) unc-119(ed4)* homozygous worms were found to be lethal. Since either *klp-7(tm2143)* or *unc-119(ed3 or ed4)* single allele is viable, the synthetic lethality of the double-mutants indicated a genetic interaction between *klp-7* and *unc-119*. Because both *ed3* and *ed4* alleles are predicted to be null alleles (Maduro and Pilgrim, 1995), I reasoned that a

weaker loss-of-function allele of *unc-119* might allow viability in combination with *klp-7(tm2143)*. Indeed, a double mutant strain was generated by using a weak allele of *unc-119*, *ky571* (Table A-1).

Table A-1 Genetic interaction between *klp-7* and *unc-119*

genotype	*unc-119 allele*	larvae viability
klp-7(tm2143) unc-119(ed3)	null	lethal
klp-7(tm2143) unc-119(ed4)	null	lethal
klp-7(tm2143) unc-119(ky571)	weak loss-of-function	viable

Genetic interactions between *klp-7* and *unc-119* occur post-embryonically, likely in neuronal cells

To address whether the synthetic lethal phenotype was caused by genetic interaction between *klp-7* and *unc-119* during embryonic or post-embryonic development, I treated *unc-119(ed3)* worms with *klp-7 dsRNA* and scored embryonic viability. Previous studies demonstrated that RNAi can be used to effectively silence genes in most cell types in early embryos and adults. However, the *C. elegans* nerve system is RNAi resistant, possibly due to limiting RNAi machinery components or factors that stabilize dsRNA in neuronal cells (Kamath et al., 2001; Timmons et al., 2001). Based on these findings, it is very likely that *klp-7(RNAi)* would not effectively knock down KLP-7 in neurons during post-embryonic development. If a *klp-7-unc-119* interaction occurs during early embryonic

development, *klp-7(RNAi) unc-119(ed3)* worms should have increased lethality, similar to the synthetic lethality of *klp-7(tm2143) unc-119(ed3)* worms. However, I found that *klp-7(RNAi) unc-119(ed3)* worms exhibited 65% embryonic viability compared to *unc-119(ed3)* worms, which is not significantly different from the viability of *klp-7(RNAi)* alone (Figure A-2). Since embryonic lethality was observed for *klp-7(RNAi)*, KLP-7 function was likely to be effectively reduced. Overall, the above results suggested that the synthetic lethality observed in *klp-7 unc-119* worms could be due to these genes having parallel neuronal functions during post-embryonic development.

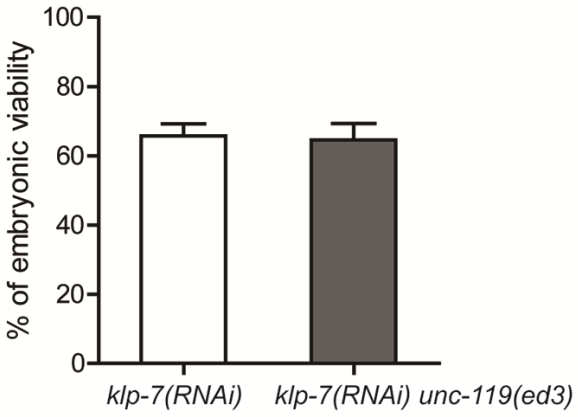

Figure A-2 *klp-7(RNAi)* to *unc-119(ed3)* worms doesn't cause synthetic lethality

dsRNA against *klp-7* was injected into *unc-119(ed3)* worms at L4 and young adult stages. Eggs laid 0-24 hrs post-injection were collected. Embryonic viability was scored at 20°C. *klp-7(RNAi)*: n=8; *klp-7(RNAi); unc-119(ed3)*: n=6.

klp-7(lf) enhances the dye-filling phenotype of *unc-119(lf)*

In order to reveal the underlying mechanism for the *klp-7* and *unc-119* interaction, I tested whether *klp-7(lf)* enhanced the reported neuronal defects of *unc-119(lf)*. One phenotype exhibited by *unc-119(lf)* worms is that they are defective in uptake of fluorescent dye into the amphid head neurons (French and Pilgrim, personal communication). In wild-type worms fluorescent dyes can be taken-up by amphid head neurons and phasmid tail neurons, possibly by extending their cilia through pores in the cuticle to the environment (Hedgecock et al., 1985; Perkins et al., 1986; Starich et al., 1995; Ward et al., 1975; White et al., 1986). Cilia are subcellular organelles formed by MT arrays emanating from a centriole-based structure, the basal body. In *C. elegans* the only type of ciliated neurons are sensory neurons. Although the exact mechanism is still unclear, a dye-filling assay has been used to determine the integrity of sensory cilia. In this study I found that as reported, none of *unc-119(ed3)* worms showed fluorescent dye in their amphid head neurons after being soaked in the dye for 20 minutes (Figure A-3). Amphid head neurons of L4 and young adult *klp-7(tm2143)* worms can uptake the fluorescent dye in a manner similar to that of the wild-type. Dye-filling by amphid head neurons are compromised in worms carrying the weak allele *unc-119(ky571)* and almost abolished in *klp-7(tm2143) unc-119(ky571)* double mutant worms (Figure A-3).

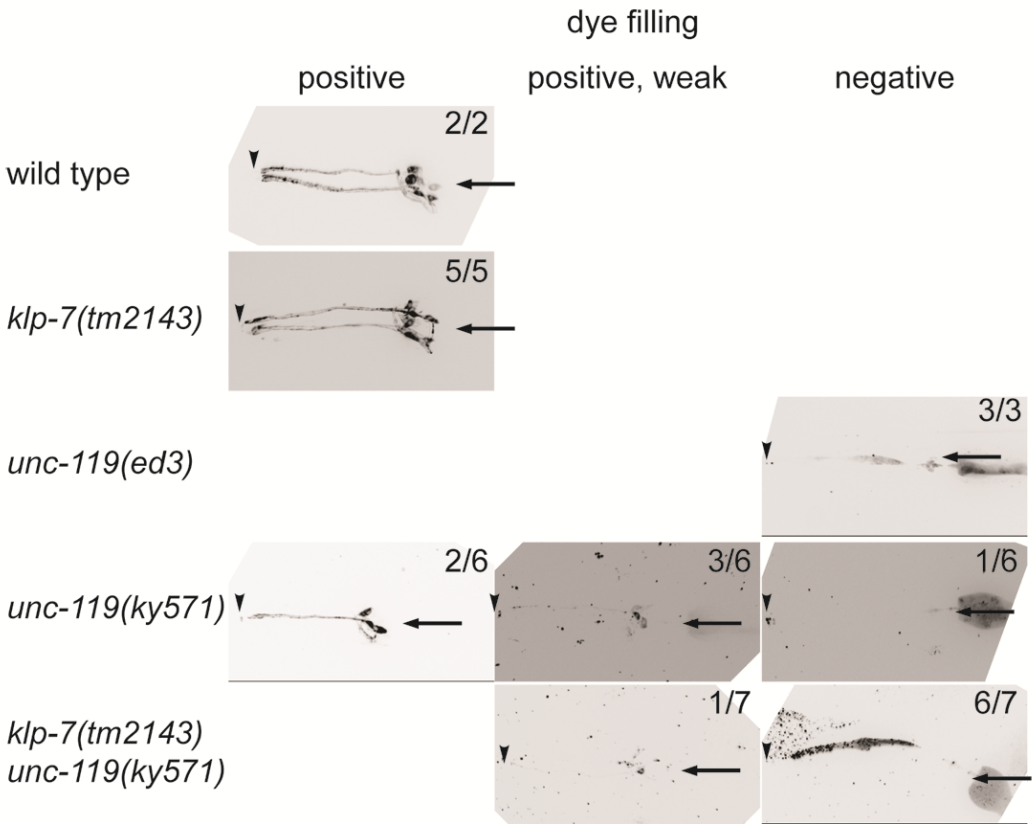

Figure A-3 Dye-filling in wild-type, *unc-119(ed3), klp-7(tm2143), unc-119(ky571)* and *klp-7(tm2143) unc-119(ky571)* worms

Amphid head neurons of L4 or young adult worms are show. Numbers indicate dye-filling positive versus total worms. Note that even some *unc-119(ky571)* worms were scored as “dye-filling positive”, the fluorescence intensity in sensory neurons seemed lower, and fewer neurons seem to take the dye compared to wild-type. Arrow heads point to the positions of the nose. Black arrows point to the approximate positions of the pharyngeal bulb. Wild-type: n=3; *unc-119(ed3)*: n=3; *klp-7(tm2143)*: n=5; *unc-119(ky571)*: n=6; *klp-7(tm2143) unc-119(ky571)*: n=7.

Possible roles of KLP-7 in *C. elegans* neuronal development and future directions

Results obtained so far suggest that UNC-119 is important for proper cilium structure or function. *klp-7(lf)* enhances defects associated with *unc-119(lf)* in ciliated sensory neurons. Loss of KLP-7 protein did not result in a dye-filling defect, indicating that *klp-7(tm2143)* worms have no gross abnormalities in ciliary function at least in amphid head neurons. It is possible that KLP-7 is not required for the assembly of the cilia structure. However, previous studies have shown that normal dye-filling behavior does not always indicate completely normal ciliary function (Schafer et al., 2006). Based on the current data I cannot rule out the possibility that KLP-7 plays a role in cilia function or signalling. It has been demonstrated that disruption of genes required for cilia assembly or function resulted in longevity in *C. elegans* via modulating the DAF-2 (insulin–IGF-1-like) receptor signaling pathway (Apfeld and Kenyon, 1999). It will be interesting to see if *klp-7(tm2143)* worms have an increased lifespan.

Another reported phenotype for *unc-119(lf)* is the excessive axon branching of the motor neurons (Knobel et al., 2001). It is possible that loss of KLP-7 exacerbates the axon branching defects in motor neurons in *unc-119(ed3)* worms. In order to address this possibility, I created worm strains that express a pan-neuronal GFP transgene in combination with *klp-7(tm2143)*, *unc-119* or the double mutant (Figure A-4). The neuronal network appeared to exhibit more branching in the double mutant. However, I was unsuccessful in quantifying axon branching due to the high complexity of the neuronal network labelled by a pan-neuronal

fluorescent marker. Future work should focus on the axon branching phenotype in a subset of *C. elegans* neurons, such as GABA neurons (Knobel et al., 2001). The structure of GABA neurons can be marked by GFP expression driven by the *unc-47* promoter (McIntire et al., 1997).

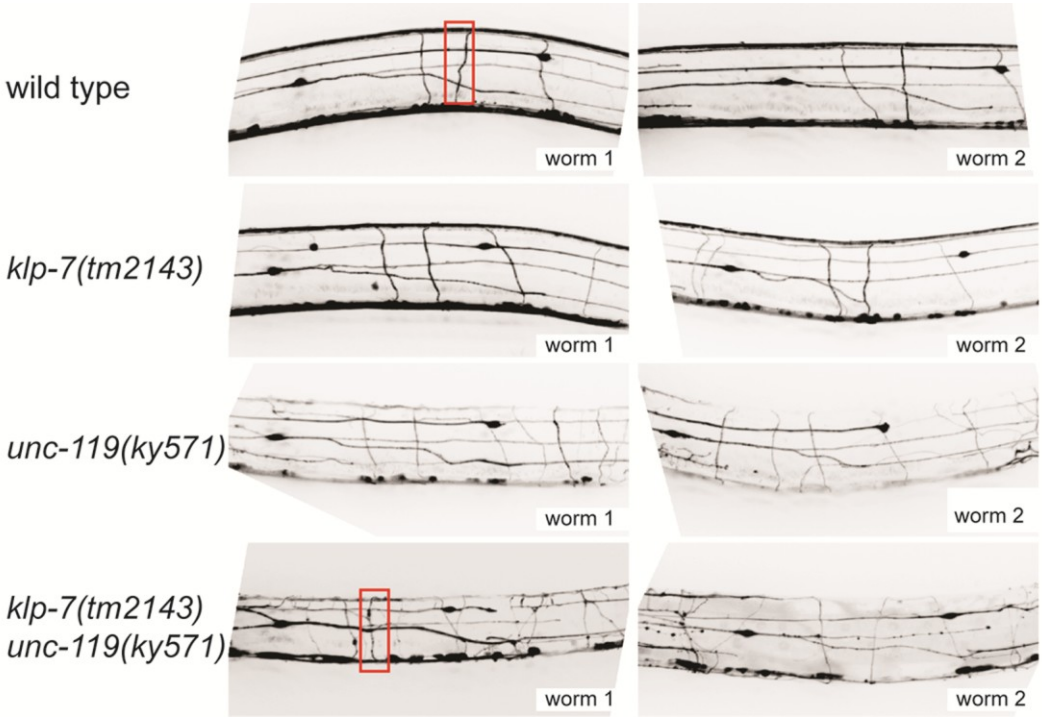

Figure A-4 *klp-7(tm2143) unc-119(ky571)* worms may exhibit excessive axon branching in their motor neurons

L4 or young adult worms expressing a pan-neuronal GFP marker were imaged. Two representative worms are shown for each strain. Red boxes indicate a motor neuron (dorsal-ventral) that may be excessively branched in *klp-7(tm2143) unc-119(ky571)* worms.

Currently it is unclear how KLP-7 interacts with UNC-119 to regulate neuron morphology or function in *C. elegans*. My genetic data that the phenotype of *unc-119(ed3)* null allele can be enhanced by *klp-7(null)* mutation supports a model whereby UNC-119 and KLP-7 acts through parallel pathways to regulate the same process, such as axon branching. One model for KLP-7 function in neurons is that KLP-7 is involved in the maintenance of neuron polarity. Neurons are polarized with a single long axon and multiple shorter dendrites. In *unc-119(ed3)* worms synapses form in the dendritic regions and also at the axon tips. The loss of distinction between axons and dendrites indicates declined polarity (Knobel et al., 2001). It will be interesting to address whether more dendrites exhibit features of axons by analysing the localization of axon- or dendrite- specific proteins in *klp-7(lf) unc-119(lf)* neurons (i.e. MAP2 is found mostly in dendrites while tau is found in axons).

Previous studies have shown that collateral branching involves fragmentation of MT arrays and local reorganization of MT fragments (Davenport et al., 1999; Dent et al., 1999; Yu et al., 1994). It is possible that MT fragmentation generates MT ends, whereas KLP-7 depolymerises MTs to suppress the formation of new branches. More work remains to be done to investigate this possibility. For example, a detailed phenotypic analysis should be performed to assess the morphology of *klp-7(tm2143)* neurons. If some neurons are found to be ectopically branched, MT growth should be measured at branching regions via fluorescence microscopy.

Bibliography

Apfeld, J., and Kenyon, C. (1999). Regulation of lifespan by sensory perception in Caenorhabditis elegans. Nature *402*, 804-809.

Bradke, F., Fawcett, J.W., and Spira, M.E. (2012). Assembly of a new growth cone after axotomy: the precursor to axon regeneration. Nat Rev Neurosci *13*, 183-193.

Conde, C., and Caceres, A. (2009). Microtubule assembly, organization and dynamics in axons and dendrites. Nat Rev Neurosci *10*, 319-332.

Craig, A.M., and Banker, G. (1994). Neuronal polarity. Annu Rev Neurosci *17*, 267-310.

Davenport, R.W., Thies, E., and Cohen, M.L. (1999). Neuronal growth cone collapse triggers lateral extensions along trailing axons. Nat Neurosci *2*, 254-259.

Dent, E.W., Callaway, J.L., Szebenyi, G., Baas, P.W., and Kalil, K. (1999). Reorganization and movement of microtubules in axonal growth cones and developing interstitial branches. J Neurosci *19*, 8894-8908.

Gallo, G. (2011). The cytoskeletal and signaling mechanisms of axon collateral branching. Dev Neurobiol *71*, 201-220.

Ghosh-Roy, A., and Chisholm, A.D. (2010). Caenorhabditis elegans: a new model organism for studies of axon regeneration. Dev Dyn *239*, 1460-1464.

Ghosh-Roy, A., Goncharov, A., Jin, Y., and Chisholm, A.D. (2012). Kinesin-13 and tubulin posttranslational modifications regulate microtubule growth in axon regeneration. Dev Cell *23*, 716-728.

Ghosh-Roy, A., Wu, Z., Goncharov, A., Jin, Y., and Chisholm, A.D. (2010). Calcium and cyclic AMP promote axonal regeneration in Caenorhabditis elegans and require DLK-1 kinase. J Neurosci *30*, 3175-3183.

Hedgecock, E.M., Culotti, J.G., Thomson, J.N., and Perkins, L.A. (1985). Axonal guidance mutants of Caenorhabditis elegans identified by filling sensory neurons with fluorescein dyes. Dev Biol *111*, 158-170.

Higashide, T., Murakami, A., McLaren, M.J., and Inana, G. (1996). Cloning of the cDNA for a novel photoreceptor protein. J Biol Chem *271*, 1797-1804.

Homma, N., Takei, Y., Tanaka, Y., Nakata, T., Terada, S., Kikkawa, M., Noda, Y., and Hirokawa, N. (2003). Kinesin superfamily protein 2A (KIF2A) functions in suppression of collateral branch extension. Cell *114*, 229-239.

Kalil, K., Szebenyi, G., and Dent, E.W. (2000). Common mechanisms underlying growth cone guidance and axon branching. J Neurobiol *44*, 145-158.

Kamath, R.S., Martinez-Campos, M., Zipperlen, P., Fraser, A.G., and Ahringer, J. (2001). Effectiveness of specific RNA-mediated interference through ingested double-stranded RNA in Caenorhabditis elegans. Genome Biol *2*, RESEARCH0002.

Kirschner, M., and Mitchison, T. (1986). Beyond self-assembly: from microtubules to morphogenesis. Cell *45*, 329-342.

Knobel, K.M., Davis, W.S., Jorgensen, E.M., and Bastiani, M.J. (2001). UNC-119 suppresses axon branching in C. elegans. Development *128*, 4079-4092.

Maduro, M., and Pilgrim, D. (1995). Identification and cloning of unc-119, a gene expressed in the Caenorhabditis elegans nervous system. Genetics *141*, 977-988.

Maduro, M.F., Gordon, M., Jacobs, R., and Pilgrim, D.B. (2000). The UNC-119 family of neural proteins is functionally conserved between humans, Drosophila and C. elegans. J Neurogenet *13*, 191-212.

McIntire, S.L., Reimer, R.J., Schuske, K., Edwards, R.H., and Jorgensen, E.M. (1997). Identification and characterization of the vesicular GABA transporter. Nature *389*, 870-876.

Nix, P., Hisamoto, N., Matsumoto, K., and Bastiani, M. (2011). Axon regeneration requires coordinate activation of p38 and JNK MAPK pathways. Proc Natl Acad Sci U S A *108*, 10738-10743.

Noda, Y., Sato-Yoshitake, R., Kondo, S., Nangaku, M., and Hirokawa, N. (1995). KIF2 is a new microtubule-based anterograde motor that transports membranous organelles distinct from those carried by kinesin heavy chain or KIF3A/B. J Cell Biol *129*, 157-167.

O'Leary, D.D., and Terashima, T. (1988). Cortical axons branch to multiple subcortical targets by interstitial axon budding: implications for target recognition and "waiting periods". Neuron *1*, 901-910.

Perkins, L.A., Hedgecock, E.M., Thomson, J.N., and Culotti, J.G. (1986). Mutant sensory cilia in the nematode Caenorhabditis elegans. Dev Biol *117*, 456-487.

Praitis, V., Casey, E., Collar, D., and Austin, J. (2001). Creation of low-copy integrated transgenic lines in Caenorhabditis elegans. Genetics *157*, 1217-1226.

Schafer, J.C., Winkelbauer, M.E., Williams, C.L., Haycraft, C.J., Desmond, R.A., and Yoder, B.K. (2006). IFTA-2 is a conserved cilia protein involved in pathways regulating longevity and dauer formation in Caenorhabditis elegans. J Cell Sci *119*, 4088-4100.

Starich, T.A., Herman, R.K., Kari, C.K., Yeh, W.H., Schackwitz, W.S., Schuyler, M.W., Collet, J., Thomas, J.H., and Riddle, D.L. (1995). Mutations affecting the chemosensory neurons of Caenorhabditis elegans. Genetics *139*, 171-188.

Swanson, D.A., Chang, J.T., Campochiaro, P.A., Zack, D.J., and Valle, D. (1998). Mammalian orthologs of C. elegans unc-119 highly expressed in photoreceptors. Invest Ophthalmol Vis Sci *39*, 2085-2094.

Timmons, L., Court, D.L., and Fire, A. (2001). Ingestion of bacterially expressed dsRNAs can produce specific and potent genetic interference in Caenorhabditis elegans. Gene *263*, 103-112.

Ward, S., Thomson, N., White, J.G., and Brenner, S. (1975). Electron microscopical reconstruction of the anterior sensory anatomy of the nematode Caenorhabditis elegans.?2UU. J Comp Neurol *160*, 313-337.

White, J.G., Southgate, E., Thomson, J.N., and Brenner, S. (1986). The structure of the nervous system of the nematode Caenorhabditis elegans. Philos Trans R Soc Lond B Biol Sci *314*, 1-340.

Witte, H., Neukirchen, D., and Bradke, F. (2008). Microtubule stabilization specifies initial neuronal polarization. J Cell Biol *180*, 619-632.

Yu, W., Ahmad, F.J., and Baas, P.W. (1994). Microtubule fragmentation and partitioning in the axon during collateral branch formation. J Neurosci *14*, 5872-5884.